Q-SWITCHED AND DARK PULSE HARMONIC MODE-LOCKED ALL-FIBER LASERS USING INTERFERENCE FILTERS

CHI MINGZHI

FACULTY OF ENGINEERING
UNIVERSITY OF MALAYA
KUALA LUMPUR

2025

Universiti Malaya

Q-SWITCHED AND DARK PULSE HARMONIC MODE-LOCKED ALL-FIBER LASERS USING INTERFERENCE FILTERS

CHI MINGZHI

DISSERTATION SUBMITTED IN FULFILLMENT OF THE REQUIREMENTS FOR THE DEGREE OF MASTER OF ENGINEERING SCIENCE

FACULTY OF ENGINEERING
UNIVERSITY OF MALAYA
KUALA LUMPUR

2025

Universiti Malaya

UNIVERSITY OF MALAYA

ORIGINAL LITERARY WORK DECLARATION

Name of Candidate: **CHI MINGZHI**

Registration/Matric No: **S2162042**

Name of Degree: **Master of Engineering Science**

Title of Project Paper/Research Report/Dissertation/Thesis ("this Work"):

Q-switched and dark pulse harmonic mode-locked all-fiber lasers using interference filters

Field of Study: Photonics

I do solemnly and sincerely declare that:

(1) I am the sole author/writer of this Work;
(2) This Work is original;
(3) Any use of any work in which copyright exists was done by way of fair dealing and for permitted purposes and any excerpt or extract from, or reference to or reproduction of any copyright work has been disclosed expressly and sufficiently and the title of the Work and its authorship have been acknowledged in this Work;
(4) I do not have any actual knowledge nor do I ought reasonably to know that the making of this work constitutes an infringement of any copyright work;
(5) I hereby assign all and every rights in the copyright to this Work to the University of Malaya ("UM"), who henceforth shall be owner of the copyright in this Work and that any reproduction or use in any form or by any means whatsoever is prohibited without the written consent of UM having been first had and obtained;
(6) I am fully aware that if in the course of making this Work I have infringed any copyright whether intentionally or otherwise, I may be subject to legal action or any other action as may be determined by UM.

Candidate's Signature Date: 2024. 8. 18

Subscribed and solemnly declared before,

Witness's Signature Date: 2024 .8. 18

Name:

Designation:

University of Malaya

Q-SWITCHED AND DARK PULSE HARMONIC MODE-LOCKED ALL-FIBER LASERS USING INTERFERENCE FILTERS

ABSTRACT

Interference filters, pivotal optical devices harnessing the principle of interference to selectively transmit or reflect specific wavelengths of light, stand as indispensable tools across diverse domains such as communication, sensing, medical, industrial, and scientific fields. This dissertation embarks on exploring the efficacy of multimode or cladding mode interference in pulse generation. Initially, it proposes and demonstrates a passively Q-switched all-fiber laser, leveraging a multimode double-clad Erbium-Ytterbium co-doped fiber as an active medium. The Q-switching mechanism, facilitated by the Kerr effect of multimode interference, induces intensity modulation within the linear cavity laser. Stable Q-switched pulses at 1552.3 nm are achieved, with a repetition rate ranging from 50.3 to 222.2 kHz and shortest pulse width of 2.1 μs, alongside a peak pulse energy of 2.7 μJ at a pump power of 2.42 W. This unveils a novel modulation mechanism for obtaining high-energy pulses within an all-fiber linear cavity. Subsequently, the study demonstrates the realization of harmonic domain-wall dark pulses in a C-band fiber laser. The self-started domain-wall dark pulse at a mere pump power of 112 mW exhibits a fundamental repetition rate of 0.96 MHz, pulse width of 250 ns, and a maximum average pulse energy of 3.24 nJ. Furthermore, the experiment reveals the visualization and quantification of dark pulses up to the 7th harmonic order, with a minimum pulse width of 60 ns recorded in the 7th order. Remarkably, the harmonic dark pulse fiber laser exhibits commendable stability, maintaining signal-to-noise ratios above 50 dB across all harmonic operations. The pursuit of harmonic dark pulse dark soliton

Universiti Malaya

presents a promising pathway for fostering sustainable industrial advancement in the future.

Keywords: Multimode interference, Kerr effect, Dark Pulses, Artificial Saturable Absorber

Universiti Malaya

TERSUIS-Q DAN RAGAM-PENGUNCIAN HARMONIK DENYUT GELAP SELURUH/SEMUA LASER BERASAKAN GENTIAN MENGGUNAKAN PENAPIS GANGGUAN

ABSTRAK

Penapis gangguan, peranti optik penting yang memanfaatkan prinsip gangguan untuk menghantar atau memantulkan panjang gelombang cahaya tertentu secara selektif, berdiri sebagai alat yang sangat diperlukan merentasi pelbagai domain seperti bidang komunikasi, penderiaan, perubatan, perindustrian dan saintifik. Disertasi ini memulakan penerokaan keberkesanan gangguan pelbagai mod atau clad mode dalam penjanaan nadi. Pada mulanya, ia mencadangkan dan menunjukkan laser sistem berasaskan semua gentian optik yang berupaya menghasilkan nadi Q-suis secara pasif, memanfaatkan gentian terdop Erbium-Ytterbium bercirikan perbagai mod sebagai medium aktif. Mekanisme pensuisan Q, difasilitasi oleh kesan Kerr untuk mendorong modulasi intensiti dalam laser rongga linear. Denyutan Q-suis yang stabil pada 1552.3 nm dicapai, dengan kadar pengulangan antara 50.3 hingga 222.2 kHz dan lebar nadi 2.1 μs, bersama tenaga nadi puncak 2.7 μJ pada kuasa pam 2.42 W. Ini memperkenalkan mekanisme modulasi baru untuk mendapatkan denyutan tenaga tinggi dalam laser sistem berasaskan semua gentian. Selepas itu, kajian menunjukkan realisasi denyutan gelap dinding domain harmonik dalam laser gentian C-band. Nadi gelap dinding domain yang dimulakan sendiri pada kuasa pam 112 mW sahaja mempamerkan kadar pengulangan asas 0.96 MHz, tempoh nadi 250 ns, dan tenaga nadi purata maksimum 3.24 nJ. Tambahan pula, eksperimen mendedahkan visualisasi dan kuantifikasi denyutan gelap sehingga tertib harmonik ke-7, dengan lebar nadi minimum 60 ns direkodkan dalam susunan ke-7. Laser gentian nadi gelap harmonik mempamerkan kestabilan yang terpuji, mengekalkan nisbah isyarat-ke-bunyi melebihi 50 dB merentas semua operasi harmonik. Pembangunan

Universiti Malaya

soliton gelap nadi gelap harmonik memberikan laluan yang menjanjikan untuk memupuk kemajuan industri yang mampan pada masa hadapan.

Kata Kunci: Mod perbagai interferensi, Kesan Kerr, Denyutan gelap, Penyerap Tepu Buatan

Universiti Malaya

TABLE OF CONTENTS

Q-SWITCHED AND DARK PULSE HARMONIC MODE-LOCKED ALL-FIBER LASERS USING INTERFERENCE FILTERS.....iii

Abstract.....iii

Abstrak.....v

Table of Contents.....vii

List of Figures.....ix

List of Tables.....xi

List of Abbreviations.....xii

CHAPTER 1: INTRODUCTION.....1

1.1 Background.....1

1.2 Thesis Objectives.....5

1.3 Outline of the Dissertation.....6

CHAPTER 2: LITERATURE REVIEW.....8

2.1 Introduction to Fiber Laser.....8

2.2 Q-switching Principle and Technique.....13

2.3 Mode-locking Principle and Technique.....16

2.3.1 Harmonic Mode-Locking (HML).....19

2.4 Dark Solitons.....21

2.4.1 NLSE Dark Soliton.....21

2.4.2 CQNLSE Dark Soliton.....27

2.4.3 DW Dark Solitons.....30

2.5 Doped Fiber Based SAs.....34

Universiti Malaya

2.6 MMI Interferometer Based SAs 38

2.7 Summary 43

CHAPTER 3: PASSIVE Q-SWITCHING INDUCED BY THE KERR EFFECT OF INTERFERENCE FILTERS 44

3.1 Introduction 44

3.2 Q-switched Laser Configuration 45

3.3 Laser Performance 47

3.4 Summary 52

CHAPTER 4: HARMONIC DOMAIN-WALL DARK PULSE GENERATION USING UNPUMPED THIN-CORE THULIUM FIBER AS INTERFEROMETER 54

4.1 Introduction 54

4.2 Experimental Arrangements 57

4.3 Mode-Locking Performance 61

4.4 Summary 68

CHAPTER 5: CONCLUSION AND FUTURE WORKS 70

5.1 Conclusion 70

5.2 Future Work 72

References 74

List of Publications and Papers Presented 86

Universiti Malaya

LIST OF FIGURES

Figure 2.1 EDF energy level diagram showing transition of absorption and emission spectrum of Er^{3+} ion (Matniyaz, 2014). 11

Figure 2.2 Simplified levels and ion transition process for 9xx/10xx nm pumped EYDF. (a) Energy transfer and ion transition process for Er ions and Yb ions in EYDF; (b) energy transfer and ion transition process for Er ion pairs (Li et al., 2025). 13

Figure 2.3 Temporal evolution of gain and losses in (a) an actively Q-switched laser, and (b) a passive Q-switched laser (Paschotta, 2006). 15

Figure 2.4 Illustration basic principle of mode-locking (a) simplest mode-locked laser cavity, and (b) Mode locked laser output signal (Bagheri et al., 2018; Ennejah et al., 2013). 17

Figure 2.5 Dispersion vs. Wavelength in SMF (Kharazi et al., 2012). 23

Figure 2.6 (a) Configuration of ring YDFL using GO as SA, (b) Pulse train of the bright pulse (inset shows the corresponding output spectrum), and (c) The evolution of the dark pulse width at different pump powers (Lin et al., 2014). 24

Figure 2.7 (a)-(c) The dark square pulse bunches consist of 2, 3, and 4 dark pulses in a round-trip time, (d)-(f) Corresponding single dark pulse width of different bunches (Lin et al., 2014). 25

Figure 2.8 Schematic diagram of the EDFL for generating multiwavelength NLSE dark pulses (Tiu et al., 2014). 26

Figure 2.9 Output spectra and the corresponding oscilloscope traces of (a) Fundamental harmonic, (b) 2nd-order harmonic, (c) 3rd-order harmonic, (4) 4th-order harmonic NLSE dark pulses (Tiu et al., 2014). 27

Figure 2.10 Schematic diagram of the EDFL producing CQNLSE dark pulse (Tiu et al., 2015). 29

Figure 2.11 (a) CQNLSE dark pulse train, (b) output spectrum, and (c) RF spectrum (Tiu et al., 2015). 30

Figure 2.12 (a) EDFL cavity to generate DW solitons, (b) output spectrum, and (c) oscilloscope trace of the single dark pulse (Zhang et al., 2011). 33

Figure 2.13 (a) Experimental setup for generating bidirectional DW dark soliton, (b) decomposed dark pulse trains in x orthogonal axis, and (c) y-axis (Zhang et al., 2019). 33

Universiti Malaya

Figure 2.14 (a) Schematic of the EDFL. (b) nonlinear absorption profile of TDF FSA (Zhang et al., 2022). 36

Figure 2.15 (a) Passively mode-locked and CW optical spectra of fiber lasers at pump power 178 mW. (b) Experimental data and $Sech^2$ fit curve of mode-locked pulse shape. (c) typical pulse train of fiber laser. (d) RF spectrum around the fundamental repetition rate, and the inset figure is the RF spectrum with high-order harmonic of the repetition rate (Zhang et al., 2022). 37

Figure 2.16 (a) Combined mode and CW optical spectra of the fiber laser. (b) The pulse train in combined mode operation. (c) RF spectrum with the span of 30 MHz and the inset figure is the RF spectrum with initial span of 10 MHz (Zhang et al., 2022). 38

Figure 2.17 The relative power transmission is plotted as a function of $\tilde{\gamma}$ (thus the total power) for $L = 4.5\pi$ for the case of five modes, when $p_0 = 0.5, 0.25, 0.75$ at $\zeta = 0$, in solid, dashed, and dotted lines, respectively (Nazemosadat et al., 2013). 39

Figure 2.18 (a) Experimental setup of the DW dark pulse EDFL. (b) Wavelength domain of DW dark pulse throughout the operating pump power range. Inset figure is the optical spectrum at pump power of 195.4 mW (Chen et al., 2024). 42

Figure 3.1 The schematic arrangement of the Q-switched EYDFL. 46

Figure 3.2 Q-switched laser characteristics (a) output spectrum (b) typical oscilloscope trace (c) RF spectrum. 48

Figure 3.3 : The Q-switched laser performance at various launched pump power (a) Measured average output power and pulse energy (b) Repetition and pulse width versus input pump power. 50

Figure 3.4 Typical pulse train obtained by the laser when EYDF is fixed at 2 m (a) Q-switched pulses at 1.71 W pump power (b) mode-locked pulse at 2.75 W pump power. 51

Figure 4.1 (a) Cavity setup of harmonic DW dark pulse EDFL. (b) Micrograph of splicing point between SMF and TCTDF. (c) Schematic diagram of light propagation through TCTDF. 59

Figure 4.2 (a) Microscopic view of TDF, (b) The distribution curves of different dopants along the fiber diameter, (c) The attenuation profile in visible and (d) the attenuation profile in NIR region (Lip et al., 2024). 60

Figure 4.3 The nonlinear optical absorption curve of the fabricated TCTDF. 61

Universiti Malaya

LIST OF TABLES

Table 1 Q-switched pulse generation using different SAs in EDFLs 53

Table 2 DW dark pulse generation using different SAs in EDFLs..... 69

Universiti Malaya

LIST OF ABBREVIATIONS

ASE	:	Amplified Spontaneous Emission
AW	:	Acoustic Wave
CNT	:	Carbon Nanotube
CQNLSE	:	Cubic-Quintic Nonlinear Schrödinger Equation
CW	:	Continuous Wave
DCF	:	Dispersion Compensation Fiber
DSF	:	Dispersion Shifted Fiber
DW	:	Dispersive Wave
DW	:	Domain Wall
EDF	:	Erbium-Doped Fiber
EDFA	:	Erbium-Doped Fiber Amplifier
EDFL	:	Erbium-Doped Fiber Laser
EPMA	:	Electron Probe Microanalyses
ESA	:	Excited State Absorption
EYDF	:	Erbium-Ytterbium Co-doped Fiber
EYDFL	:	Erbium-Ytterbium Co-doped Fiber Laser
FBG	:	Fiber Bragg Grating
FSA	:	Fiber Saturable Absorber
FSR	:	Free Spectral Range
FWHM	:	Full Width at Half Maximum
GDD	:	Group Delay Dispersion
GDR	:	Gain Depletion and Recovery
GIMF	:	Graded-Index Multimode Fiber
GOSA	:	Graphene-Oxide Saturable Absorber

Universiti Malaya

GVD	:	Group Velocity Dispersion
HML	:	Harmonic Mode Locking
LD	:	Laser Diode
MFA	:	Mode Field Area
MMI	:	Multi-Mode Interference
MMF	:	Multimode Fiber
NALM	:	Nonlinear Amplifying Loop Mirror
NIR	:	Near-Infrared
NLSE	:	Nonlinear Schrödinger Equation
NOLM	:	Nonlinear Optical Loop Mirror
NPR	:	Nonlinear Polarization Rotation
OSA	:	Optical Spectrum Analyzer
PC	:	Polarization Controller
PIQ	:	Pair Induced Quenching
Q-Factor	:	Quality Factor
RF	:	Radio Frequency
SA	:	Saturable Absorber
SAM	:	Self-Amplitude Modulation
$SECH^2$	:	Hyperbolic Secant Squared
SESAM	:	Semiconductor Saturable Absorber Mirror
SIMF	:	Step-Index Multimode Fiber
SMF	:	Single-Mode Fiber
SMS	:	Single-Mode Fiber-Multimode Fiber-Single-Mode Fiber
SNR	:	Signal-to-Noise Ratio

Universiti Malaya

TBF	:	Tunable Bandpass Filter
TBP		Time-Bandwidth Product
TCTDF	:	Thin-Core Thulium Doped Fiber
TDF	:	Thulium-Doped Fiber
TMD	:	Transition Metal Dichalcogenides
WDM	:	Wavelength Division Multiplexer
YDF	:	Ytterbium Doped Fiber
1-D	:	One-Dimensional
2-D	:	Two-Dimensional

Universiti Malaya

CHAPTER 1: INTRODUCTION

1.1 Background

Since its creation decades ago, the fiber laser has developed into a sophisticated technology that is now indispensable for various scientific, medicinal, and industrial purposes (Ashforth et al., 2020; Cerami et al., 2013). Due to their versatility, dependability, and small design, these light sources are more advantageous than bulk lasers, including alignment-free and turn-key operation for end users (Nishizawa, 2014). Fiber lasers operating in a pulsed fashion are essential because they can drive nonlinear optical processes and boost peak power. The pulsating laser output is appropriate for tasks involving cutting, material processing and remote sensing. To date, numerous methods have been proposed by researchers to generate pulsed laser emissions. However, a promising new approach utilizes saturable absorbers (SAs), often favored for their significant potential in producing Q-switching or mode-locking pulses. Q-switching involves the modulation of the laser cavity quality factor (Q-factor), while mode-locking is achieved through the phase-locking of multiple longitudinal cavity modes. Passive approaches employing SA offer access to a wide range of pulse parameters without the need for expensive and intricate electrically driven modulators, which can otherwise limit the achievable pulse width from the laser source (Keller, 2003).

Q-switching is a widespread technique in fast optics, primarily used to generate microsecond or sub-microsecond pulses. There are two ways to realize Q-switching operation: active and passive methods. On the one hand, an active Q-switching method typically requires an electro-optic or an acoustic-optic device to constantly modulate the intra-cavity losses (Cui et al., 2019; Zhang et al., 2021). Moreover, Pérez-Millán et al.

Universiti Malaya

(2005) generated the Q-switching pulse using magneto-strictive transducers. On the other hand, passive Q-switching techniques benefit from the availability of the nonlinear absorption of the SAs to modulate Q-factor, which, in other words, modulates the intra-cavity losses (Popa et al., 2011; Wang et al., 2014). Passive methods are widely preferred over active methods in Q-switching because of their compactness, design simplicity, and operation versatility (Chi et al., 2023). To date, there are many different SAs have been reported, such as graphene (Luo et al., 2010; Popa et al., 2011), black phosphorus (Chen et al., 2015), carbon nanotubes (CNTs) (Zhou et al., 2010), rare-earth-doped fiber (Tsai et al., 2010), semiconductor saturable absorber mirror (SESAMs) (Li et al., 2012), and transition metal dichalcogenides (TMDs) (Chen et al., 2015).

Even though the above SAs had been extensively studied and proved to be potential SA candidates, inevitable drawbacks, and limitations of these SAs were also pointed out. Graphene is low in modulation depth and has a small optical absorption range. Black phosphorus is easily damaged and prone to water and oxygen exposure. Also, black phosphorus raised concerns as it could be dangerous to human health when exposed to long-term operations. In addition, CNTs require a relatively complicated bandgap control, which prevents their operation from specific wavelengths. Moreover, SESAMs are expensive and complex in design and fabrication. Finally, TMDs suffer from low impurities and low uniformities, as well as a low damage threshold, which limits the long-term stability of the fiber laser.

Therefore, looking for SAs with the merits of high damage threshold, good stability (signal-to-noise ratio (SNR) above 40 dB and stably operates over 24 hours) to various operating environments, wide wavelength operation range, cheap fabrication cost, and simplicity in structure are necessary for the emerging fiber laser industry. A cascaded fiber structure that consists of a segment of single-mode fiber (SMF), a piece of

Universiti Malaya

multimode fiber (MMF), and another SMF segment to formalize a SMF-MMF-SMF structure (SMS) utilizing multimode interference (MMI) to generate Q-switching or mode-locking pulses received considerable attention in recent years (Chen et al., 2024; Fu et al., 2015; Zhao et al., 2019).

Multiple modes are excited inside the MMF when the lead-in light shoots from the core of SMF to MMF. Consider mono-mode light propagates inside SMF and it has a stable filed E at the SMF-MMF interface for $z = 0$. When the lead-in light enters from SMF into MMF, multiple modes are excited inside the MMF due to the intrinsic characteristics of the MMF can carry many modes. Field E can be decomposed into the modes' modal functions of multimode waveguide (Zhu, 2008):

$$E(x, y, 0) = \sum_l c_{l0} \varphi_{l0}(x, y), \tag{1.1}$$

where φ_{l0} is the orthogonal wave function of $(l, 0)$ mode with propagation β_{l0} and c_{l0} are the excitation coefficients. Different modes exist different phase velocities, and thus, the field at the end of MMF where the position is $z = z$ (Zhu, 2008):

$$E(x, y, z) = \sum_l c_l \varphi_l(x, y) \exp(-j\beta_l z) \tag{1.2}$$

Consequently, an interference pattern happens when the light shoots out from lead-out SMF. This phenomenon is also related to the self-imaging effect. Since the superposition of different z can lead to different interference patterns. Nazemosadat et al. (2013) have numerically investigated and proved that MMI exists nonlinear phenomenon, which made SMS structure a novel SA especially in the ultrafast pulse generation (Ding et al., 2011; Nazemosadat et al., 2013; Renninger et al., 2013; Wright et al., 2015; Wright et al., 2015).

Contrary to the conventional bright pulses emitted by most pulsed lasers, experimental observations have unveiled a fascinating phenomenon: fiber lasers can produce dark pulses under specific conditions, especially when a polarizer is introduced into the cavity. Dark pulses manifest as a series of narrow intensity dips superimposed on a continuous wave (CW) background of laser emission (Tiu et al., 2022; Zhang et al., 2009). Numerical simulations have indicated that dark pulses exhibit reduced sensitivity to fiber loss and enhanced stability against noise, distinguishing them from their bright counterparts. This characteristic hints at significant potential for dark pulses in applications such as long-haul communication (Baronio et al., 2018).

Significant attention has been devoted to exploring the emission of dark pulses from fiber lasers across different wavelength regions (Tiu et al., 2015; Xomalis et al., 2018; Xue et al., 2015). This intriguing phenomenon is considered an intrinsic characteristic of fiber lasers, regardless of whether they operate in anomalous or normal dispersion regimes (Xue et al., 2015). Typically, fiber lasers with net anomalous dispersion generate dark pulses through a mechanism elucidated by the domain-wall theory. This theory proposes that two laser beams, arising from the two Eigen operation states of the fiber lasers, undergo incoherent coupling with each other (Wang et al., 2024). Achieving these states involves managing either the two orthogonal polarization states of the lasers or inducing two separated wavelengths through an intra-cavity birefringent filter. Subsequently, the resulting dual light beams interact via the nonlinear effect of optical fibers, with the lasers typically requiring a pump threshold of around 100 mW for dark pulse formation (Zhao et al., 2013).

To enhance the cross-coupling effect between the lasing beams for dark pulse generation, a nonlinear gain medium is essential. Previous studies have shown that incorporating a segment of highly nonlinear fiber into the laser resonator can reduce the

Universiti Malaya

threshold pump power for dark pulse generation to as low as 43.4 mW (Wang et al., 2012). Recent advancements have explored various materials for their potential as SAs to generate dark pulses within mode-locked fiber lasers. For instance, Nizamani et al. (2021) demonstrated the generation of mode-locked dark pulses using a novel SA based on aluminum zinc oxide (AZO) .

This dissertation aims to investigate the utilization of multimode interference for pulse generation. Initially, a passively Q-switched all-fiber laser is proposed and demonstrated, employing a multimode double-clad Erbium-Ytterbium co-doped fiber as the active medium. Q-switching is achieved through the Kerr effect of multimode interference, inducing intensity modulation within the linear cavity laser. Subsequently, experimental demonstration of harmonic domain-wall dark pulses is conducted in an Erbium-doped fiber laser (EDFL). This is achieved by employing an unpumped thin-core Thulium-doped fiber (TCTDF) to trigger multiwavelength oscillations within the cavity. The interaction of these multiwavelength oscillations results in the emergence of topological defects in the temporal domain, leading to the formation of narrow intensity dips amidst the strong CW emission background.

1.2 Thesis Objectives

The study of SAs is crucial in passive Q-switching and mode-locking technologies for generating short pulses. Among various SAs, the SMS structure stands out as a unique type, its transmission spectrum depends on the length of the multimode fiber (MMI mechanism) and the light intensity circulating inside the laser cavity. There are multiple reports regarding either Q-switching or mode-locking operation utilizing SMS or similar structures. However, most of them require a more complex ring resonator scheme. In addition, forementioned papers reported that the typical Q-switching pulse energy and

Universiti Malaya

peak power is commonly below 1μJ and 300 mW, respectively (Fu et al., 2015; Wang et al., 2014; Wang et al., 2019). The SMS fiber structure's intrinsic high optical damage threshold gives it a notable edge in high-power laser systems. Due to the spatial self-imaging effects within the multimode fiber segment, optical intensity is redistributed over a wider effective mode area (usually 50–100 μm², as opposed to 10–15 μm² in single-mode fibers). In addition to reducing thermal lensing effects, this intensity redistribution allows stable operation under high pump power regimes (>500 mW CW emission) by lowering localized power density at the SA interface. Thus, SMS-based systems exhibit improved pulse energy scalability, with the average output power scaling linearly with pump power until it reaches the nonlinear threshold, which is usually between 1 and 3 W, depending on the shape of the fiber.

This research focuses on exploring the SMS structure's effectiveness as an artificial SA in passive Q-switching and as the comb filter in domain-wall dark pulse generation via passive mode-locking operation. The fundamental objective is to experimentally demonstrate the generation of Q-switched and mode-locked dark pulses. The following objectives have been outlined to achieve this aim:

1. To design, construct, and validate the Q-switched Erbium Ytterbium fiber laser operating at C-band by using the Kerr effect of multimode interference.
2. To utilize the TCTDF as the fiber saturable absorber (FSA) and interferometer in EDFL to generate Domain-Wall (DW) dark pulse.
3. To characterize the DW dark pulse by its pulse width, spectral width, repetition rate, harmonic order, output power and SNR.

1.3 Outline of the Dissertation

This thesis is systematically organized into five chapters, each meticulously dedicated to exploring and analyzing the generation of Q-switched and mode-locked fiber lasers

Universiti Malaya

operating within the C-band region, utilizing the SMS structure as an artificial SA or comb filter. The first chapter serves as an introductory foundation, offering a concise overview of the practical applications of pulsed lasers and the methodologies employed for passively generating Q-switched and mode-locked lasers. This chapter not only establishes the rationale for the current investigation but also articulates the motivations, objectives, and substantive contributions of this thesis to the existing body of knowledge.

The second chapter provides a comprehensive literature review, focusing on the fundamental principles of fiber lasers and the two operational regimes: Q-switching and mode-locking, which are essential for generating short and ultrashort pulses. Additionally, it delves into the techniques for dark pulse generation in subsequent subsections, offering a thorough theoretical background. Chapter 3 is dedicated to the detailed exploration of passively Q-switched pulse generation based on the optical Kerr effect, while Chapter 4 offers an in-depth exposition on the generation of DW dark pulses using a fiber interferometer. Finally, the fifth chapter synthesizes the key findings of the research, drawing conclusions and proposing potential avenues for future experimental advancements to further enhance the field.

Universiti Malaya

CHAPTER 2: LITERATURE REVIEW

2.1 Introduction to Fiber Laser

A fiber laser is a type of laser that utilizes optical fiber as its gain medium, where the amplification of light occurs. In a fiber laser, the gain medium is typically doped with rare-earth ions such as erbium, ytterbium, or thulium, which provide the necessary energy levels for lasing action. The fiber itself serves as a waveguide, confining and guiding the light along its length. Fiber lasers offer several advantages over traditional bulk lasers, including compact size, high efficiency, excellent beam quality, and flexible integration into various systems. They are widely used in industrial applications such as cutting, welding, marking, and engraving, as well as in telecommunications, medicine, defense, and scientific research. Additionally, fiber lasers can be operated in CW mode or pulse mode, depending on the specific application requirements.

An EDFL is a type of fiber laser that uses an optical fiber doped with erbium ions (Er^{3+}) as the gain medium. Erbium-doped fibers (EDFs) are commonly used in telecommunications, amplifiers, and various other applications due to their ability to amplify light in the 1550 nanometer (nm) wavelength range, which is widely used in optical communication systems. EDFL requires an external energy source to excite the erbium ions within the fiber and raise them to higher energy levels. This process is called pumping. Typically, the erbium ions are pumped with a laser diode or another laser source at a shorter wavelength, such as around 980 nm or 1480 nm. When the erbium ions absorb energy from the pump source, they are raised to higher energy levels, creating a population inversion. This means that there are more ions in the higher energy states than in the lower ones. As the excited erbium ions return to their lower energy states, they emit

Universiti Malaya

photons at the desired wavelength of around 1550 nm through a process called stimulated emission. These emitted photons are coherent and have the same frequency, phase, and direction as the incident photons. The emitted photons are then amplified as they travel back and forth through the erbium-doped fiber, which serves as the laser cavity. This amplification process is due to the stimulated emission and the population inversion within the fiber.

This study primarily focuses on generating laser output within the 1.5-micron range, utilizing EDF as the amplifying medium. Figure 2.1 illustrates an energy level diagram for Erbium ions (Er^{3+}). The energy levels exhibit broadening attributed to the dc-Stark effect, resulting in a relatively wide emission bandwidth. When a 980 nm pump laser diode beam is introduced into the EDF, Er^{3+} ions transition from the ground state ($^4I_{15/2}$) to a higher excited state ($^4I_{11/2}$). From there, these excited ions quickly decay to the metastable energy level ($^4I_{13/2}$) via nonradiative emission. Subsequently, the ions at $^4I_{13/2}$ return to the ground state ($^4I_{15/2}$) through spontaneous emission, emitting photons within the wavelength band of 1520 – 1570 nm. This spontaneous emission becomes amplified as it traverses through the fiber, particularly with increasing pump laser power. As the amplified spontaneous emission (ASE) spans a broad wavelength range of 1520-1570 nm, it serves effectively as a broadband light source.

When both a laser signal with a wavelength ranging between 1520 and 1570 nm and a 980 nm pump laser are simultaneously introduced into an EDF, several outcomes are possible, as depicted in Figure 2.1. Firstly, the signal photon may undergo stimulated absorption, wherein it excites an erbium ion from the ground state ($^4I_{15/2}$) to a higher level ($^4I_{13/2}$), and in the process, becomes absorbed. Alternatively, stimulated emission can occur, where the signal photon stimulates an erbium ion at state $^4I_{13/2}$to decay to $^4I_{15/2}$,

thereby generating another identical photon, thus amplifying the signal. Lastly, the signal photon may propagate through the unaffected fiber.

Meanwhile, spontaneous emission consistently occurs between energy levels $^4I_{13/2}$ and $^4I_{15/2}$. When the pump laser power reaches a sufficient level to achieve population inversion between these energy levels within the EDF, the input laser signal passing through the fiber is amplified. This process allows for the construction of an optical amplifier known as an erbium-doped fiber amplifier (EDFA). Additionally, the pump laser can amplify spontaneous emission, resulting in ASE, which constitutes the primary source of noise in these amplifiers.

A laser is an optical amplifier with positive feedback. By feeding the output of an EDFA back into its input to form a fiber loop and adding pump laser power into this loop, the EDFA is transformed into a fiber laser, termed an EDFL. The wavelength of the laser can be adjusted by tuning the cavity loss, thereby varying the laser wavelength accordingly.

If a laser signal with a wavelength between 1520 and 1570 nm, and a 980 pump laser are fed into an EDF simultaneously as shown in Figure 2.1, there are three possible outcomes for the signal photon: i) stimulated absorption: signal photon excites an erbium ion from the ground state $^4I_{15/2}$ to a higher level $^4I_{13/2}$ and become annihilated in the process; ii) stimulated emission: signal photon stimulates an erbium ion at state $^4I_{13/2}$ to decay to $^4I_{15/2}$, producing another identical photon. Thus, the signal is amplified; iii) signal photon can propagate unaffected through the fiber. In the meanwhile, spontaneous emission always occurs between level $^4I_{13/2}$ and level $^4I_{15/2}$. When pump laser power is high enough that the population inversion is achieved between the energy level $^4I_{13/2}$ and $^4I_{15/2}$ of EDF, the input laser signal passing through the fiber is then be amplified.

Universiti Malaya

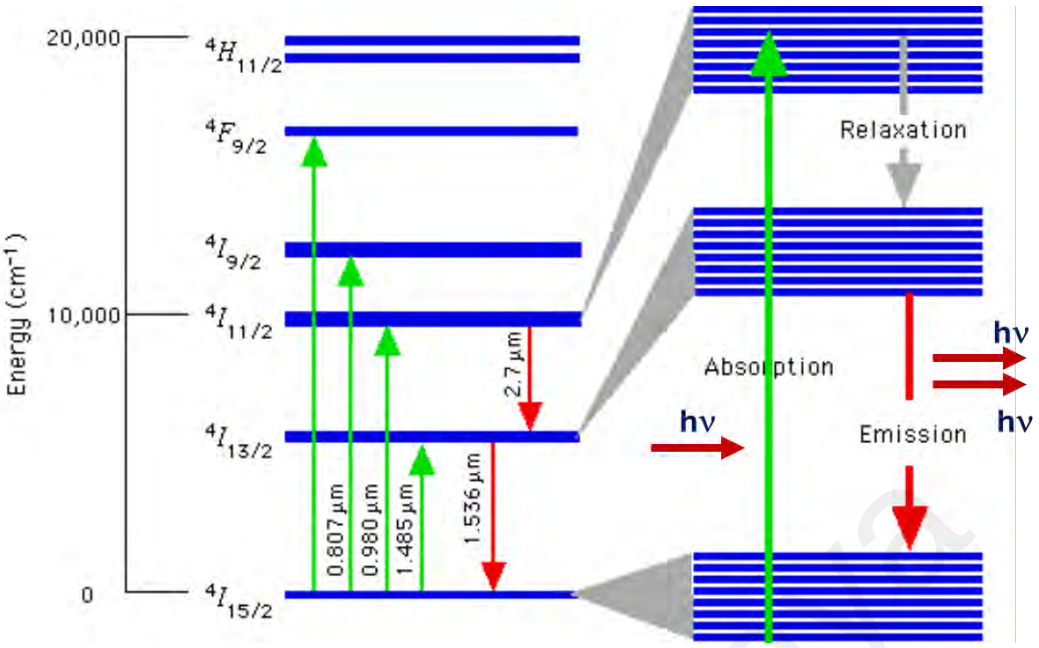

Figure 2.1 EDF energy level diagram showing transition of absorption and emission spectrum of Er^{3+} ion (Matniyaz, 2014).

EDFs have long been the mainstay of optical amplification systems, especially for the telecom C-band (1530-1565 nm), because of the erbium's (Er^{3+}) distinct metastable energy level structure. However, EDFs in high-power applications are limited by their weak cross absorption sections at typical pump wavelengths (such as 980 nm or 1,480 nm), which results in low pump efficiency (<30%). Erbium-ytterbium co-doped fiber (EYDF) is a hybrid fiber architecture that co-dopes ytterbium (Yb^{3+}) with Er^{3+} to address this difficulty. Superior performance in high-power fiber lasers and amplifiers is made possible by this synergistic combination, which uses Yb^{3+} as a sensitizer to improve pump absorption and facilitate effective energy transfer to Er^{3+}. With an absorption cross section ten times greater than Er^{3+} at 980 nm, Yb^{3+} acts as a sensitizer in EYDF. Over 95% of the absorbed pump energy is transferred from Yb^{3+} to Er^{3+} via resonant energy transfer (Förster mechanism).

The simplified energy transfer mechanism in EYDF is depicted in Figure 2.2 (a): Yb^{3+} ions at the $^2F_{7/2}$ ground state absorb 9xx/10xx nm pump photons, exciting them to the $^2F_{5/2}$ level. These excited Yb^{3+} ions transfer energy via cross-relaxation to adjacent Er^{3+} ions in the $^4I_{15/2}$ ground state, promoting Er^{3+} to the $^4I_{11/2}$ level. Subsequent nonradiative decay rapidly populates the $^4I_{13/2}$ metastable state, enabling signal amplification through stimulated emission from $^4I_{13/2}$ to $^4I_{15/2}$. However, two detrimental effects limit power scaling:

1. Excited-State Absorption (ESA): Signal photons are absorbed by Er^{3+} in the $^4I_{13/2}$ state, exciting them to $^4I_{9/2}$. Subsequent nonradiative decay to $^4I_{11/2}$ results in the loss of one signal photon.
2. Pair-Induced Quenching (PIQ): When two neighboring Er^{3+} ions are simultaneously excited to $^4I_{13/2}$, instantaneous energy transfer occurs. One ion transitions non-radiatively to $^4I_{9/2}$ while the other returns to $^4I_{15/2}$, effectively depleting one excited Er^{3+} ion.

Both ESA and PIQ significantly reduce optical efficiency in Er^{3+}-band lasers. The Er^{3+} ion pairs are assumed can be in two states: the 0-photon state (no ion excited) and the 1-photon state (one ion excited) (Delevaque et al., 1993; Sanchez et al., 1993).

Universiti Malaya

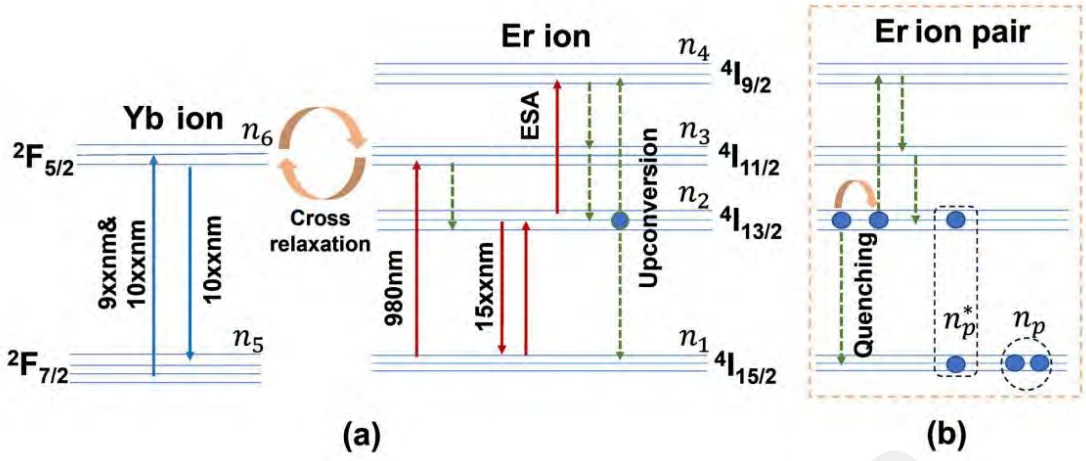

Figure 2.2 Simplified levels and ion transition process for 9xx/10xx nm pumped EYDF. (a) Energy transfer and ion transition process for Er ions and Yb ions in EYDF; (b) energy transfer and ion transition process for Er ion pairs (Li et al., 2025).

2.2 Q-switching Principle and Technique

The Q-switching technique is a method used to generate a powerful pulse, also known as Q-spoiling. It earns its name because it alters the optical Q-factor of the resonant cavity where it is applied. The Q-factor denotes the ratio of energy stored in the cavity to the energy lost per cycle. Mathematically, this can be represented by the equation (Yu et al., 2024):

$$Q = 2\pi v_o \left(\frac{W}{\delta}\right), \tag{2.1}$$

here, v_o represents the central frequency of the Q-switcher, W symbolizes the energy stored in the cavity, and δ stands for the rate of energy loss per cycle of light propagating in the laser cavity.

Considering L as the resonator length, n as the refractive index of the medium, and c as the speed of light, the time taken by light to travel in a cycle can be expressed as nL/c.

Consequently, the energy loss per cycle due to light propagation in the cavity can be represented as $\delta W/(nL/c)$. Thus, the Q-factor can be expressed as (Deng et al., 2025):

$$Q = 2\pi v_o \frac{W}{\delta W^c/_{nL}} = \frac{2\pi nL}{\delta \lambda_o}, \tag{2.2}$$

here, λ_o signifies the central wavelength of the laser in a vacuum. The equation suggests that the Q-factor is inversely proportional to the loss of the laser cavity. A lower Q-factor implies lower cavity loss and a higher laser threshold, while a higher Q-factor indicates lower cavity loss and a lower laser threshold, making laser oscillation easier to initiate. This technique enables the generation of laser pulses with very high peak power in a short duration.

The process begins with the pumping of the gain medium, while energy extraction is prevented by keeping the resonator losses high. This is achieved through active or passive approaches. Consequently, population inversion can exceed the population threshold significantly, which would not happen without the shutter. When the shutter abruptly opens, the laser's gain surpasses the losses, releasing the held energy in the form of a short, intense light pulse. This switching of the cavity Q-factor from low to high is why these processes are termed Q-switching techniques. Figure 2.3 (a) and (b) demonstrate the temporal evolution of gain and losses in an active Q-switched laser and passive Q-switched laser, respectively.

Universiti Malaya

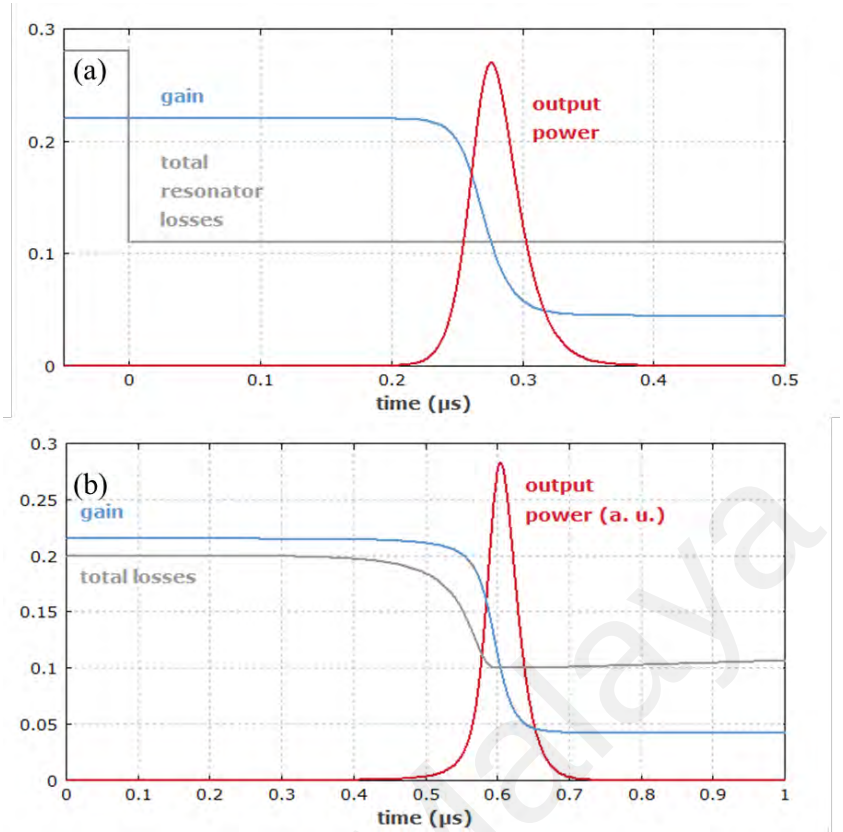

Figure 2.3 Temporal evolution of gain and losses in (a) an actively Q-switched laser, and (b) a passive Q-switched laser (Paschotta, 2006).

Active Q-switching relies on actively modulating loss. This method necessitates an external active operation modulator, such as mechanical Q-switches, electro-optical Q-switches, or acousto-optic Q-switches, to achieve loss modulation. Alternatively, SA devices can substitute the modulator to create a passive Q-switched laser. The optical nonlinearity inherent in SA triggers the switching process. Initially, the SA induces significant optical loss until it reaches the gain level. Once the gain surpasses the loss level, the gain of a SA becomes saturated, leading to the generation of brief pulses. This approach eliminates the need for an external active modulator, offering advantages in terms of flexibility and cost-effectiveness, and it is particularly suitable for higher pulse repetition rates.

2.3 Mode-locking Principle and Technique

The mode-locking method is employed to generate ultra-short pulses from lasers. It involves locking several axial modes within a laser cavity, a process referred to as mode-locking. By ensuring coherence between the phases of these modes, a radiation pulse can be generated, resulting in a sequence of extremely narrow laser pulses with a high pulse repetition rate, often measured in MHz, evenly spaced apart in time. Initially, the laser oscillates simultaneously at various frequencies. However, these light waves lack coherence because they oscillate at distinct frequencies, causing them to be out of phase with each other. The interference among these modes creates beating effects in the laser output, leading to random fluctuations in the intensity of the output beam. Figure 2.4 illustrates the fundamental concept of mode-locking.

Within the resonant cavity of a laser resides a gain medium alongside an optical loss modulator or SA, which dynamically alters the cavity's loss over time. A SA is an optical element characterized by a decreasing absorption coefficient as the intensity of incident light increases. It selectively absorbs weak pulses while allowing strong ones to transmit with minimal absorption. As pulse intensities rise, the material's ground state within the SA becomes depleted, leading to reduced resonator losses. Typically situated inside the optical resonator cavity adjacent to the gain medium, as depicted in Figure 2.4 (a), SAs obviate the need for an external signal for this form of mode-locking. Changes in the intra-cavity elements are induced solely by the laser light within the cavity itself.

Universiti Malaya

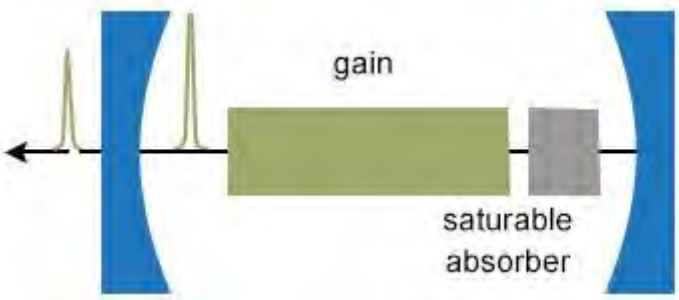

(a)

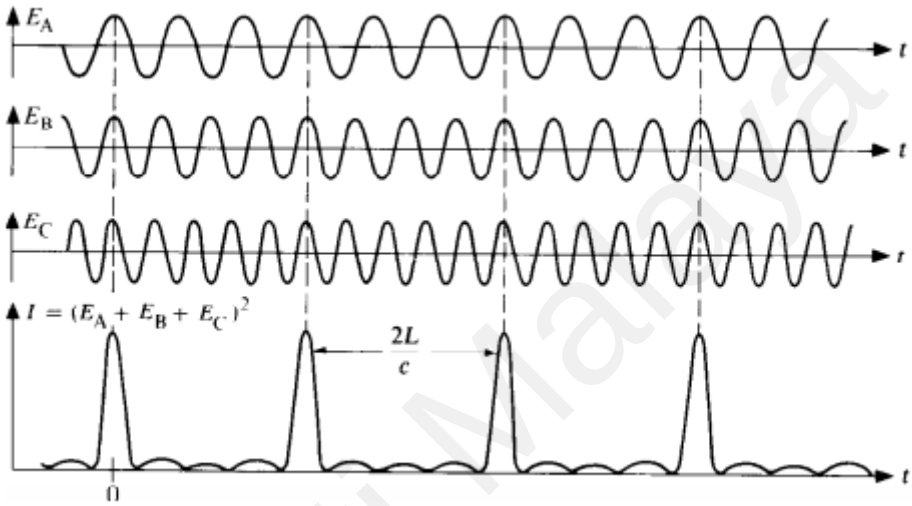

(b)

Figure 2.4 Illustration basic principle of mode-locking (a) simplest mode-locked laser cavity, and (b) Mode locked laser output signal (Bagheri et al., 2018; Ennejah et al., 2013).

To achieve mode-locked pulses, as illustrated in Figure 2.4 (b), multiple phases of modes must be synchronized. Once the phases are locked, each mode operates with a fixed phase relative to the others, resulting in light pulses that periodically interfere with one another. The output pulse train of a mode-locked device exhibits a repeated series of pulses, a phenomenon known as mode-locking. The linear Fabry-Pérot cavity, determined by (Quimby, 2006):

$$\Delta v = \frac{c}{2L} \tag{2.3}$$

Universiti Malaya

For a ring cavity, the mode separation is equal to c/L, where L is the cavity's length and c is the speed of light. The number of phase-locked modes influences the pulse duration. With N mode-locked devices, the total bandwidth becomes $N\Delta v$. This equation illustrates that the pulse width becomes narrower as the bandwidth widens. In practice, the shape of each pulse can be used to determine the precise amplitude and phase relationship of each longitudinal mode. For example, the minimal pulse duration for a pulse with a Gaussian shape is given as (Keller, 2021):

$$\Delta t = \frac{0.441}{N\Delta v}, \tag{2.4}$$

the value 0.44 is known as the time-bandwidth product (TBP), which varies depending on the shape of the pulse. For ultra-short, pulsed lasers, the TBP value is 0.315, and the pulse is expected to be a hyperbolic secant squared ($sech^2$) shape. This suggests that the pulse duration is inversely proportional to the mode count. With a higher number of interacting modes, the peak intensity increases, leading to a shorter pulse duration.

In general, there are two methods to generate mode-locking fiber lasers. The first technique, known as active mode locking, is based on the addition of an amplitude or phase modulator to the laser cavity in order to accomplish mode locking. Conversely, other approaches rely on the application of passive mode locking strategies. This method's basic idea is to provide the extra loss for low-intensity radiation by adding an intensity-dependent component to the laser cavity (Grudinin et al., 1997).

Acousto-optic or electro-optic modulators serve as examples of optical loss modulators utilized in active mode-locking processes. Alternatively, a SA can be employed to achieve self-amplitude modulation (SAM) of the light within the laser cavity, facilitating the production of passive mode-locked pulses. The speed of the loss modulation increases as

Universiti Malaya

the pulse length decreases, enhancing the efficiency of this method. The pulse duration is determined by a delicate balance of various effects, including the pulse shaping action of the SA and the pulse broadening caused by the limited gain bandwidth. Optical nonlinearities and dispersion can also play significant roles, particularly as pulses become increasingly rapid. The achieved pulse duration may be orders of magnitude shorter than the SA's recovery time. If other effects are not constraining the pulse duration, the pulse bandwidth may constitute a significant percentage of the gain bandwidth, for instance, due to higher-order dispersion.

Passive mode-locking provides a simplified alternative to active techniques by enabling automatic loss modulation synchronization, thereby eliminating the requirement for an external electronic modulator. However, the pulse formation mechanism in such systems is inherently complex due to interrelated dynamic stability challenges. These include: (1) stringent synchronization requirements between the SA recovery time and the cavity round-trip period, (2) sensitivity to pump source power fluctuations, (3) spectral-temporal distortions induced by higher-order dispersion effects, and (4) nonlinear interactions that exacerbate multi-pulse instabilities. Additionally, practical limitations arise from the SA damage threshold under high peak power conditions and the frequent inability to achieve self-starting operation without external perturbations. These compounded factors necessitate careful cavity design and material selection to ensure robust ultrashort pulse generation.

2.3.1 Harmonic Mode-Locking (HML)

In 1997, Grudinin et al. theoretically and experimentally investigated passive harmonic mode-locking in soliton fiber lasers (Grudinin et al., 1997). They noted that

Universiti Malaya

soliton pulses and non-soliton components make up the output radiation of soliton fiber lasers. The ratio of stored intracavity energy to soliton energy determines the number of circulating pulses. The non-soliton component, which serves as a buffer, is created because of the non-integer ratio. An almost uniform distribution of pulses occurs in the cavity as a consequence of the contact force being repulsive for a specific phase difference between solitons and the non-soliton component. However, given other specific phase difference requirements, repulsive force may also lead to a non-uniform pulse distribution. This demonstrated that when the pump power is raised to a greater level, a fiber laser may generate many light pulses inside its cavity. The long-range interaction of pulses via the acoustic wave (AW), the non-soliton component (i.e., the dispersive wave (DW) or CW) of radiation in the cavity, and the gain depletion and recovery (GDR) process are the root causes of the HML produced in passively mode-locked lasers. (Liu et al., 2019). Mode-locked lasers have shown the passive HML phenomenon in a broad range of theoretical and practical settings (Dianov et al., 1992; Sobon et al., 2011). Liu et al. (2019) revealed that the whole process of HML buildup successively undergoes seven different ultrafast phases: raised relaxation oscillation, spectral beating behavior, birth of a giant pulse, self-phase-modulation-induced instability, pulse splitting, repulsion and separation of multiple pulses, and stable HML state.

A 285th HML laser was reported in 1993 (Grudinin et al., 1993). In recent years, more and more HML phenomenon is reported in the generation of dark pulse or bright-dark pulse pairs. Lin et al. (2014) presented the generation of up to 8th order of HML dark square pulses by incorporating the graphene-oxide saturable absorber (GOSA); Tiu et al. (2014) exploited the nonlinear polarization rotation (NPR) technique to generate HML dark pulses up to 4th harmonic order; Zhang et al. (2019) generated maximum 8th

harmonic order in a bidirectional EDFL ring cavity using a short segment of Thulium-doped fiber (TDF) as the FSA.

2.4 Dark Solitons

A soliton is a self-reinforcing solitary wave that maintains its shape and travels at a constant speed, as first discovered by John Scott Russell in 1844 (Russell, 1844). In laser systems where dispersion components dominate, soliton formation is primarily governed by the Nonlinear Schrödinger Equation (NLSE), as noted by Hasegawa and Tappert (Hasegawa et al., 1973, 1973). Typically, bright solitons emerge in anomalous dispersion, while dark solitons arise in normal dispersion conditions. However, it has been observed that dark solitons can be generated not only by the NLSE but also through mechanisms such as the Cubic-Quintic Nonlinear Schrödinger Equation (CQNLSE) and DW techniques. The upcoming subsections will delve into these three typical dark soliton generation methods, providing theoretical insights, explanations, and reviews of previous research.

2.4.1 NLSE Dark Soliton

In the context of laser pulse transmission through a single-mode fiber, the propagation can be described by an extended NLSE when both the dispersion length (L_D) and nonlinear length (L_{NL}) in the system exceed the cavity length. These lengths are defined as follows (Tiu et al., 2022):

$$L_D = {T_0^2}/{\beta_2}, \tag{2.5}$$

$$L_{NL} = {}^{1}/_{\gamma P_0}, \tag{2.6}$$

here, T_0 represents the RMS value of the pulse width in intensity, and β_2 denotes the group velocity dispersion (GVD) or second order dispersion. Anomalous dispersion occurs when $\beta_2 < 0$, while normal dispersion is indicated by $\beta_2 > 0$. The nonlinear coefficient is denoted by γ, and P_0 represents the peak power of the optical pulse. A represents the slowly varying envelope of the optical pulse. The NLSE governing bright and dark pulse formations is expressed as (Hasegawa et al., 1973, 1973):

$$\frac{\partial A}{\partial z} = -i\frac{\beta_2}{2}\frac{\partial^2 A}{\partial t^2} + i\gamma|A|^2 A \tag{2.7}$$

Bright soliton formation under anomalous dispersion ($\beta_2 < 0$) is described by (Lee et al., 2006):

$$A(z,t) = \sqrt{2\gamma}\eta \exp\{-4(\xi^2 - \eta^2)z - 2i\xi t + i\varphi\} \operatorname{sech}(2\eta(t - t_0) + 8\eta\xi z), \tag{2.8}$$

where η, ξ, φ, and t_0 are constants. On the other hand, dark soliton formation under normal dispersion ($\beta_2 > 0$) is given by (Zakharov et al., 1970):

$$A(z,t) = \sqrt{-\frac{2\gamma}{\gamma}\frac{(\lambda+iv)^2+\exp\{2v(t-t_0-2\lambda z)\}}{1+\exp\{2v(t-t_0-2\lambda z)\}}} \tag{2.9}$$

where $\lambda^2 + v^2 = 1$.

In Figure 2.5, the silica optical fiber exhibits both normal and anomalous dispersion characteristics, with a transition point occurring around ~1330 nm (Kharazi et al., 2012). This property makes it suitable for use as an optical waveguide in fiber laser cavities operating in the near-infrared and mid-infrared regions below 2000 nm. Consequently, the GVD or group delay dispersion (GDD) within the fiber laser cavity is primarily

Universiti Malaya

governed by the intra-cavity SMF. For fiber lasers operating above 1330 nm, such as EDFLs, bright pulses can be generated in anomalous dispersion regions without the need for additional dispersion control fibers like dispersion compensating fiber (DCF) or dispersion shifted fiber (DSF). On the other hand, the setup for generating NLSE dark solitons, whether at wavelengths below or above 1330 nm, differs significantly. Below 1330 nm, the typical experimental setup involves inserting artificial SAs or material type of natural SAs into Ytterbium-doped fiber laser (YDFL) cavities. These cavities exhibit normal dispersion as Ytterbium-doped fiber (YDF) emits around 1064 nm.

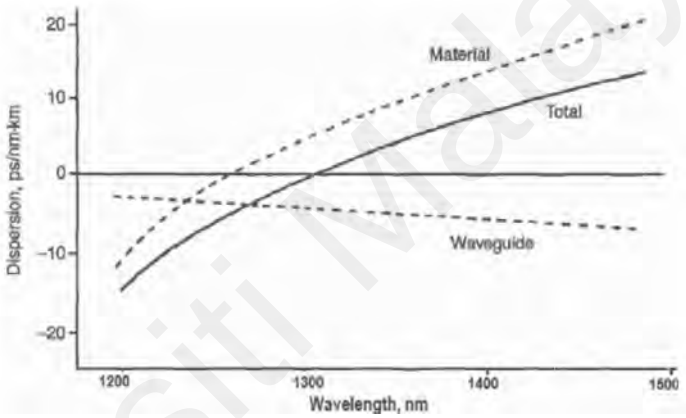

Figure 2.5 Dispersion vs. Wavelength in SMF (Kharazi et al., 2012).

Figure 2.6 (a) illustrates the configuration of a YDFL employing a GOSA for the generation of both bright and harmonic dark square pulses. Lin et al. (2014) devised and implemented this fiber laser within a ring cavity setup. The laser diode operates as the pump source, emitting light at a wavelength of 976 nm. A 976/1064 nm Wavelength Division Multiplexer (WDM) facilitates the coupling of the pump light into the YDF. To control the intra-cavity polarization state, a polarization controller (PC) is employed, while an isolator ensures unidirectional propagation of light. An optical coupler is incorporated to provide an output tap for monitoring and measurement purposes.

The experimental observations revealed the generation of bright pulses at a pump power of 200 mW (Figure 2.6 (b)). However, at a significantly higher pump power of 450 mW, dark square pulses were obtained. Furthermore, the authors observed the HML behavior of dark pulses as the pump power increased, reaching a threshold of 600 mW. They adjusted the PC in various orientation combinations to achieve this effect. The width of the dark square pulses exhibited a decreasing trend from 90.8 ns to 42.05 ns with increasing pump power between 450 mW and 600 mW, as depicted in Figure 2.6 (c). Additionally, an intriguing phenomenon known as dark pulse bunches was observed at the maximum power of 600 mW as shown in Figure 2.7 (a)-(f). Here, two, three, or four dark pulses coexisted within a single round-trip time, further highlighting the complexity and versatility of the system.

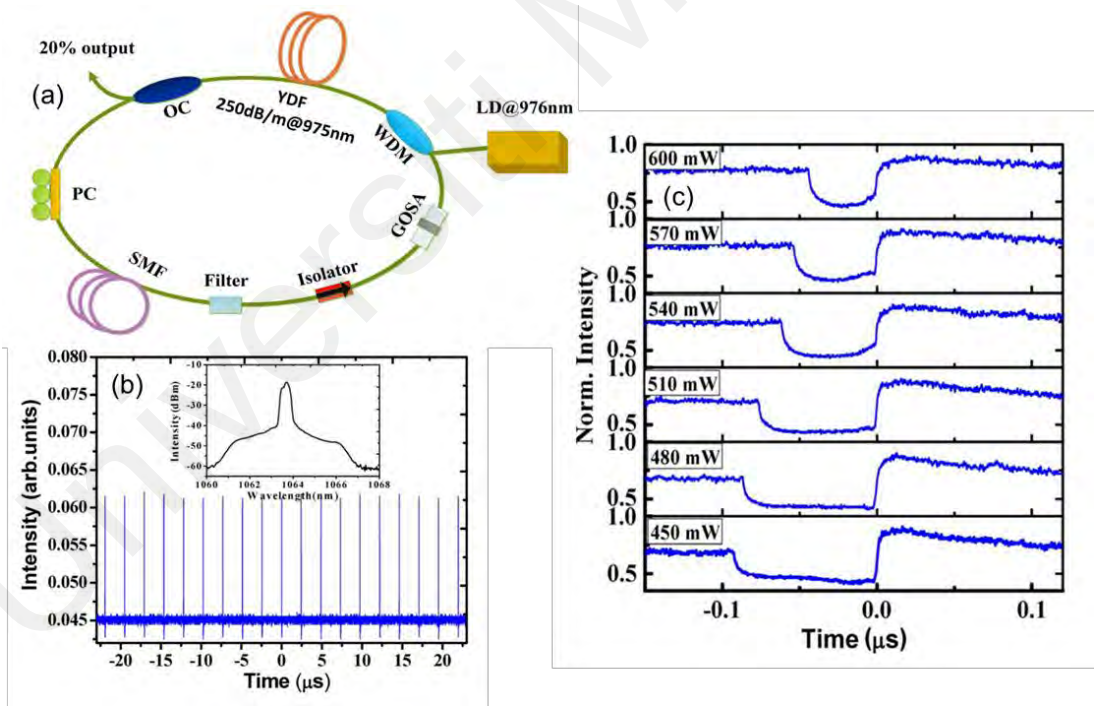

Figure 2.6 (a) Configuration of ring YDFL using GO as SA, (b) Pulse train of the bright pulse (inset shows the corresponding output spectrum), and (c) The evolution of the dark pulse width at different pump powers (Lin et al., 2014).

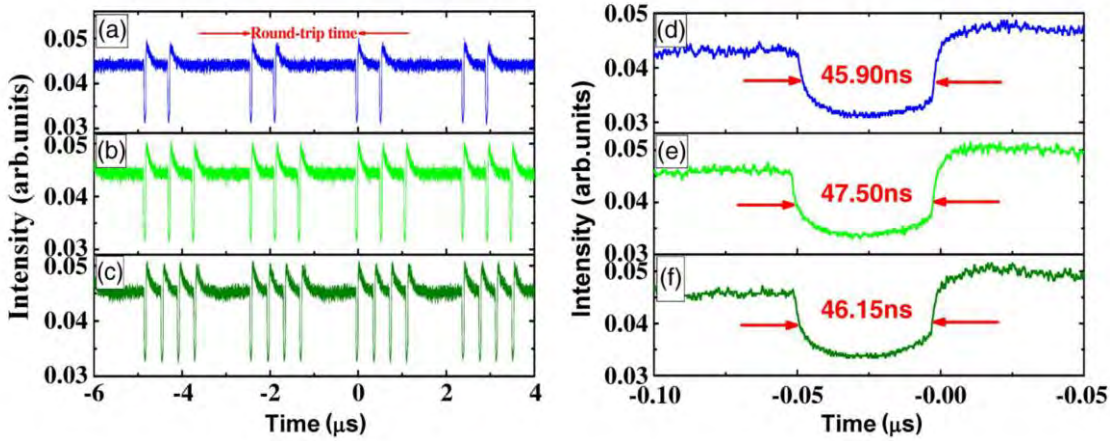

Figure 2.7 (a)-(c) The dark square pulse bunches consist of 2, 3, and 4 dark pulses in a round-trip time, (d)-(f) Corresponding single dark pulse width of different bunches (Lin et al., 2014).

As previously discussed, generating NLSE dark pulses above 1330 nm typically involves compensating for the anomalous dispersion of SMF by inserting a DCF or DSF spool. In another study by Tiu et al. (2014), multiwavelength NLSE dark pulses were generated using NPR technique within an EDFL cavity. This setup included an additional 6.9 km DCF and a 50 m photonic crystal fiber (PCF), as depicted in Figure 2.7. A 1480 nm laser diode pumped the EDF to create a population inversion for laser generation in 1.55-micron region.

Universiti Malaya

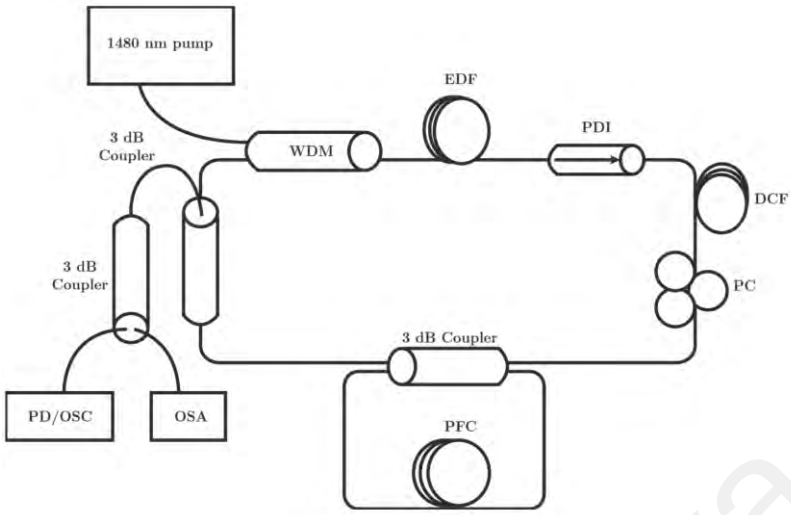

Figure 2.8 Schematic diagram of the EDFL for generating multiwavelength NLSE dark pulses (Tiu et al., 2014).

The multiwavelength operation was facilitated by the NPR technique and a Sagnac loop, which comprised a 50:50 coupler and a spool of PCF. Multiwavelength operation commenced at a pump power of 24 mW and continued until reaching the maximum pump power of 145 mW. As the pump power increased from 24 mW to 145 mW, the number of lines in the optical spectrum output and the output power also increased. Figure 2.8 illustrates that at least 9 lines were obtained in the optical spectra, with a free spectral range (FSR) of approximately 0.47 nm.

In the temporal domain, oscilloscope traces of NLSE dark pulses were acquired when the pump power exceeded 133 mW. The fundamental repetition rate was measured at 29 kHz, with a pulse width of 2.7 µs. As the pump power increased and the PC was adjusted, 2nd, 3rd, and 4th harmonic dark pulses were observed. Figure 2.8 demonstrates the harmonic dark pulse output spectra along with the corresponding pulse train.

Universiti Malaya

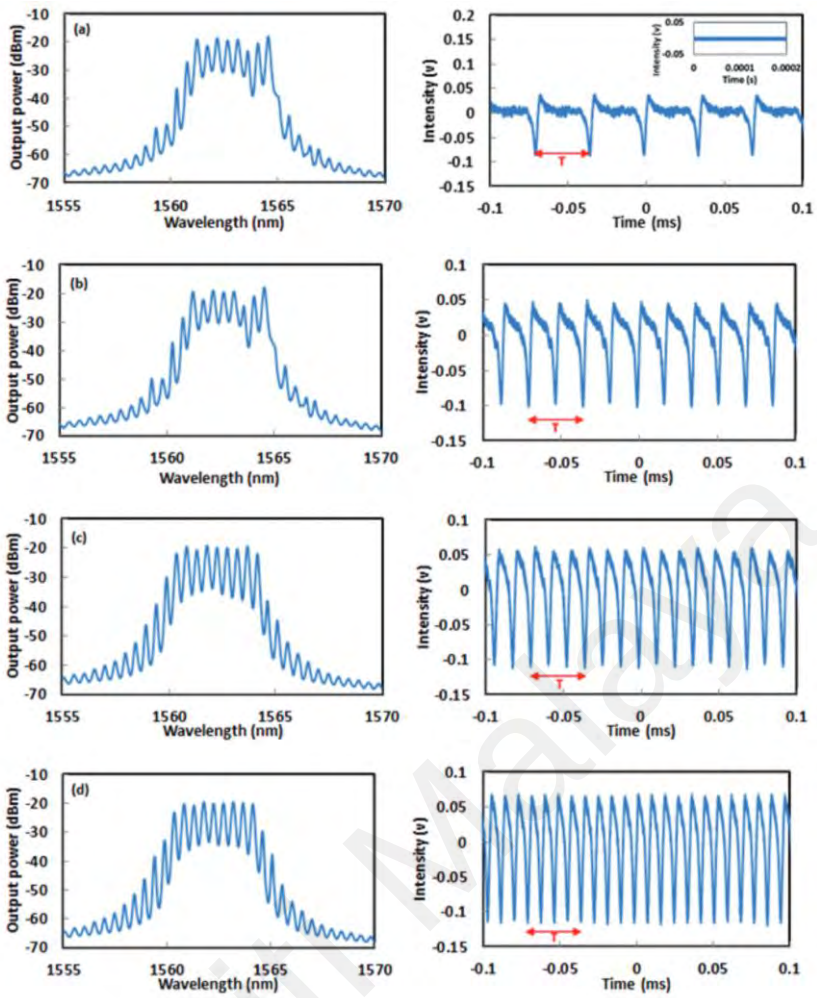

Figure 2.9 Output spectra and the corresponding oscilloscope traces of (a) Fundamental harmonic, (b) 2nd-order harmonic, (c) 3rd-order harmonic, (4) 4th-order harmonic NLSE dark pulses (Tiu et al., 2014).

2.4.2 CQNLSE Dark Soliton

As outlined in the preceding section, the formation of NLSE solitons arises from the interplay between GVD and Kerr nonlinearity. The Kerr effect can be expressed as follows (Keller, 2021):

$$n = n_0 + n_2|\mathbf{E}|^2 + n_4|\mathbf{E}|^4, \tag{2.10}$$

here, n represents the total refractive index, n_0 denotes the linear refractive index, n_2 signifies the first-order Kerr nonlinear coefficient, n_4 represents the second order Kerr nonlinear coefficient, and $|E|$ is the magnitude of the electric field. Considering the relationship between the electric field $|E|$ and light intensity I (Keller, 2021):

$$I \propto |E|^2 \tag{2.11}$$

We can express n as (Keller, 2021):

$$n = n_0 + n_2 I + n_4 I^2 \tag{2.12}$$

Hence, it is evident that higher-order Kerr nonlinearity cannot be disregarded when the light intensity becomes sufficiently strong. The second and fourth-order Kerr nonlinear coefficients are directly proportional to the third and fifth-order nonlinear susceptibilities χ^3 and χ^5 (Tiu et al., 2022):

$$n_2 = \frac{3\chi^3}{8n_0}, \tag{2.13}$$

$$n_4 = \frac{5\chi^5}{32n_0} \tag{2.14}$$

In scenarios of intense light intensity, considerations of third order and particularly fifth-order nonlinear susceptibilities become pertinent in the formation of dark pulses. Consequently, a specific solution, known as the CQNLSE, emerges. When a spool of High Nonlinear Fiber (HNLF) is inserted into the fiber laser cavity, significantly enhancing the nonlinearity in the system, realization of CQNLSE dark solitons becomes feasible in both anomalous and normal dispersion laser systems.

Universiti Malaya

YANG et al. (2005) and Arshad et al. (2017) conducted theoretical analyses of the CQNLSE, laying the groundwork for understanding its properties and behavior. Subsequently, experimental validation was provided by Tiu et al. (2015), who demonstrated CQNLSE dark solitons by incorporating a 100 m long HNLF into the laser cavity. In their experiment, the total cavity length was approximately 130 m, and the EDFL operated within the anomalous dispersion region. The proposed schematic diagram of the cavity is depicted in Figure 2.10. Measurements yielded a pulse width of 219 ns and a fundamental repetition rate of 1.52 MHz. Figure 2.11 (a)-(c) illustrate the corresponding oscilloscope trace, output spectrum, and Radio Frequency (RF) spectrum, respectively, providing a comprehensive overview of the experimentally observed CQNLSE dark soliton behavior.

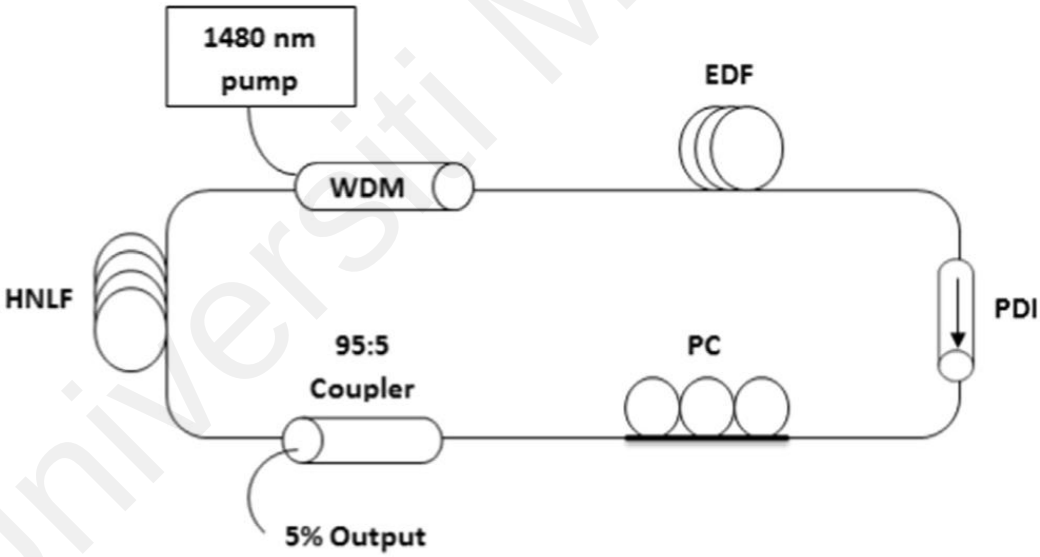

Figure 2.10 Schematic diagram of the EDFL producing CQNLSE dark pulse (Tiu et al., 2015).

Universiti Malaya

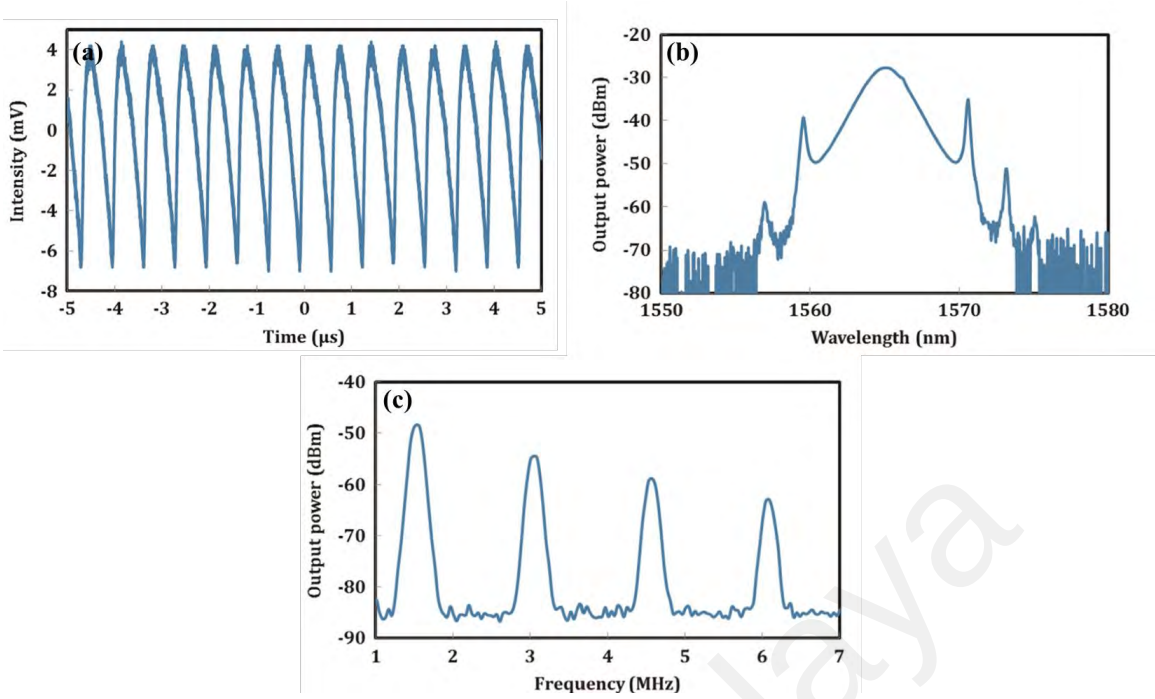

Figure 2.11 (a) CQNLSE dark pulse train, (b) output spectrum, and (c) RF spectrum (Tiu et al., 2015).

2.4.3 DW Dark Solitons

Apart from NLSE and CQNLSE dark solitons, DW solitons have also garnered significant attention since their discovery. A DW represents a topological defect acting as a structural entity that connects two stable and static states within a physical system. The theoretical prediction of the existence of stable optical domain walls was first proposed by Zakharov et al. (1987). They emphasized that the formation of optical domain walls arises from the interactions between two counter-propagating electromagnetic waves and is entirely unaffected by dispersion. This interaction in a third-order nonlinear medium leads to the creation of polarization DW solitons.

In the context of optical fibers, Wabnitz et al. (1993) theoretically predicted that polarization switching could generate DW solitons. Subsequently, Pitois et al. (1998)

experimentally validated this theory. Additionally, another type of DW soliton known as dual-wavelength DW solitons has been studied (Wang et al., 2017; Zhang et al., 2011). Dual-wavelength DW solitons consist of two components with different center wavelengths. The interaction between optical waves of these two distinct wavelengths gives rise to a topological defect in the temporal domain, resulting in the establishment of localized intensity minima, which constitutes the dark pulse. Due to the birefringent characteristics of optical fibers, light propagating inside typical SMFs can be decomposed into two orthogonal polarization modes. Incoherent polarization mode coupling can then lead to the formation of DW solitons (Zhang et al., 2008; Zhao et al., 2008).

Theoretically, domain walls exhibit kinks, and by applying Bäcklund transformation to NLSE, single-kink solitons can be derived, as described by (Boiti et al., 1982):

$$A(z,t) = 2\sigma \tanh\left[\sqrt{2}\sigma_0(t - t_0) + 4\xi_0 z\right] \exp\{i[-2\xi_0 t - 4(\sigma_0^2 + \xi_0^2)z - \theta_0]\}, \quad (2.15)$$

here, σ_0 and ξ_0 are two real parameters, and the real constants θ_0 and t_0 fix the location of the traveling wave at the initial time. Unlike the NLSE, DW solitons can exist in both anomalous and normal dispersion regimes. Additionally, DW solitons typically involve dual- or multi-wavelength operation in the spectral domain, distinguishing them from CQNLSE dark solitons.

DW solitons can be generated using both artificial and material SA. Zhang et al. (2011) proved dual-wavelength DW solitons by employing the NPR technique in an anomalous dispersion EDFL cavity. Figure 2.12 (a) shows the laser configuration. The dual-wavelength operation occurred at 1588.5 nm and 1591.0 nm, respectively (Figure 2.12 (b)). As the pump power increased from 0.25 W to 0.85 W, the duration of the dark pulse decreased from 4.5 ns to 1 ns (Figure 2.12 (c)). By altering the PC, and consequently

the birefringent filter, the bandpass wavelength changed, leading to different combinations of wavelength components (single wavelength and dual wavelength). Notably, no dark pulse was obtained when the laser system operated at a single wavelength. Then, a tunable bandpass filter (TBF) with a range from 1570 nm to 1610 nm was employed. By adjusting the filter, wavelength shifting was observed. Dark pulses consistently appeared at the position where the laser emission switched from one single wavelength to another. The work verified that the phenomenon of wavelength alternation is not only attributed to gain competition but to the incoherent coupling between the two polarization modes existing in the two orthogonal axes of the birefringent fibers. Under strong pump power, the pulse evolved into the type of dark pulse previously reported by Zhang et al. (2010), named dual-wavelength DW solitons.

In another study by Zhang et al. (2019), DW solitons were demonstrated using a different approach. A short segment of TDF was employed as the SA within a bidirectional EDFL cavity as depicted in Figure 2.13 (a). In this work, a polarization beam splitter was employed at the output port. The key observation in this study was the in-phase feature of the dark pulse train of the two orthogonal polarization components (Figures 2.13 (b) and (c)). This indicated that the formation of the DW soliton was primarily due to the mutual interaction of two counter-propagating beams and the intensity coupling of the bidirectional beams. The use of the polarization beam splitter facilitated the separation of the orthogonal polarization modes, allowing for a clearer observation and characterization of the DW soliton phenomenon.

Universiti Malaya

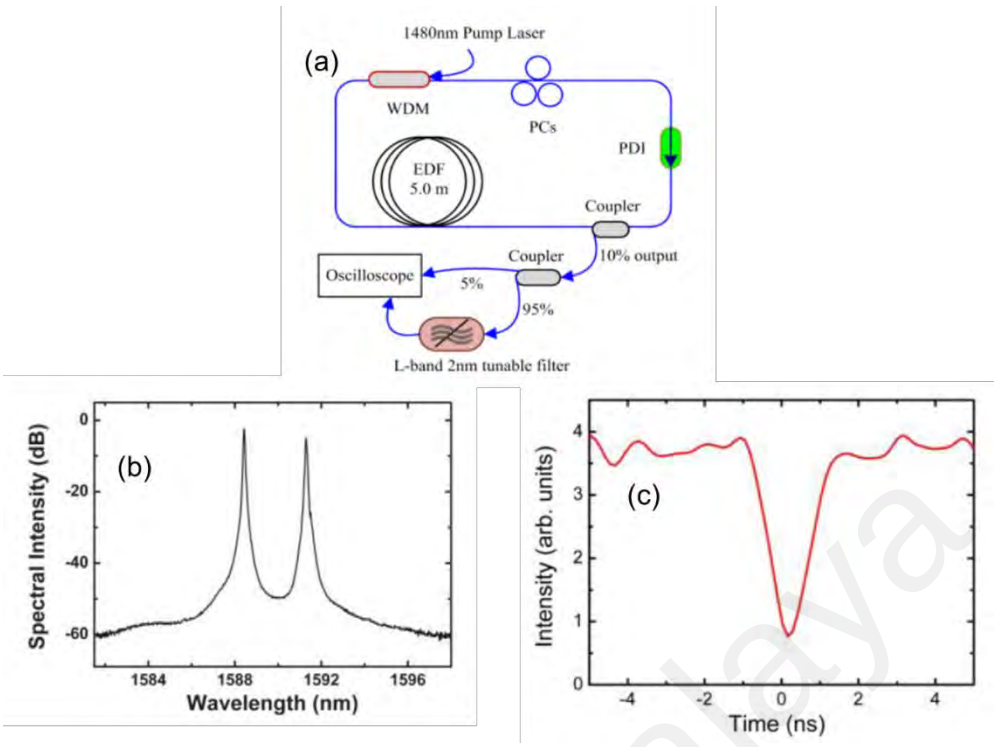

Figure 2.12 (a) EDFL cavity to generate DW solitons, (b) output spectrum, and (c) oscilloscope trace of the single dark pulse (Zhang et al., 2011).

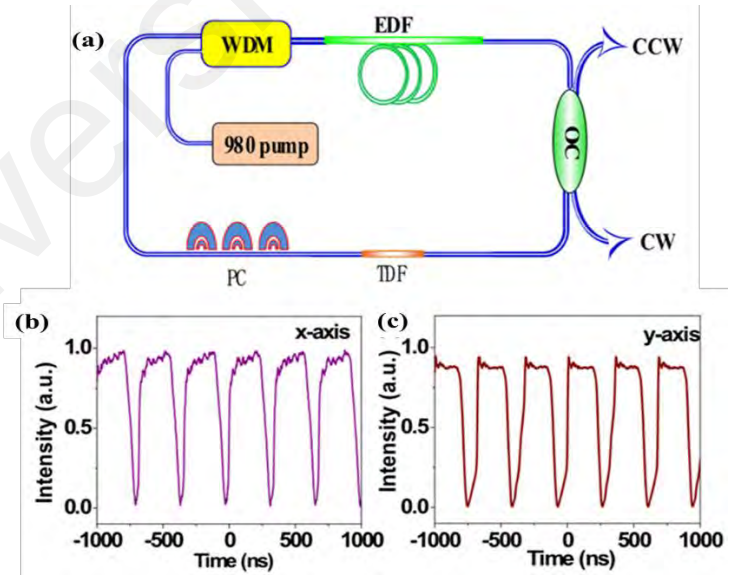

Figure 2.13 (a) Experimental setup for generating bidirectional DW dark soliton, (b) decomposed dark pulse trains in x orthogonal axis, and (c) y-axis (Zhang et al., 2019).

Universiti Malaya

2.5 Doped Fiber Based SAs

In the context of fast or ultrafast pulse generation, thin-film SAs have emerged as preferred options in various configurations. Utilizing one-dimensional (1-D) or two-dimensional (2-D) materials as SAs to generate dark pulses or dark-bright pulse pairs has been extensively studied (Ahmad et al., 2016; Lin et al., 2014; Wang et al., 2019). These thin, lightweight, and simple materials with good optical nonlinearity hold great potential for generating such pulses. However, material based or natural SAs often suffer from drawbacks such as low damage threshold, susceptibility to exposure to air, and instability caused by variations in material size and uniformity. On the other hand, artificial SAs like NPR and nonlinear amplifying loop mirror (NALM) are some of the earliest developed techniques to generate dark pulses (Tiu et al., 2014; Zhang et al., 2011; Zhang et al., 2009; Zhou et al., 2019). Nevertheless, these SAs are prone to disturbances by ambient temperature fluctuations (Silva et al., 2021).

FSAs have garnered significant interest as well. FSAs are fibers doped with rare earth elements such as erbium, thulium, ytterbium, holmium, samarium, etc. On one hand, these fibers serve as gain media in fiber laser schemes. Particles in such fibers are excited by photon energy, transitioning from the ground state to the upper state. Stimulated emission occurs when the following photon energy triggers the upper state particles to fall, emitting another photon energy. This process amplifies the light beam. When a piece of the doped fiber is placed into the laser cavity, low-intensity light causes stimulated emission. However, if the gain is less than the loss, the photon energy is briefly retained inside the fiber. When the light intensity increases to a threshold where the gain surpasses the loss, the stored energy is released in nanoseconds or sub-nanoseconds, dramatically increasing the light flux to form the pulse. This transmission, dependent on light intensity, is analogous to the role of SAs in the generation of Q-switching pulses. Moreover, by

Universiti Malaya

modulating the intra-cavity loss, FSAs can operate in the mode-locking regime. Benefiting from the all-fiber structure, FSAs have high damage thresholds, making them suitable for Q-switching pulse generation in high-power schemes, and they can usually hold large gain excited in the fiber from lasing (Tsai et al., 2010). Additionally, FSAs have the potential for mass production due to the established silicate optical fiber manufacturing industry.

Sanchez et al. (1993) discussed the self-pulsing phenomenon in EDF in specific erbium ion pair concentration. Tsai et al. (2010) proposed an all-fiber EDFL using TDF as the Q-switching SA. Tm^{3+} ions have a broad absorption and emission wavelength range 1.5 to 1.9 µm and 1.6 to 2.1 µm, respectively. The SA Q-switching criterion considering level degeneracy and mode-field-area (MFA) can be expressed as (Tsai et al., 2010):

$$C_q \equiv \frac{P_a A_g \sigma_a}{P_g A_a \sigma_g} > 1, P_a = 1 + g_a, P_g = 1 + g_g, \tag{2.16}$$

where g_a is $\frac{\sigma_e}{\sigma_a}$, g_a is $\frac{\sigma_a}{\sigma_e}$, and A_a and A_g are the MFA of the SA (or the gain fiber). C_q is the coupling ratio. In practice, considering the loss of the laser cavity, $C_q > 1.5$ is favored and then we have the relationship (Tsai et al., 2010):

$$\sigma_a \cong \left(1.5\sigma_g\right) \times \frac{P_g A_a}{P_a A_g}, \tag{2.17}$$

notably, the absorption cross section of Tm^{3+} (~3.5-4.5×10^{-21} cm^2) is larger than the emission cross section of Er^{3+} (~1×10^{-21} cm^2), makes TDF a suitable FSA to generate Q-switched and mode-locked pulses in the region of 1.55 µm.

Zhang et al. (2022) exploited the potential of a short segment TDF as the FSA to the generation of mode-locking ultrashort pulses in an all-fiber net anomalous dispersion

EDFL cavity, as shown in Figure 2.14 (a). The FSA was fabricated by a 12 cm long single-mode TDF. Figure 2.14 (b) depicts the FSA's nonlinear absorption profile, which reveals its capability as a mode-locker.

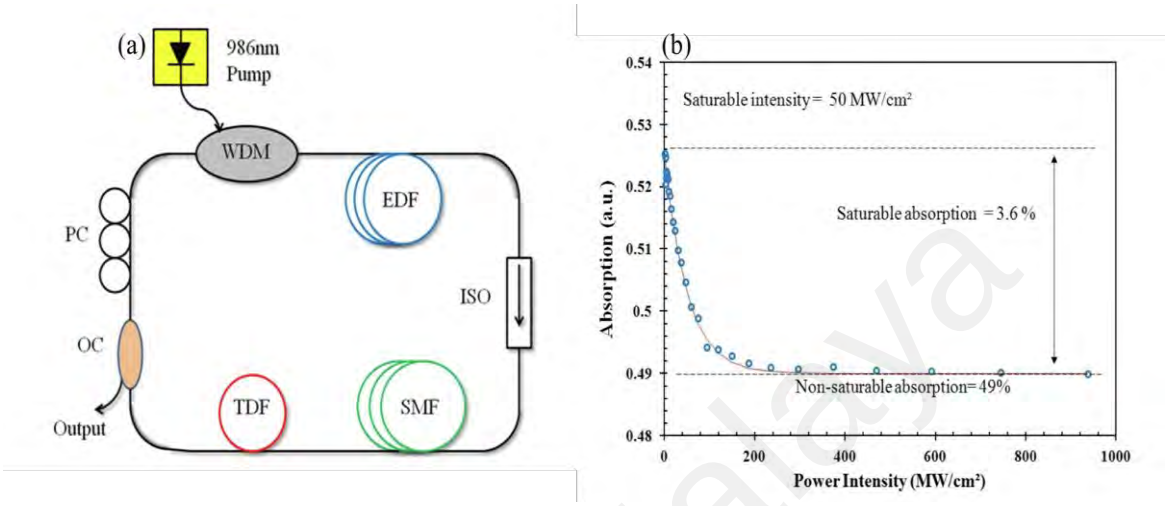

Figure 2.14 (a) Schematic of the EDFL. (b) nonlinear absorption profile of TDF FSA (Zhang et al., 2022).

The EDFL operated in CW mode in the beginning. Raised the pump power beyond 96 mW, the mode-locking operation was kicked in. The wavelength of the EDFL is centered at 1568.2 nm with a pulse width of 2.27 ps. The RF spectrum indicated that there was a constant repetition rate of 0.99 MHz during the mode-locking operation. The maximum peak power and pulse energy are calculated as 1.75 kW and 3.93nJ, respectively. The mode-locking operation had a very robust stability whose SNR was maintained at 63 dB. The wavelength spectrum, $Sech^2$ fit curve of mode-locked pulse shape, mode-locking pulse train, and RF spectrum are displayed in Figure 2.15 (a) – (d), respectively.

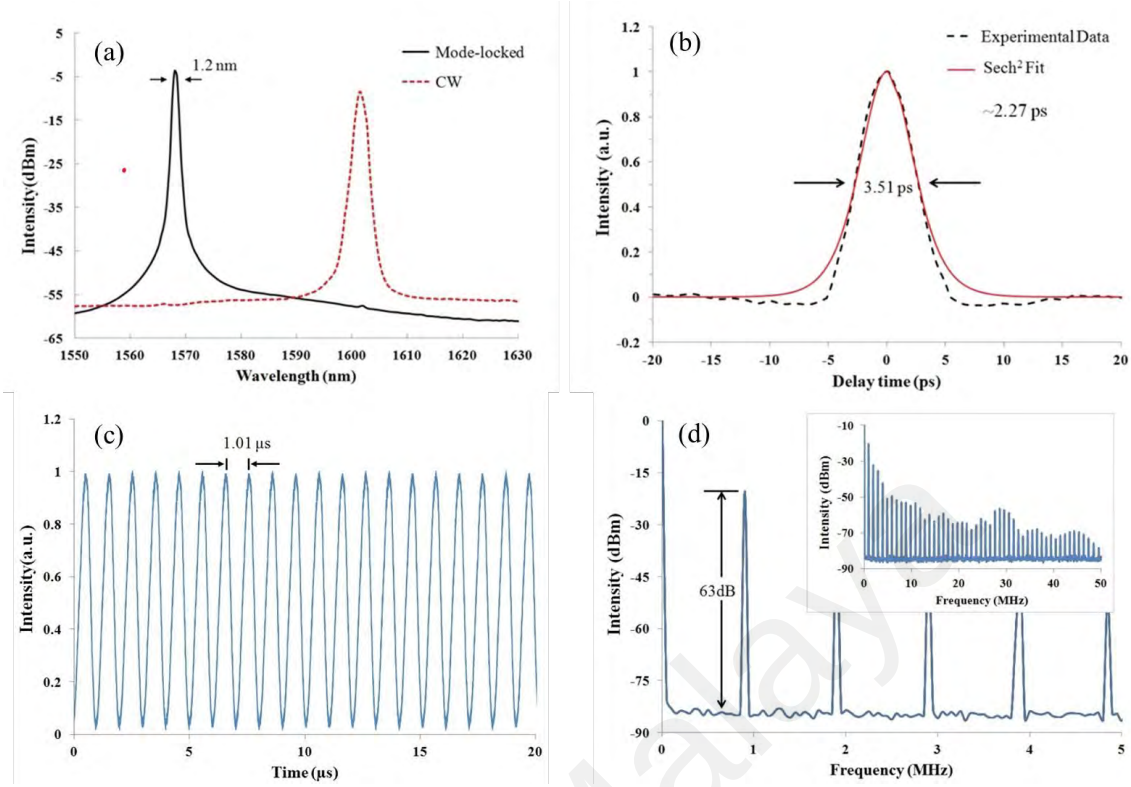

Figure 2.15 (a) Passively mode-locked and CW optical spectra of fiber lasers at pump power 178 mW. (b) Experimental data and Sech^2 fit curve of mode-locked pulse shape. (c) typical pulse train of fiber laser. (d) RF spectrum around the fundamental repetition rate, and the inset figure is the RF spectrum with high-order harmonic of the repetition rate (Zhang et al., 2022).

Once the pump power exceeded 178 mW, the EDFL was operated at combine mode. From the plumed part of the 3 dB linewidth of the wavelength spectrum and distorted bottom of the temporal pulse shape shown in Figure 2.16 (a) and (b), respectively, the author speculated that partially saturated FSA resulted in the adjacent longitudinal mode coupling contributing to the combine-mode phenomenon. In addition, RF spectrum in Figure 2.16 (c) manifests that there was an equidistant frequency interference between the lower-order harmonics due to the mutual coherence of different modes. What is more, a group of uniformly spaced frequency components was observed from RF spectrum,

which is caused by the intracavity and nonlinear interaction. As a result, the SNR of fundamental frequency dropped to approximately 50 dB.

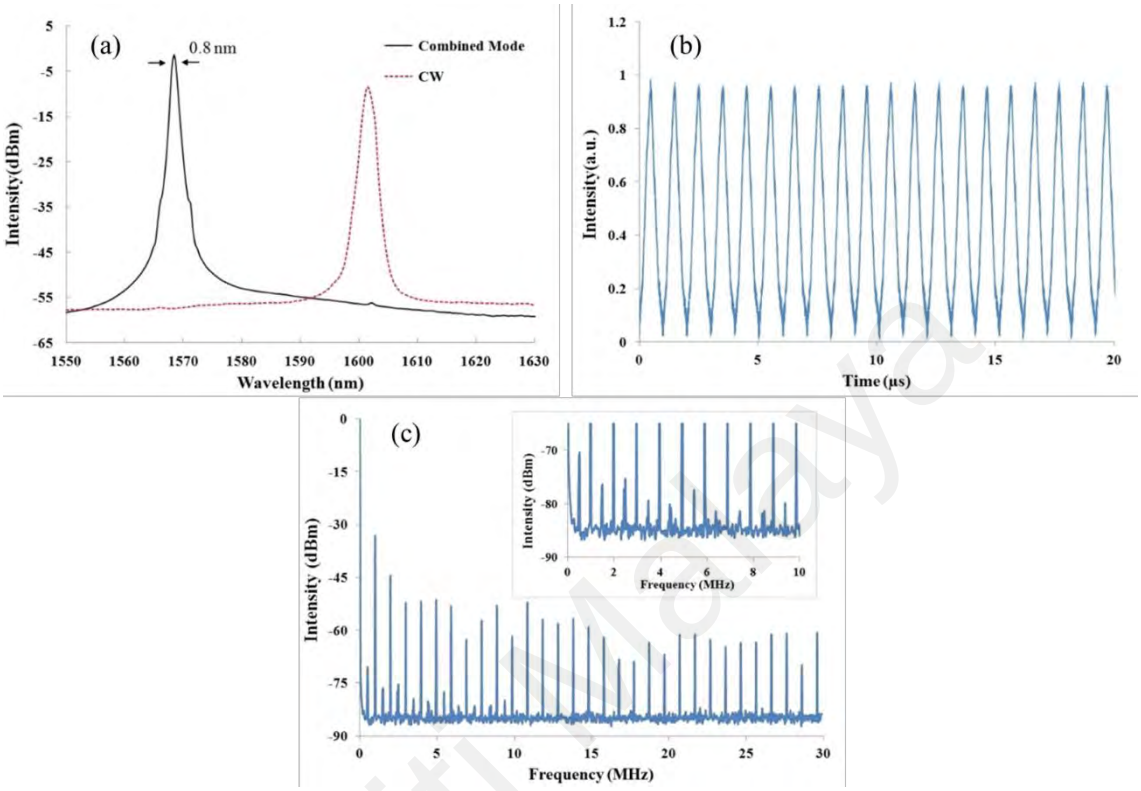

Figure 2.16 (a) Combined mode and CW optical spectra of the fiber laser. (b) The pulse train in combined mode operation. (c) RF spectrum with the span of 30 MHz and the inset figure is the RF spectrum with initial span of 10 MHz (Zhang et al., 2022).

2.6 MMI Interferometer Based SAs

Nazemosadat et al. (2013) presented a detailed investigation regarding the nonlinear multimodal interference in a short graded-index multimode fiber. Figure 2.17 depicts the behavior of the relative power transmission τ as a function of normalized nonlinear coefficient $\tilde{\gamma}$ for a fixed value of the normalized graded-index multimode fiber (GIMF) length $L = 4.5\pi$ in a SMF-GIMF-SMF configuration. For relative fundamental mode power $p_0 = 0.5, 0.25, 0.75$ at dimensionless longitudinal coordinate $\zeta = 0$, in solid,

dashed, and dotted lines. The value of L is chosen such that in the linear case, the relative power transmission is at its minimum value. For $p_0 = 0.5$, the relative power transmission increases from τ_{min} to $\tau_{max} \approx 1$ monotonically as $\tilde{\gamma}$ is increased from 0 to $\tilde{\gamma} = 0.75$. Beyond $\tilde{\gamma} = 0.75$, τ goes through a few low amplitude oscillations and saturates at $\tau_{max} = 1$. In essence, the SMF-GIMF-SMF structure exhibits minimal power transmission under low-intensity conditions, while demonstrating near-total transparency at higher power intensities. This behavior closely approximates the ideal characteristics of a SA, with the sole limitation in this simulation being that the minimum transmission value (τ_{min}) remains non-zero.

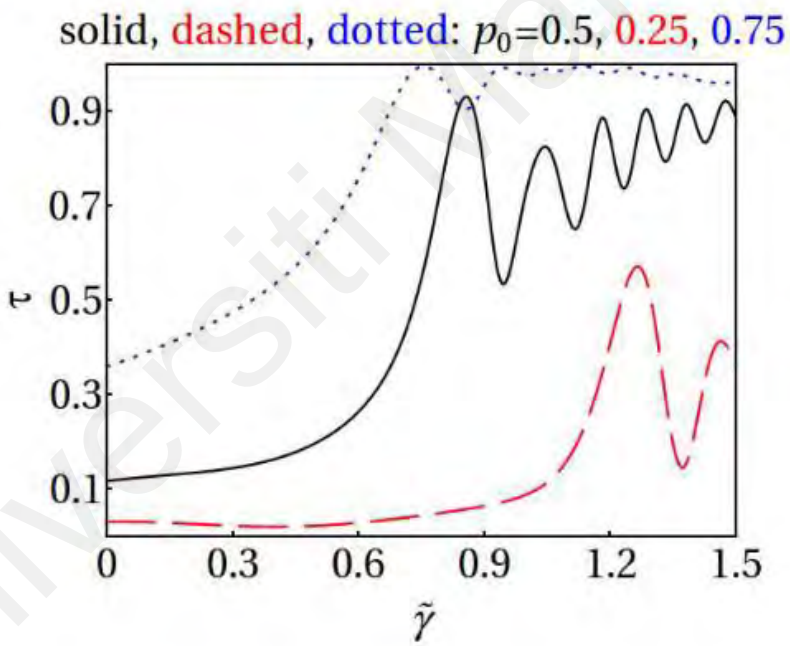

Figure 2.17 The relative power transmission is plotted as a function of $\tilde{\gamma}$ (thus the total power) for L = 4.5π for the case of five modes, when p_0 = 0.5, 0.25, 0.75 at ζ = 0, in solid, dashed, and dotted lines, respectively (Nazemosadat et al., 2013).

When the light propagates from SMF to MMF, multiple modes are excited in MMF due to MMF's intrinsic characteristic. Thereafter, the field distribution can be

decomposed into modes' modal function of multimode waveguide, as mentioned in equation 1.1 and consequently the different modes exist different phase velocities, and thus, the filed distribution of different modes along the MMF is governed by equation 1.2. Equation 1.2 can be expressed in terms of the phase difference between the fundamental mode and the excited higher order modes in the cylindrical coordinates (Fu et al., 2015):

$$E_{MM}(r,\varphi,z) = \exp(-j\beta_l z)\sum_{n=1}^{N} C_n e_n(r,\varphi,z)\exp[-j(\beta_n-\beta_l)z], \quad (2.18)$$

where β_l and β_n are the propagation constants of the fundamental mode and the nth excited higher mode modes inside MMF, respectively.

Self-imaging occurs in MMF when fulfill the condition (Fu et al., 2015):

$$(\beta_n-\beta_l)z_{Self-Imaging} = \Delta\beta_n z_{Self-Imaging} = m_n 2\pi, \quad (2.19)$$

where m_n is integer and $z_{Self-Imaging}$ is the position along MMF where self-imaging occurs.

When the length of the MMF segment L is chosen to allow self-imaging to occur at a certain wavelength, equation 2.19 can be rewritten as (Fu et al., 2015):

$$\Delta n_{eff,n} L = m_n \lambda_0, \quad (2.20)$$

where $\Delta n_{eff,n} = (\beta_n-\beta_l)\lambda_0/2\pi = n_{eff,n} - n_{eff,1}$ and m_n is integer.

Considering the optical Kerr effect, the effective refractive index depends on the light intensity and therefore equation 2.20 can be expressed as (Fu et al., 2015):

$$\Delta n_{eff,n}(I) L = m_n \lambda \quad (2.21)$$

Universiti Malaya

As a result, the wavelength of self-imagining at a high laser intensity can be described as below (Fu et al., 2015):

$$\lambda_{Self-Imagining} = \frac{\Delta n_{eff,n}(I_{High})}{\Delta n_{eff,n}(I_{Low})}\lambda_0, \tag{2.22}$$

where interpretation can be made from equation 2.21 and equation 2.22 that within the same MMF segment length L, the optical Kerr effect will modulate the self-imaging wavelength $\lambda_{Self-Imagining}$ in the MMF. As a result, the MMI device's transmission at a specific wavelength performs similarly to the SA, whose transmission increases as the input laser intensity increases. This is the fundamental process by which MMI devices function as the synthetic SA to generate Q-switching pulses.

Chen et al. (2024) utilized a 158 mm length of 105 µm core diameter step-index multimode fiber (SIMF) to fabricate the SMF-SIMF-SMF fiber device to incorporate into the EDFL to generate the Q-switching pulses. At maximum pump power of 343 mW, a maximum pulse repetition rate of 157.7 kHz, the shortest pulse width of 2.5 µs, a maximum output power of 2.35 mW, and a pulse energy of 15 nJ were recorded, respectively.

The unique interference pattern of the MMI devices can not only act as a Q-switcher or mode-locker but can be used to generate dark pulse. Aforementioned, The formation of DW dark pulses are relied on interaction of two or more lasing centered at different wavelengths to induce the topological defects in temporal domain (Tiu et al., 2022). The DW dark pulse production in a ring EDFL using the SMF-GIMF-SMF structure was described by Chen et al. The interplay between MMI device's interference and the filtering effect of the PC merges as the artificial SA with the aid of dark pulse development. Figure 2.17 (a) shows the laser cavity configuration. The dark pulse was

Universiti Malaya

stable when the pump power was between 97 and 195.4 mW. The pulse width and repetition rate were reported as 5 ns and 21.5 MHz, respectively. As seen in Figure 2.17 (b), the wavelength spectrum remained consistent throughout the DW dark pulse regime, whereas the dual wavelength peaks, located at 1567.2 nm and 1569.4 nm.

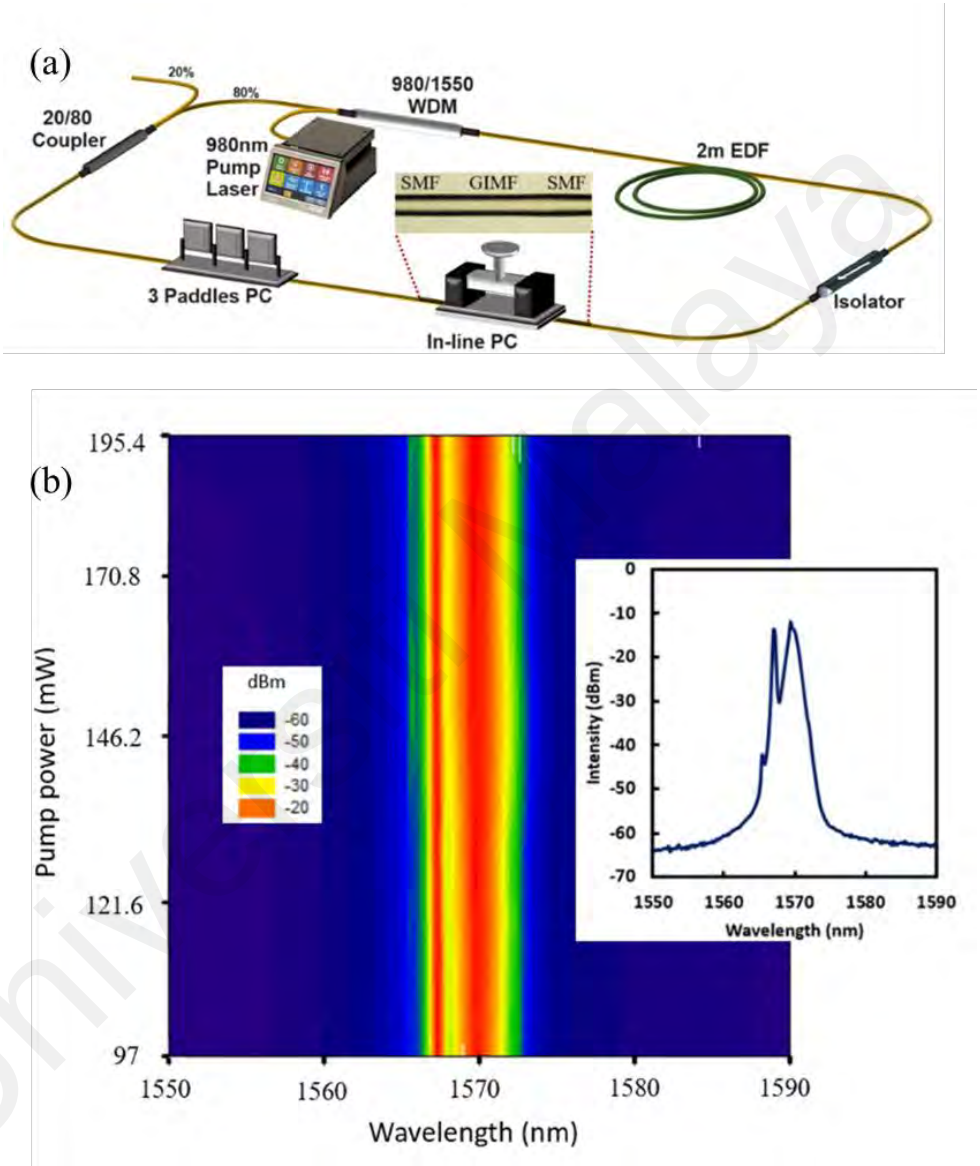

Figure 2.18 (a) Experimental setup of the DW dark pulse EDFL. (b) Wavelength domain of DW dark pulse throughout the operating pump power range. Inset figure is the optical spectrum at pump power of 195.4 mW (Chen et al., 2024).

2.7 Summary

In Chapter 2, a general introduction to fiber lasers is provided, with particular emphasis on the energy transition mechanisms in EDF and EYDF. The subsequent section delves into Q-switching and mode-locking techniques, covering their fundamental principles, classifications, and key characteristics. Following this, three aspects of dark pulses are reviewed and discussed, including an overview of reported methods for generating various types of dark pulses. Additionally, the saturable absorption mechanism of FSA is explored. Finally, the use of MMI spectral filter as SAs is discussed in detail, supported by theoretical equations and references to relevant literature.

Universiti Malaya

CHAPTER 3: PASSIVE Q-SWITCHING INDUCED BY THE KERR EFFECT OF INTERFERENCE FILTERS

3.1 Introduction

Fiber lasers are attractive for many applications owing to their excellent combination of high efficiency and spatial beam quality (Shiner, 2016; Zervas et al., 2014). They are also more dependable, require less maintenance and are more compact than those of other types of lasers. Cladding pumping scheme is commonly used to realize high power fiber laser. It uses cheap high-power diodes to excite rare-earth ions doped into the core via inner cladding of the double-clad fiber. Recently, many works have been focused on Q-switched fiber lasers to produce short and high energy pulses by modulating the cavity loss (Ghafar et al., 2022; Soboh et al., 2021). These pulses are useful in many applications including range finding, nonlinear frequency conversion, and remote sensing.

Up to date, numerous Q-switched fiber lasers have been reported using either active or passive methods. Active methods typically employ electro-optic and acousto-optic devices to modulate the intra-cavity losses (Cui et al., 2019; Zhang et al., 2021). On the other hand, the passive methods employ gain switching (Zenteno et al., 1989), various SA devices (Mirov et al., 2015; Popa et al., 2011; Wang et al., 2014), and other approaches. Passive techniques are desirable due to their merits of simplicity, compactness, simplicity, all-fiber format, and low cost. Therefore, up to now, many SA materials have been explored for Q-switching including SESAMs (Wang et al., 2014), transition metal-doped crystals (Mirov et al., 2015), graphene (Popa et al., 2011), CNTs (Ahmed et al., 2015), transition metal dichalcogenide (Wei et al., 2021) and rare-earth-doped fibers (Rahman et al., 2018). However, SESAMs, transition-metal-doped crystals,

Universiti Malaya

CNTs, and rare-earth doped fibers have a narrow operating region due to their limited absorption bands. Graphene and transition metal dichalcogenide have a broader operating wavelength range, but they require complicated fabrication processes and exhibit low optical damage threshold.

Alternatively, the nonlinear effect in the optical fiber-based laser cavity could also be used to generate Q-switched pulses. In this chapter, we demonstrate a compact Q-switched Erbium-ytterbium co-doped fiber laser (EYDFL) with 222.2 kHz of repetition rate and 2.1 µs of full width at half maximum (FWHM) at an average output power of 500 mW. The Q-switched operation in the EYDFL was achieved due to a nonlinear effect induced modulation mechanism. It employed the Kerr-effect of MMI in a few modes double clad EYDF, which was deployed in the laser's linear cavity as the active medium. This approach has advantages of its inherently high optical damage threshold, wavelength independence and all-fiber setup.

3.2 Q-switched Laser Configuration

The schematic configuration of the Q-switched EYDFL is illustrated in Figure 3.1. A 975-nm multimode laser diode with maximum output power of 10 W served as the pump source to excite Yb^{3+} ions, enabling energy transfer to Er^{3+} ions via a cooperative upconversion mechanism for 1.5-µm band laser generation (Supe et al., 2021). A 3-meter segment of double-clad EYDF (Coherent MM-EYDF-10/125-XPH) was employed as the gain medium, the fiber supports few-mode operation around 1.5 µm region. The double clad EYDF has a peak core absorption of 106.7 dB/km at 1530 nm and a core/outer diameter of 10.5/125.4 µm. The cladding absorption is 2.95 dB/m at 915 nm. The pump light was coupled into the inner cladding of the EYDF through a commercial multimode pump combiner. A fiber Bragg grating (FBG) with a Bragg wavelength of 1552.3 nm (3-

dB bandwidth: 0.5 nm, reflectivity: >95%) constituted the linear cavity boundary to establish resonant feedback for laser oscillation. The other end of the EYDF was spliced to a passive single clad 6/125 µm SMF. As a result, a Fabry-Pérot resonator was formed between the FBG and the single clad SMF. The FBG used has a Bragg wavelength of 1552.3 nm, a reflectivity of 99.9%, and 3-dB bandwidth of 0.2 nm. The spectral and temporal laser signal was detected by an optical spectrum analyzer (OSA) (Yokogawa AQ6370D) and an InGaAs photodetector (Electro-Optics Technology, Inc: ET-3500), respectively. The photodetector was connected to a digital oscilloscope (GWINSTEK GDS-3352, 350 MHz) and radiofrequency (RF) spectrum analyzer (Anritsu MS2683A, 7.8 GHz) to characterize the pulse train in time and frequency domain, respectively. The optical power meter (Thorlabs: S415C) conducts laser power measurement. It is worth noting that no residual 975 nm pump was observed from OSA during the experiment. This proves that the pump light was fully absorbed in the gain medium.

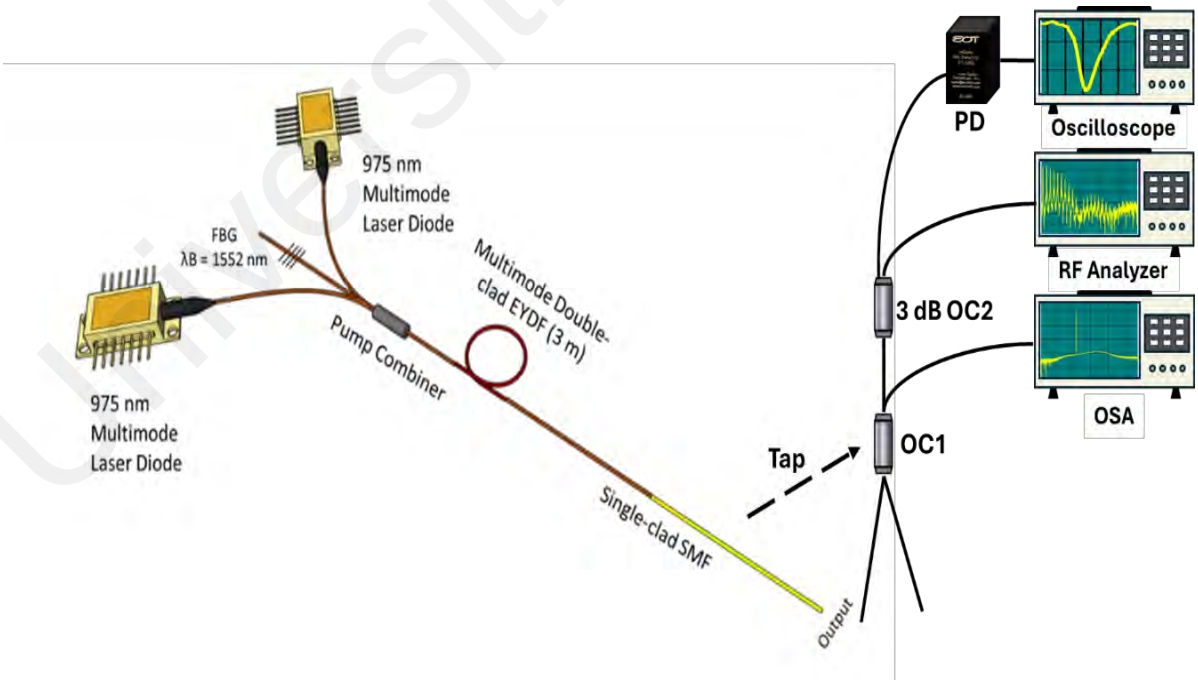

Figure 3.1 The schematic arrangement of the Q-switched EYDFL.

3.3 Laser Performance

The EYDFL started to generate stable Q-switched pulses at a pump power of 1 W. The stable pulses were maintained as the pump power rose to 3.09 W. However, as the pump power was further increased, the pulse train was diminished, and the laser operated in continuous-wave regime. The spectrum of the laser in logarithmic scale is illustrated in Figure 3.2(a). It is centered at 1552.3 nm with a 3dB spectrum width of 0.04 nm. Figure 3.2(b) showed the laser's pulse train at 3.09 W pump power. The output pulses are stable, and no noticeable intensity fluctuation captured in the oscilloscope trace. Figure 3.2(c) illustrates the RF spectrum of output laser at 1.00 W pump power. It shows the SNR of 42.8 dB at the fundamental frequency of 50.3 kHz. The laser also operated stable in the laboratory condition for 24 hours without any obvious degradation of performance.

Q-switching pulses were obtained due to employment of multimode EYDF, which formed SMS fiber structure in the EYDFL cavity. The SMS excited additional modes in the multimode waveguide as the single mode light was launched into the multimode fiber and caused the MMI to happen. Owing to the optical Kerr effect of MMI, the transmission of the oscillating light at 1552.3 nm through the SMS structure increases with increase of laser power density. Thus, it performs like a SA and the Q-switched laser operation can be achieved at this wavelength.

Universiti Malaya

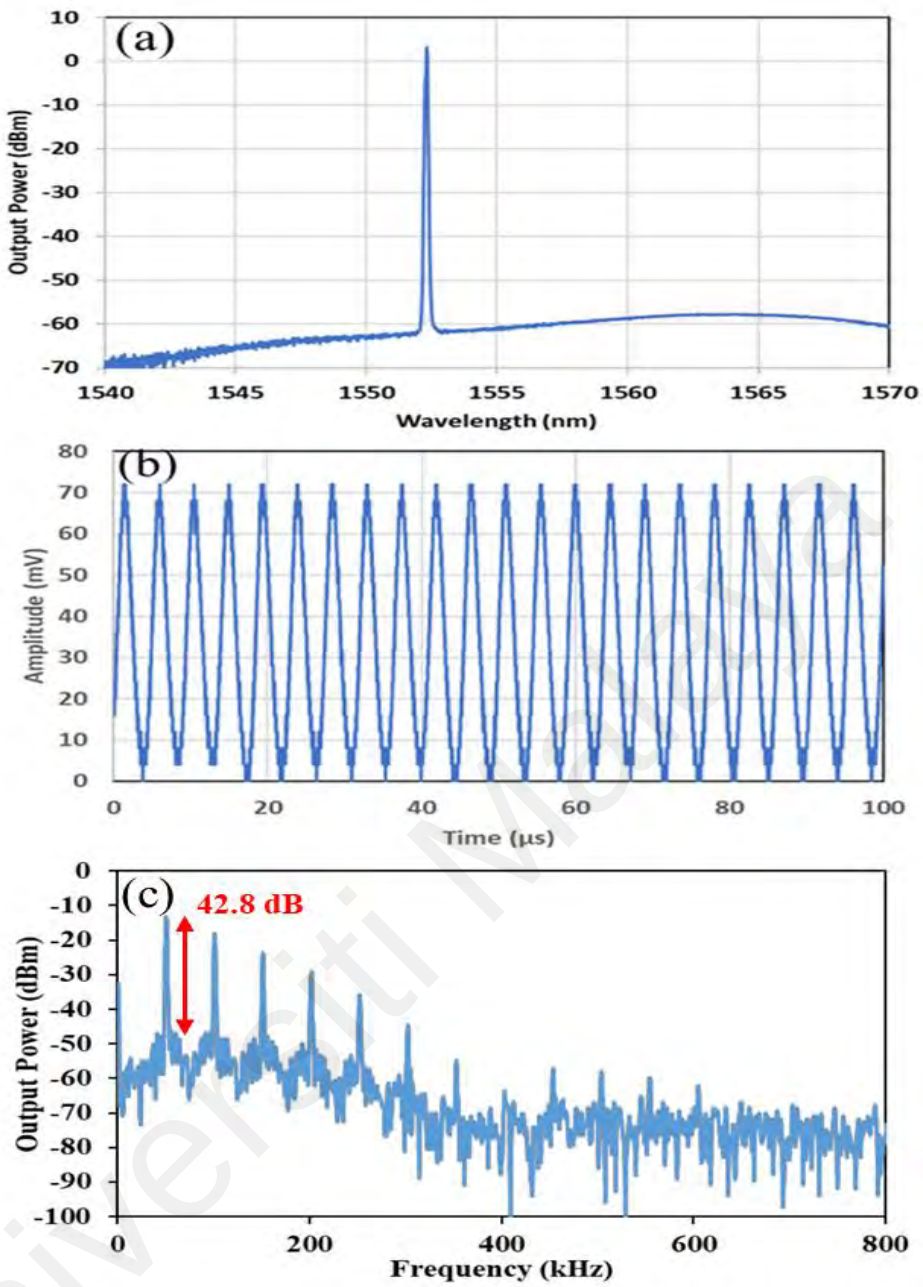

Figure 3.2 Q-switched laser characteristics (a) output spectrum (b) typical oscilloscope trace (c) RF spectrum.

The output power of the Q-switched pulses was measured as a function of the pump power using a power meter and the result is presented in Figure 3.3 (a). The output power linearly increased with the pump power and the slope efficiency was 10.35 %. A maximum output power of 500 mW was obtained at a pump power of 3.09 W for the

proposed Q-switched EYDFL. The pulse energy also rose from 1.0 to 2.7 μJ with the ascending pump from 1.00 to 2.42 W. However, the pulse energy reduces as the pump power is further increased due to sudden increase in the repetition rate due to the cavity noise. The cavity noise can be attributed to the sudden increase of the ASE due to the partial or full saturation of the SMS structure. Using OSA with a wide span from 1000 nm to 1600 nm will take a glance at the clear ASE background in the spectrum. The proposed method to mitigate the background noise is to increase the saturation intensity of the SMS structure. Future investigation will focus on leveraging the SMS structure maximum saturation intensity. Figure 3.3(b) presents the variation of repetition rate and pulse width at different pump powers. The pulse repetition rate increases from 50.3 kHz to 222.2 kHz with the ascending pump power from 1.00 to 3.09 W. Conversely, the FWHM decreases from 4.1 to 2.1 μs owing to the gain compression that occurs in the laser cavity as the pump power is increased. This behavior is typical for a Q-switched fiber laser.

Universiti Malaya

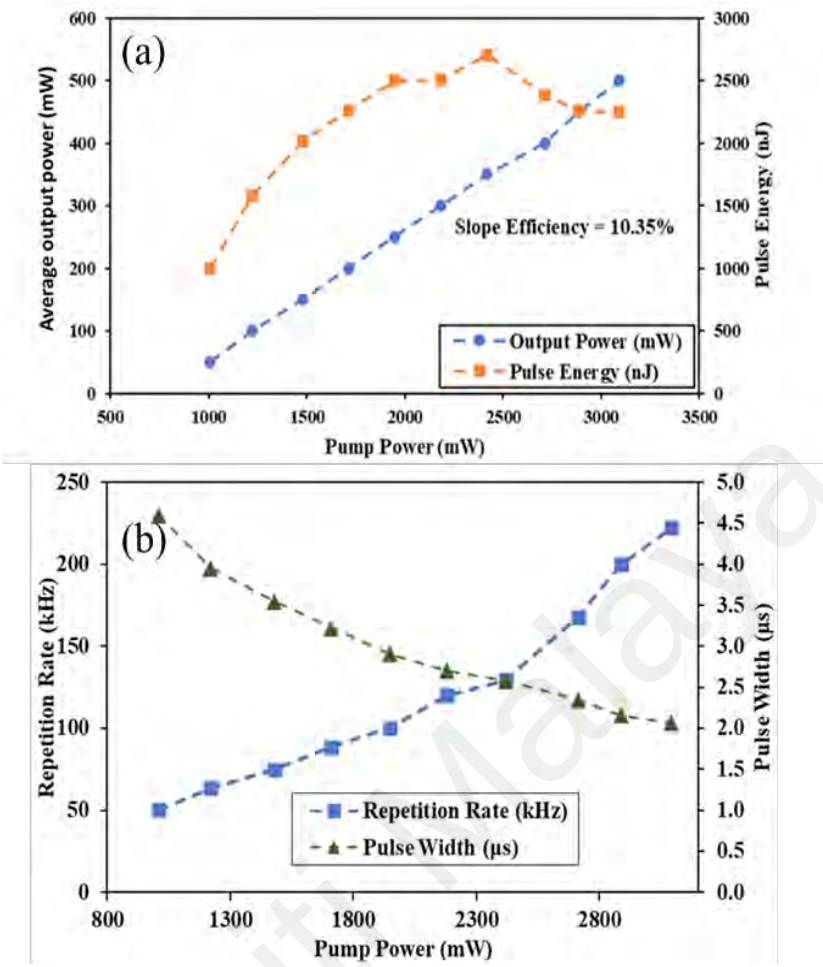

Figure 3.3 : The Q-switched laser performance at various launched pump power (a) Measured average output power and pulse energy (b) Repetition and pulse width versus input pump power.

The Q-switching generation observed in this work could also be ascribed to relaxation oscillations in the laser cavity with a segment of unexcited fiber owing to excessive EYDF length. As a 975 nm pump laser light is launched into the EYDF, it generates the population inversion necessary for the stimulated emission process of the EYDF. From another point of view, if an EDF is not under pump, it could modulate the laser light intensity and thus might behave as a slow SA to initiate Q-switching lasing. We have repeated the experiment with a shorter length of EYDF (2 m) to verify that the Q-

switching operation is due to the Kerr effect rather than the unexcited fiber segment. It is observed that the Q-switched laser was obtained within a pump power range from 1.71 and 2.45 and the unstable mode-locked pulses were observed as the pump power is further increased up to the maximum pump power of 3.09 W. Figures 3.4 (a) and (b) show the samples of Q-switched and mode-locked pulses, generated at pump power of 1.71 W and 2.75 W, which operated at repetition rate of 37.9 kHz and 111.1 MHz, respectively. These results indicate that the pulse generation was caused by multimode interference rather than the unexcited active fiber.

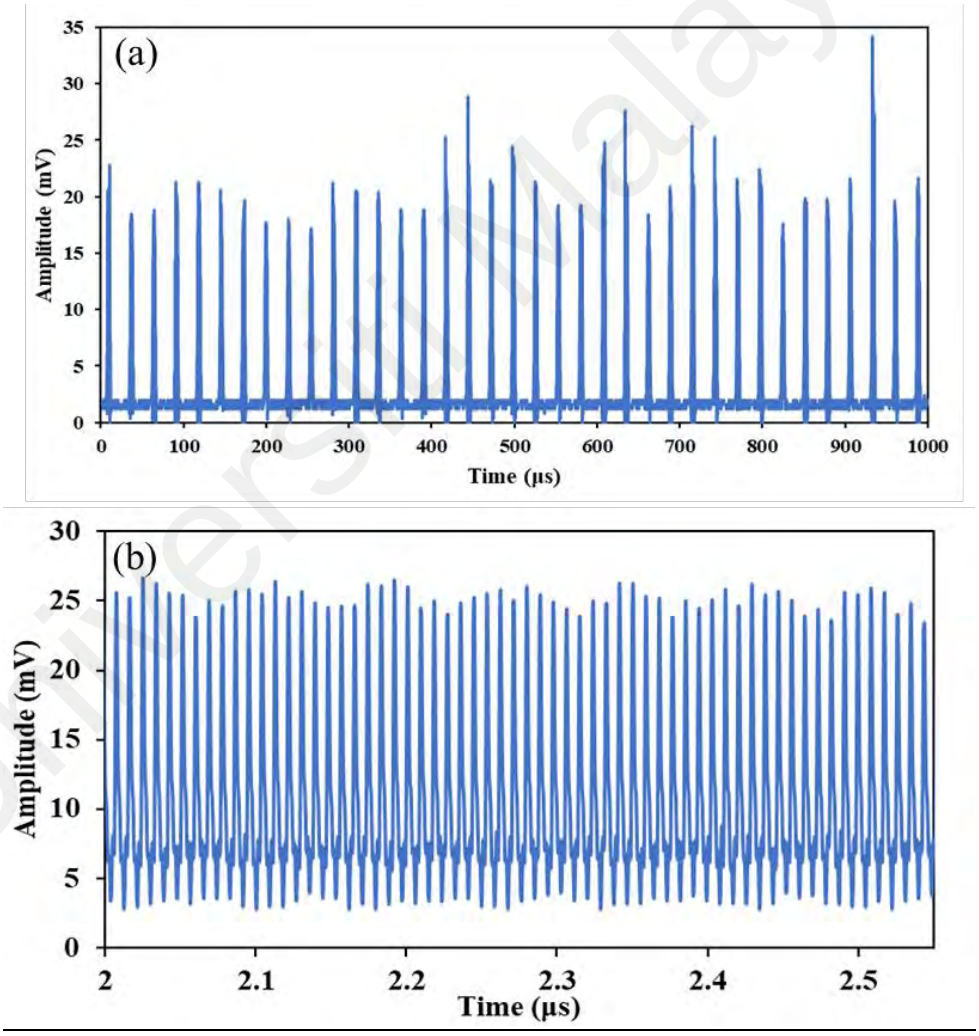

Figure 3.4 Typical pulse train obtained by the laser when EYDF is fixed at 2 m (a) Q-switched pulses at 1.71 W pump power (b) mode-locked pulse at 2.75 W pump power.

3.4 Summary

This chapter demonstrated a new Q-switching mechanism using the Kerr effect of MMI. A Q-switched fiber laser operating at 1552.3 nm was demonstrated using a multimode double-clad EYDF as a gain medium in a linear configuration. Stable Q-switched pulses were realized for pump powers from 1 W to 3.09 W. At a pump power of 3.09 W, the laser exhibited a maximum repetition rate of 222.2 kHz, and minimum pulse width of 2.1 μs. The maximum pulse energy of 2.7 μJ was recorded at pump power of 2.42 W. This new Q-switching mechanism could be deployed to produce short pulse in all-fiber laser configuration at any wavelength region.

Table 1 provides a comparative analysis of the findings of this study with other reported works in the field. The results clearly indicate that this work outperforms previous studies in several key metrics, including average power, repetition rate, and single pulse energy. However, it is worth noting that the SNR remains relatively lower in comparison. Furthermore, the Q-switched pulse width achieved in this study is on par with those reported in other works, demonstrating competitive performance in this aspect.

Universiti Malaya

Table 1 Q-switched pulse generation using different SAs in EDFLs

Pulsing Method	Pump Threshold (mW)	Pulse Width (µs)	Average Output Power (mW)	Repetition Rate (kHz)	Pulse Energy (nJ)	SNR (dB)	Ref
SMS	1000 - 3090	2.1 - 4.1	200-500	50.3 - 222.2	2700	42.8	-
EYDF	208 - 800	4	65	-	1500	-	(Zhou et al., 2010)
Organic metal 8-hydroxy quinoline chelate (Znq_2)	38 -198	2.8 - 6.6	1.9 - 8.2	45 - 85	41.8 - 95.4	57.4	(Salam et al., 2023)
SMS	115 - 343	2.5 - 4.2	0.61 - 2.35	87 - 158	7 - 15	72	(Chen et al., 2024)
Nanodiamond	59 - 187	1.565 - 4.24	0.447	77.84 - 127.2	1.5 - 3.5	73	(Shakaty et al., 2022)

Universiti Malaya

CHAPTER 4: HARMONIC DOMAIN-WALL DARK PULSE GENERATION USING UNPUMPED THIN-CORE THULIUM FIBER AS INTERFEROMETER

4.1 Introduction

Since John Scott Russell et al. first reported the observation of a heap of water remained unchanged while traveling for one to two miles that was caused by the stoppage of a boat in a canal, the soliton phenomena have been extensively reported and studied in many branches of physics (Guan et al., 2022; Ikezi et al., 1970; Li et al., 2023; Li et al., 2023; Liu et al., 2019; Liu et al., 2019; Liu et al., 2018; Nishida, 1982; Panoiu et al., 2004). Notably, soliton formation in nonlinear optics has attracted many researchers' attention over the past decades (Caudrey et al., 1973; Gibbon et al., 1972). The unremitting venture in optical soliton has paved a solid foundation for the ultrafast laser. In the year 2023, the Nobel Prize in Physics was awarded to Pierre Agostine, Ferenc Krausz, and Anne L'Huillier for their exceptional contribution in generating attosecond pulses of light that can give a snapshot of changes within atoms (Pierre et al., 2004). The importance of ultrafast laser is not confined to fundamental science but has been widely used in emerging and advanced technologies, particularly in micromachining and highly precision surgery applications (Ashforth et al., 2020; Cerami et al., 2013).

Hasegawa and Tappert first theoretically predicted the soliton formation in optical fibers using the NLSE (Hasegawa et al., 1973, 1973). The equation established the fundamental concept of dark and bright soliton generation in normal and anomalous dispersion cavities, respectively. Within the anomalous dispersion regime, bright solitons are localized, solitary wave solutions in NLSE, it is typically expressed as a hyperbolic secant function, with a localized peak under a background of CW (Seadawy et al., 2022).

Universiti Malaya

On the other hand, in the normal dispersion regime of NLSE solution, a dark soliton is expressed as the hyperbolic tangent function, with a localized dip under a background of CW (Alexander et al., 2022; Feng et al., 2010). The bright soliton has been extensively investigated for the past decades (Zhang et al., 2022; Zhang et al., 2022; Zhao et al., 2020) and achieved tangible applications in emerging industries (Nelson et al., 1997). As compared to bright soliton, the investigation of dark soliton is still hesitant to move forward. In fact, dark soliton exhibits unique properties that are described as "a solution looking for a problem" (Baronio et al., 2018; Krökel et al., 1988). For instance, dark soliton is highly immune to noise and loss from long-haul propagation. Additionally, without the high pulse peak power as exhibited by the bright pulse, the dark pulse can minimize the formation of nonlinear effects.

In the experimental work, NLSE dark pulse generation in fiber laser systems is normally reported at the wavelength below 1310 nm, due to the normal dispersion region of SMF (Lin et al., 2014; Wang et al., 2017; Wang et al., 2019). Alternatively, it can be achieved in longer wavelengths with the aid of additional dispersion shifted or dispersion compensating fibers (Guo et al., 2016; Tiu et al., 2014). Zooming into the dark pulse, the NLSE equation provides another solution with the consideration of higher order (3rd to 5th) of nonlinearity, called CQNLSE (Tiu et al., 2022). For the CQNLSE formation in fiber laser systems, it required a sufficient length of nonlinear medium to induce non-Kerr nonlinearity that dominates the Kerr nonlinearity (Tiu et al., 2015). Aside from the dispersion and nonlinearity condition that NLSE and CQNLSE had considered, there is another mechanism to generate the dark soliton, called DW dark pulse (Haelterman et al., 1995; Haelterman et al., 1994). DW dark pulse refers to the interaction among multiple lases at different wavelengths to induce the topological defects under the temporal domain. Unlike NLSE or CQNSE, the condition to induce DW dark pulse is not limited

Universiti Malaya

by dispersion or nonlinearity, which provides alternatives to form the dark pulse in fiber laser designs. Typically, the formation of DW dark pulse required an interferometer mechanism to stimulate the multiwavelength oscillation in the cavity. Interferometer mechanism can be achieved in fiber laser arrangements such as tapered fiber (Peng et al., 2013), NPR (Luo et al., 2011), nonlinear optical loop mirror (NOLM) (Feng et al., 2006), and NALM (Liu et al., 2012). However, the tapered fiber is sensitive to peripheral, whereas NOLM and NALM are complex in cavity configuration.

In this work, we have experimentally demonstrated harmonic DW dark pulse in an EDFL, by using an unpumped TCTDF to trigger multiwavelength oscillations in the cavity. The interaction of multiwavelength oscillation leads to the emergence of topological defects in temporal domain and forms a narrow intensity dip under the strong CW emission background. In addition, throughout the pump power tuning range, fundamental to the 7th order harmonic dark pulse are visualized and measured. All the harmonic orders manifest good stability (All the harmonic frequency components are 20 dB above all the super-mode noise, and overall SNR is above 50 dB for fundamental and each harmonic order) to oscillate in the cavity, with all SNRs above 50 dB, which shows the merits of the proposed design for potential industrial applications. The proposed thin-core thulium fiber as interferometer does not require additional optical components, and the all-fiber solution has further enhanced the feasibility for all-fiber system integration. These advantages are crucial for this method to be commercialized in the future. Furthermore, with the advantages of low loss and exceptional noise immunity in long-haul propagation, the dark pulse fiber laser could be a potential carrier in the next generation of optical communication system.

Universiti Malaya

4.2 Experimental Arrangements

The cavity setup of harmonic DW dark pulse EDFL is illustrated in Figure 4.1(a). In the cavity, a 40 cm long EDF (Liekki Er110-4/125) functioned as the gain medium. The EDF was pumped by a single-mode semiconductor laser diode (LD) whose wavelength centered at 980 nm, and the pump power could reach up to 421 mW. A 980nm/1550nm WDM was employed to couple the LD pump light into the EDF. A polarization-independent isolator forced the light to propagate unidirectionally in the cavity. A 3-paddle PC serves as a polarization state tuner to optimize the dark pulse formation. A 200 m SMF was inserted into the cavity to provide an additional birefringence effect to enhance the incoherent coupling of the decomposed polarization modes. The 10 cm TCTDF was spliced between the 3-paddle PC and SMF to act as an interferometer. A 50:50 optical coupler in the ring cavity was to tap 50% of light for analysis purposes. The total cavity length was 214 m and operated in anomalous dispersion, with GVD of -4.86 ps^2. Essential measurement instruments are depicted in Figure 4.1(a), and details will elaborate in the "Mode-locking performance" section.

The employed TCTDF was fabricated by one of the lab's collaborators. The fiber was designed to be single mode with N.A.~ 0.20 and cladding/core diameters of 125±0.5/6.5 μm . Figure 4.2 (a) displays the fiber cross-section under a microscope. Using electron probe microanalyses (EPMA), the integrated doping levels of several elements were assessed along the fiber's diameter. Along the fiber core, the distribution curve of several dopants with 6.15 wt% Al2O3, 2.2 wt% Y2O3, 0.47 wt% Tm2O3, 2.12 wt% GeO2, 1.57 wt% HfO2 and 0.05 wt% Bi2O3 is shown in Figure 4.2 (b). Figure 4.2 (c) and (d) display the TDF's attenuation curves, which were measured in the visible and near-infrared (NIR) regions, respectively (Lip et al., 2024; Paul et al., 2024).

Universiti Malaya

The splicing point between the TCTDF and SMF is visualized by optical microscope shown in Figure 4.1(b). Judging from 10x magnification image, the SMF and TCTDF were well spliced, with a splicing loss of ~ 0.02 dB. By 40x magnification, the core sizes of SMF and TCTDF were able to be estimated as 9 μm and 6.5 μm, respectively. When the light propagated from SMF to TCTDC, it would excite the cladding mode that co-propagated with the core mode. When both core and cladding modes are recombined at another end of the TCTDF and SMF joint, phase differences of core and cladding modes could induce constructive and destructive modal interferences. A spectrum filtering effect was successively induced by the interference and then led to the development of multi-wavelength oscillation within the laser cavity. The intensity of the transmission spectrum can be expressed as (Li et al., 2010; Tian et al., 2008):

$$I = I_{core} + \sum_m I_{cladding}^m + \sum_m 2\sqrt{I_{core} I_{cladding}^m} cos\Delta\varphi^m, \quad (4.1)$$

where I_{core} and $I_{cladding}^m$ are the light intensity of core mode and mth cladding mode, $\Delta\varphi^m$ represents the phase differences between fundamental mode in the core and mth cladding mode. By considering only 1st cladding mode, the intensity exhibits the minimum in spectra (Li et al., 2010):

$$\frac{2\pi\Delta n_{eff} L}{\lambda_{minimum}} = (2n+1)\pi \quad n = 1, 2, 3, 4, \ldots\ldots, \quad (4.2)$$

where $\lambda_{minimum}$ are the corresponding wavelengths that exist the intensity minima. The effective refractive index difference between core and cladding is denoted as Δn_{eff}, and L is the length of the TCTDF. Hence, the expression of FSR as the difference between the adjacent intensity minima is (Li et al., 2010):

$$FSR = \frac{{\lambda_{minimum}}^2}{\Delta n_{eff} L} \quad (4.3)$$

Universiti Malaya

Due to the short length of the interference length, it is difficult to precisely control the TCTDF length in practice. To optimize the DW dark pulse performance, we fabricated multiple pieces of TCTDF with different lengths. And TCTDF, with 10 cm length possessed the best performance in terms of HML DW dark pulse generation stability.

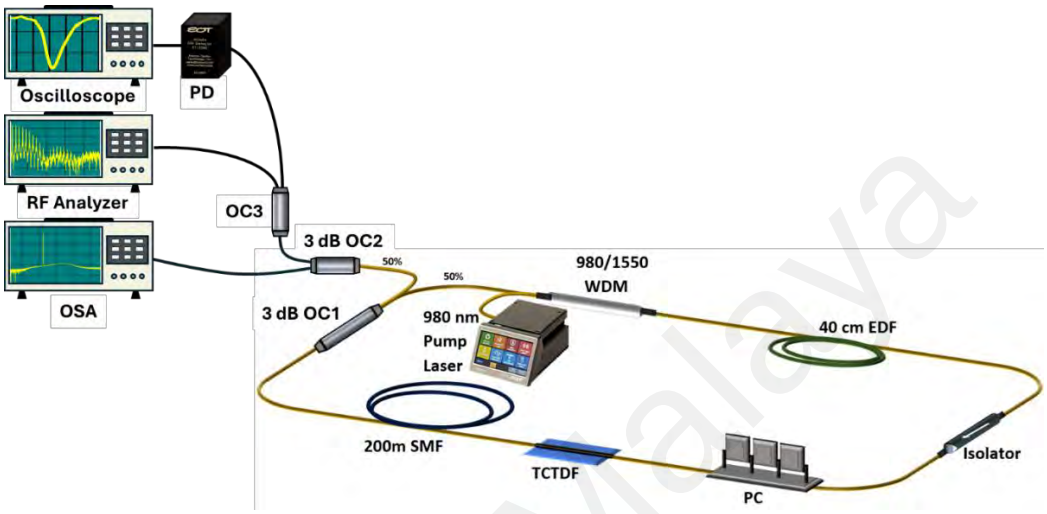

(a)

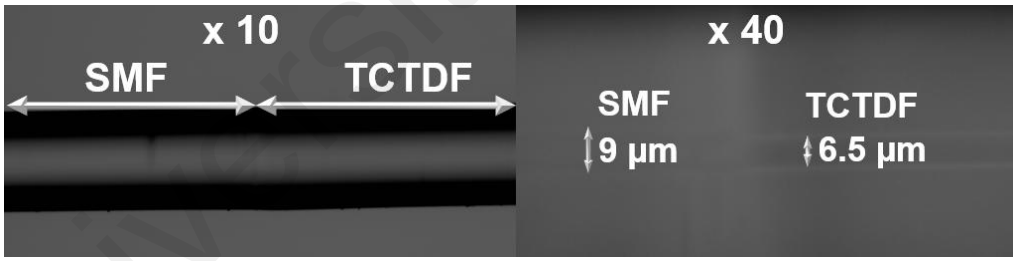

(b)

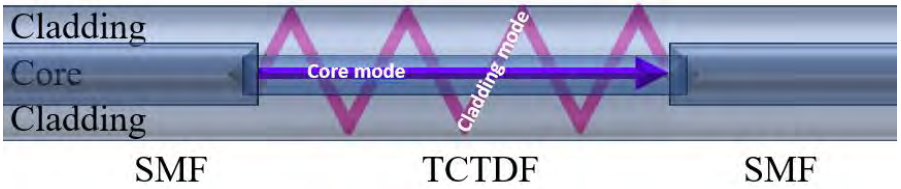

(c)

Figure 4.1 (a) Cavity setup of harmonic DW dark pulse EDFL. (b) Micrograph of splicing point between SMF and TCTDF. (c) Schematic diagram of light propagation through TCTDF.

Universiti Malaya

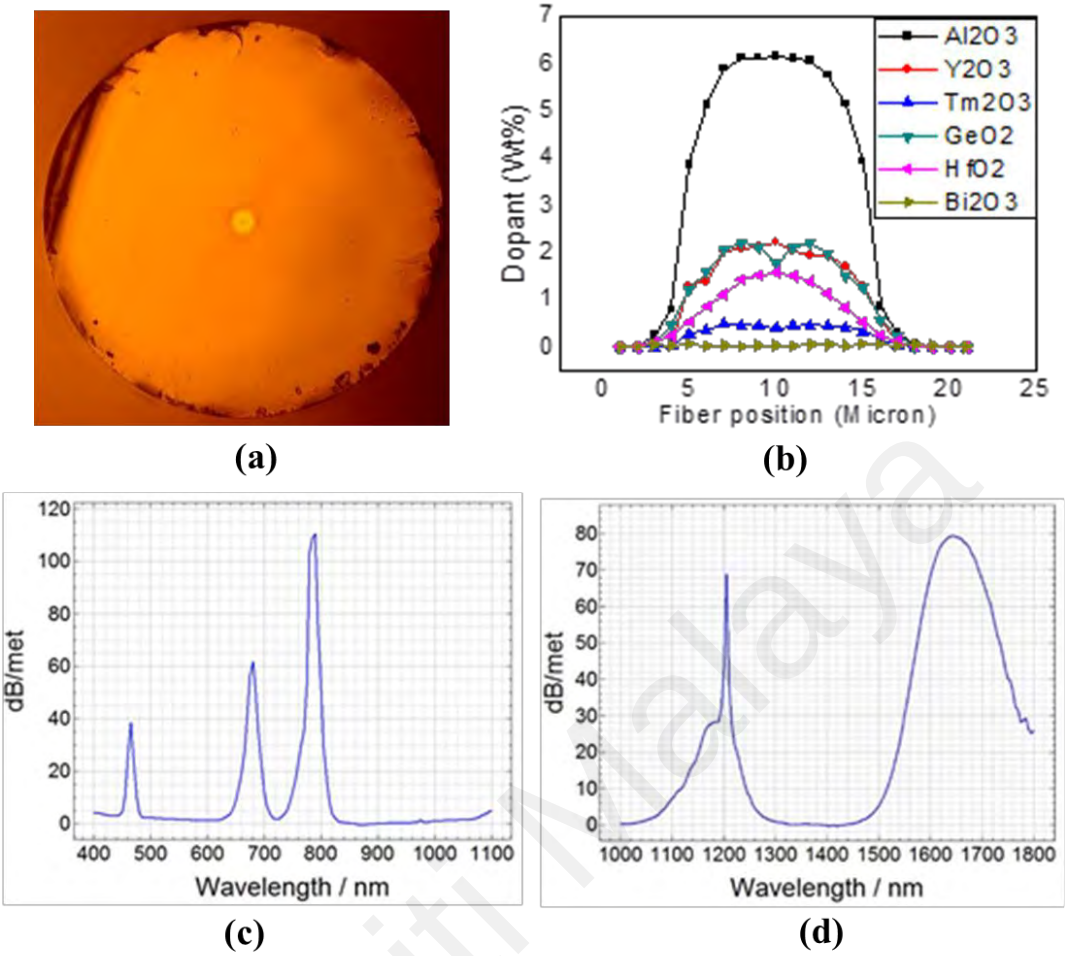

Figure 4.2 (a) Microscopic view of TDF, (b) The distribution curves of different dopants along the fiber diameter, (c) The attenuation profile in visible and (d) the attenuation profile in NIR region (Lip et al., 2024).

The saturable absorption rate is calculated utilizing twin detector method. The saturable absorption rate is approximately 3.7%. The data plot is shown in Figure 4.3.

Universiti Malaya

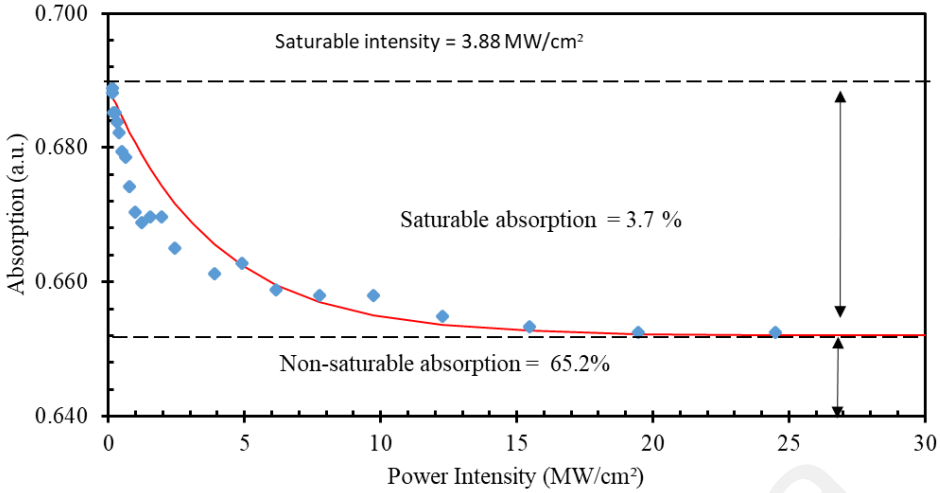

Figure 4.3 The nonlinear optical absorption curve of the fabricated TCTDF.

4.3 Mode-Locking Performance

As the pump power rose to 15 mW, the fiber laser's CW emission was formed. When the power increased gradually to 112 mW, the stable self-started DW dark pulse was observed by the instruments. The optical spectrum was tangibly modulated by the SMF-TCTDF-SMF interferometer mechanism and achieved multiwavelength oscillation in the laser cavity, which was visualized.by an OSA (Yokogawa AQ6370D). The multiwavelength peaks located at 1556.70 nm, 1557.41 nm, and 1558.12 nm, with FSR of ~0.71 nm as shown in Figure 4.4(a). Furthermore, thulium-doped elements in TCTDF were favorable to aid the pulse formation with the nature of saturable absorption characteristic at the C-band region.

The interaction of multiwavelength centered at different wavelengths could further induce the topological defects in temporal domain. Theoretically, DW exhibits kinks, by applying Bäcklund transformation to the NLSE. The single-kink soliton is expressed in equation 2.15. As forementioned in the introduction chapter and elaborated by above

equation, the formation of DW dark pulse is independent of the dispersion condition. As a result, DW dark pulse formation is feasible to establish in the fiber laser cavity without dispersion management mechanism.

The fundamental dark pulse train was characterized under varying pump conditions using multiple optical measure instruments. As shown in Figure 4.4 (b), temporal measurements captured by a 350 MHz oscilloscope (GWINSTEK GDS-3352) at 112 mW pump power revealed stable dark pulse generation. Subsequent analysis of the CSV data from the oscilloscope demonstrated the dark pulse FWHM of 250 ns at an elevated pump power of 125.4 mW. Complementary RF spectrum characterization using a real-time spectrum analyzer (Anritsu MS2683A, 7.8GHz bandwidth) identified with a fundamental repetition rate of 0.96 MHz, as evidenced by the RF spectrum in Figure 4.4 (c). The measured fundamental frequency agreed with the calculated repetition rate which proved that the fiber laser operated in the mode-locking regime. The system exhibited robust stability, with the fundamental frequency achieving a SNR of approximately 54.4 dB in the same RF spectral measurement.

Universiti Malaya

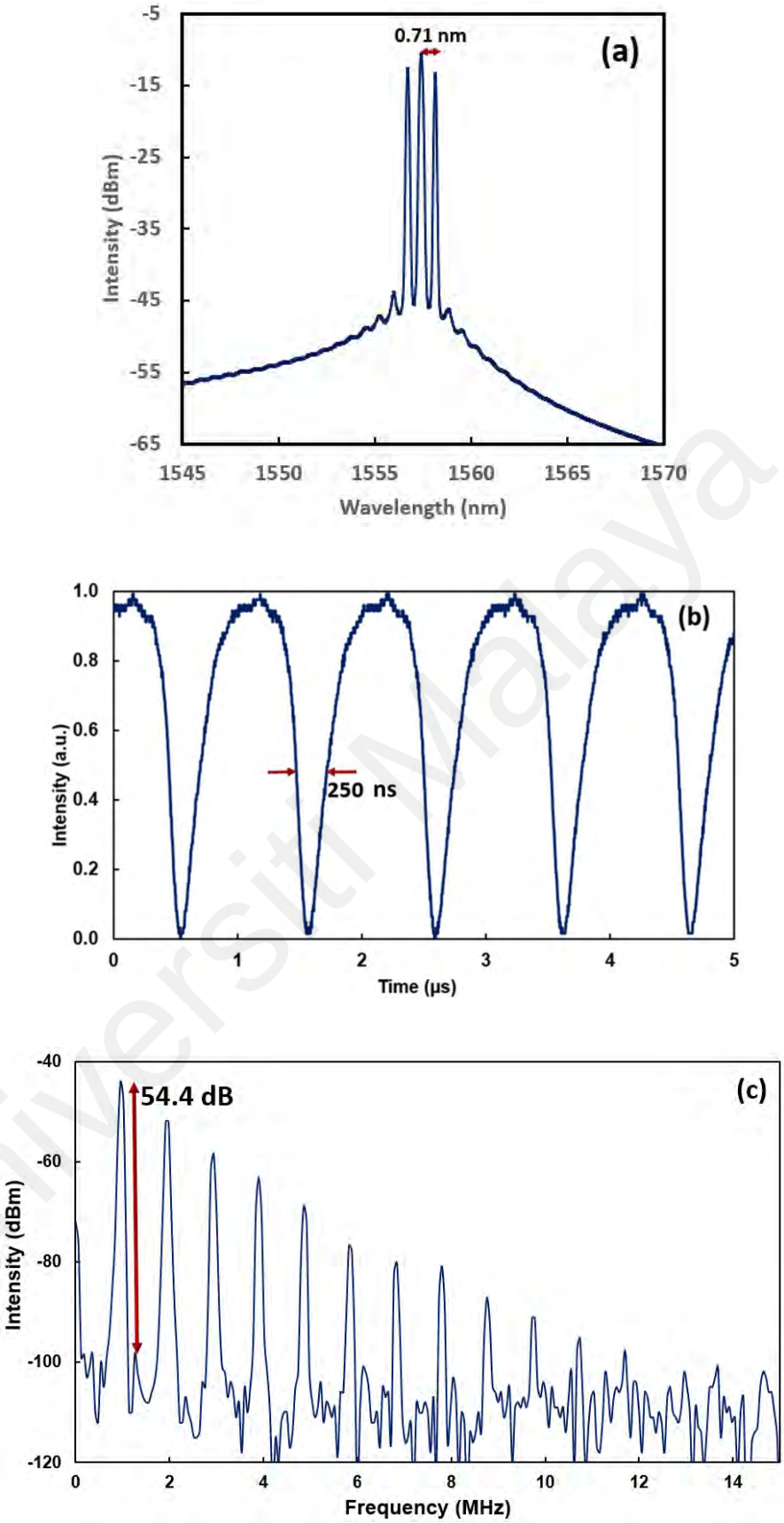

Figure 4.4 (a) Spectrum of DW dark pulse, (b) Temporal domain of DW dark pulse, and (c) RF spectrum of DW dark pulse at pump power of 125.4 mW.

Universiti Malaya

With the increase of pump power to 145.6 mW, the DW dark pulse train evolved to second harmonic order. The main indication of the second harmonic order was visualized by two dark pulses formation within a roundtrip time in temporal domain. By further increasing the pump power to 199.3 mW, 246.3 mW, 273.2 mW, 313.4 mW, and 387.3 mW, the dark pulse trains evolved to 2nd, 3rd, 4th, 5th,6th, and 7th order, respectively, as shown in Figure 4.5. The nonlinear phase shift, which is proportional to the intra-cavity light intensity, is primarily responsible for the harmonic operation. The nonlinear phase shift can be further developed to induce the harmonic mode-locking behavior by increasing the pump power and designing the cavity length (Peng et al., 2013; Wang et al., 2015; Zhang et al., 2019). Figure 4.5 shows a distinct pulse width evolution for various harmonic orders. The deep blue vertical stripe indicated the dark pulses, whereas the red color region indicated the noise floor of the laser. Inset figure is the corresponding harmonic order pulse train measured by oscilloscope. As the proposed cavity transformed into higher-order operations, more dark pulses were formed within a roundtrip time and the pulse width was suppressed with the increase in harmonic orders.

Universiti Malaya

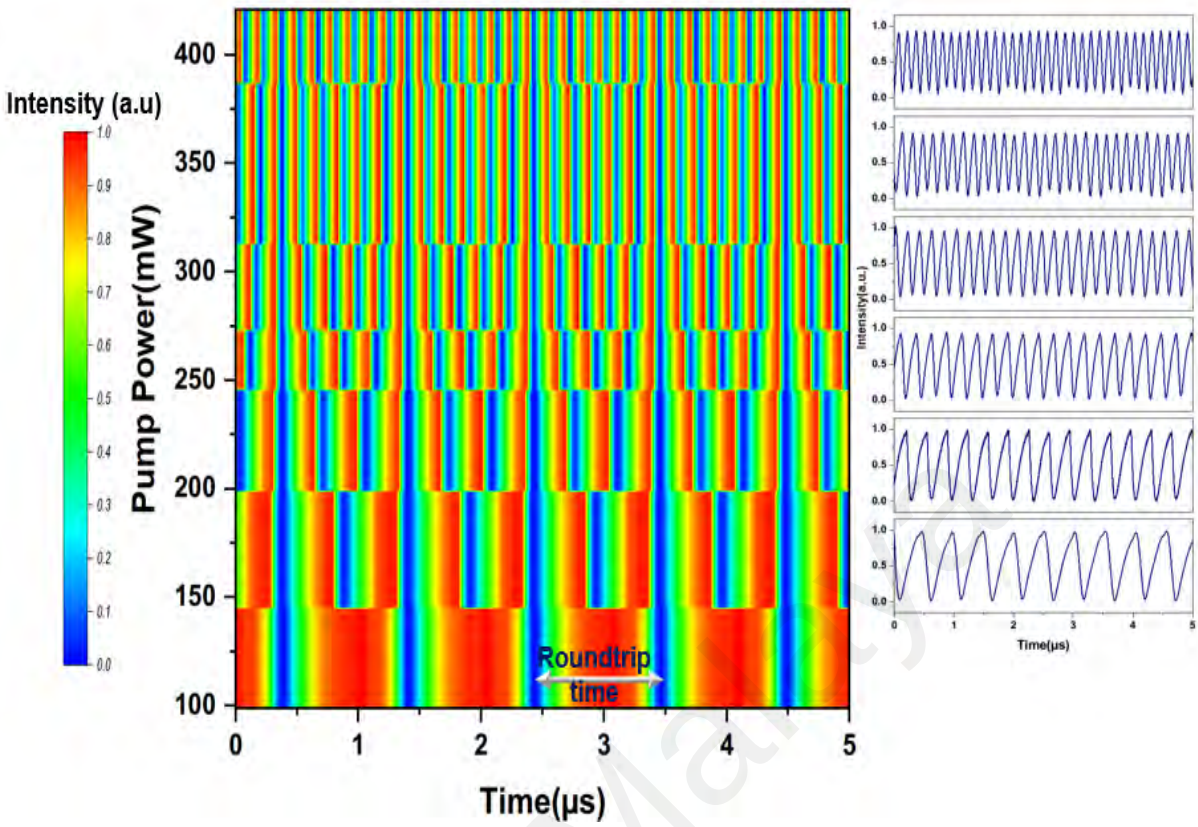

Figure 4.5 Pulse train evolution from fundamental to 7th order harmonic with the increase of pump power.

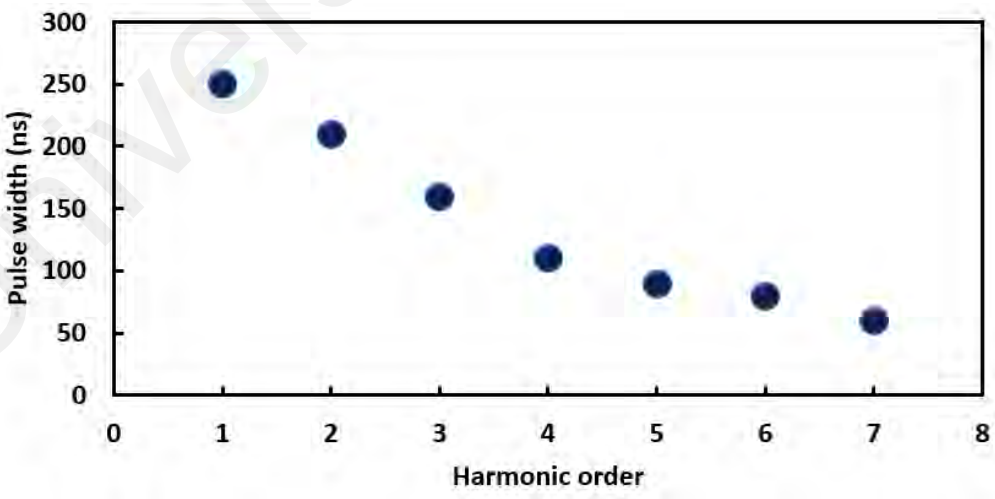

Figure 4.6 Average pulse width evolution from fundamental to 7th order harmonic.

The pulse width exhibited a clear decreasing trend with the rise of harmonic order as shown in Figure 4.6. As forementioned in the fundamental operation, the dark pulse

widths of different harmonic orders were also calculated from the CSV data files. On summary, the pulse widths for the fundamental, 2nd, 3rd, 4th, 5th, 6th, and the 7th order are 250ns, 210 ns, 160 ns, 110 ns, 90 ns, 80 ns and 60 ns, respectively.

Throughout the evolution of fundamental to 7th harmonic order, the output power was linear proportional to the pump power. As the pump power increased from 112.0 mW to 420.9 mW, the average power output increased linearly from 2.78 mW to 6.58 mW as shown in Figure 4.7. On the other hand, the dark pulse energy estimation is the same with the bright pulse, which is indicated as the average power divided by the corresponding repetition rate (Tiu et al., 2014; Zhang et al., 2019; Zhou et al., 2019). Average pulse energy increased within the same harmonic order, but experienced downward hopping with increase of harmonic order. The highest average pulse energy was recorded as 3.24 nJ at fundamental frequency, as depicted in Figure 4.7.

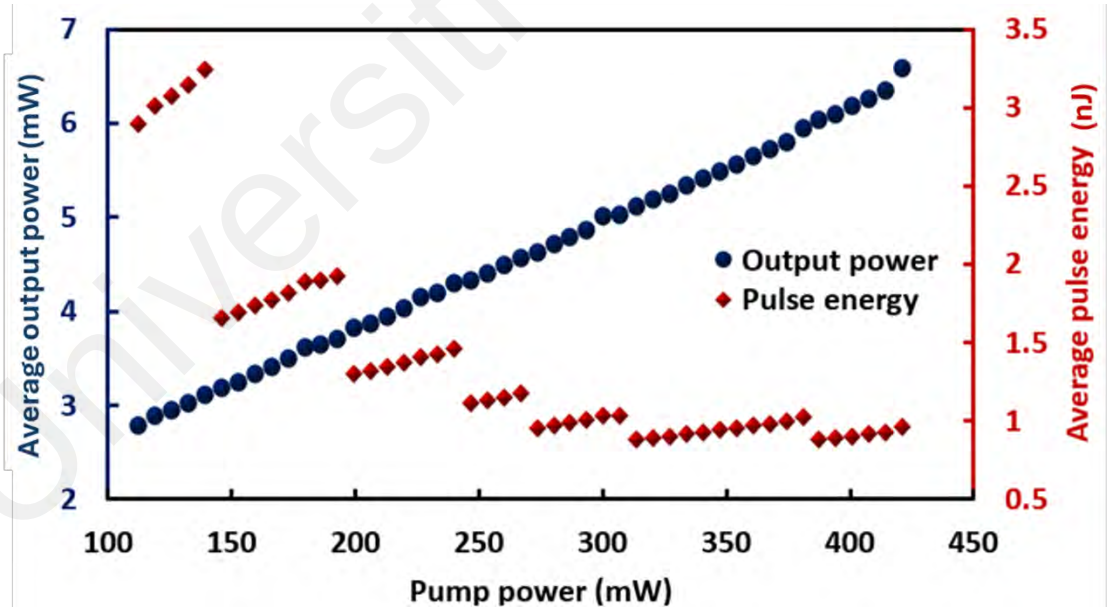

Figure 4.7 Output power and average pulse energy throughout the DW dark pulse operation range.

By determining the fundamental frequency in the previous section, fine tune the span of the RF analyzer and the RF spectrums could be extracted. Then the stability for each of the harmonic orders was investigated using RF spectrum analyzer as shown in Figure 4.7. From 2nd to 7th harmonic orders' SNR were all above 50 dB, which manifests the DW dark pulse operated stably throughout the operation of all harmonic orders. Notably, for each of the RF spectra in Figure 4.7, the super-mode noise peaks (Pottiez et al., 2002; Rana et al., 2002) are observed from fundamental frequency to N-1 harmonic order, with the spacing of fundamental frequency (0.96 MHz). The main drawback of the HML laser technology is the noise-induced irregularities of the time interval between the delivered pulses known as the HML timing jitter. From Figure 4.7, all the adjacent super-mode noise are at least 20 dB below the harmonic frequency components, which indicates the harmonic operations are not heavily interfered by the super-mode noise. However, the suppression of super-mode noise is still of great practical importance. The noise can be suppressed by resonant CW injection (Korobko et al., 2022), self-phase modulation & spectral filtering (Nakazawa et al., 1996), and semiconductor optical amplifier based high-pass filter (Wu et al., 2005). These could be potential future work to enhance the performance of the DW dark pulse fiber laser.

Universiti Malaya

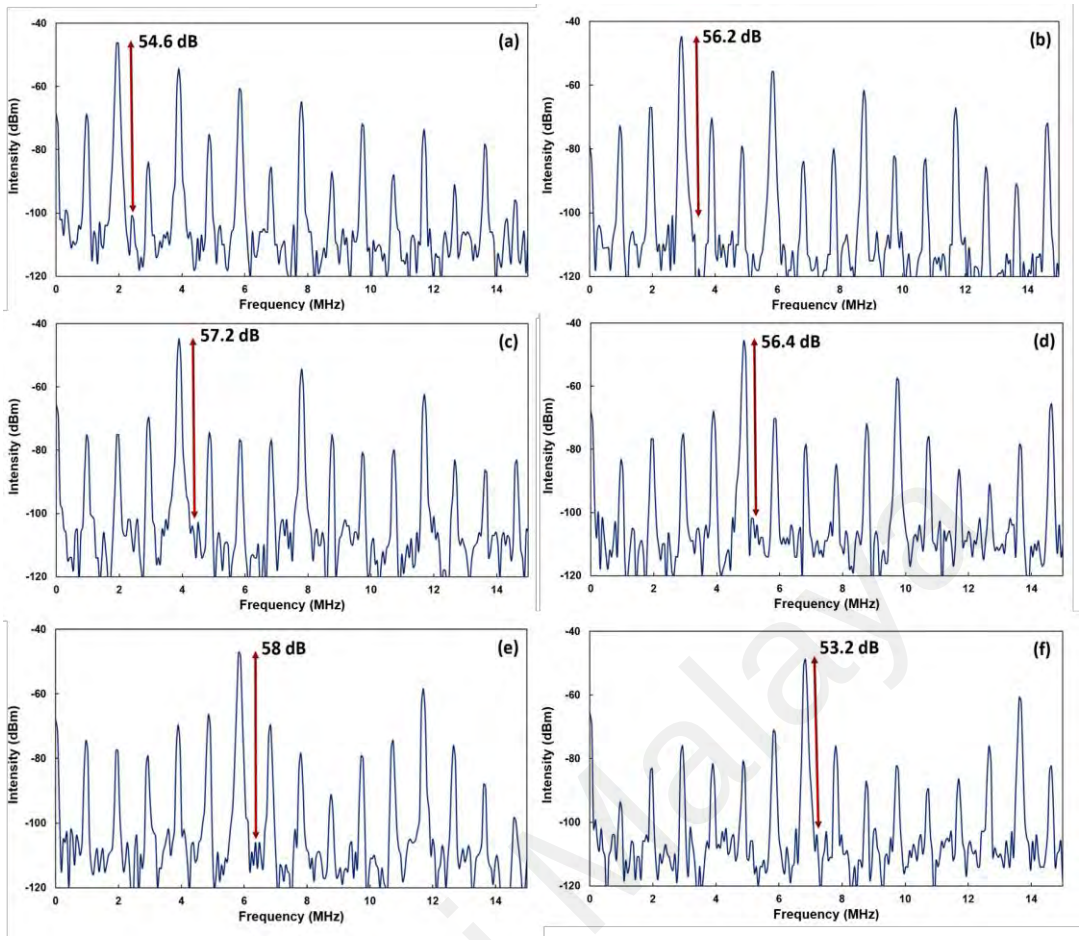

Figure 4.8 RF spectrum for 2nd to 7th harmonic orders.

4.4 Summary

In this chapter, the generation of harmonic DW dark pulse in the EDFL, by employing TCTDF as spectral filter has been successfully demonstrated. The multiwavelength oscillation in the cavity further induced the topological defects in temporal domain and developed DW dark pulse operation. Harmonic DW dark pulses of up to the 7th harmonic order have been investigated. High SNRs in each harmonic order indicated the reliability of the harmonic DW dark pulse operation in the proposed cavity. The highest average pulse energy obtained was 3.24 nJ at fundamental frequency, and the shorted pulse width was observed as 60 ns at 7th harmonic order.

Table 2 is the comparison of this thesis's work to the other reported work in terms of DW dark pulse generation in EDFLs.

Table 2 DW dark pulse generation using different SAs in EDFLs

Pulsing Method	SAs Categories	Wavelength (nm)	Pump Threshold (mW)	Pulse Width (ns)	Repetition Rate (MHz)	SNR (dB)	Ref
TCTDF	Artificial SAs	1556.7, 1557.4, 1558.1	112 - 420.9	60 - 250	0.96 - 6.72	54	-
TDF		1566.75	120 - 300	18	3.03	52.5	(Zhang et al., 2019)
SMS		1567.2, 1569.4	97 - 195.4	5	21.5	49	(Chen et al., 2024)
NPR		1546.5, 1562	43.4	-	2.5 - 20	-	(Wang et al., 2012)
Chromium Gallium Carbide (Cr_2GaC)	Material SAs	1529.6, 1531.6	83.7 - 99.8	300	1.27	69.3	(Husaini et al., 2025)
Polyacryl-onitrile		1560.43, 1561.17	97.76 - 165.26	306	0.99	67	(Song et al., 2025)
Scandium Oxide (Sc_2O_3)		1597.8	209.3 - 239.8	23	10.42	55.6	(Ahmeed et al., 2025)

In comparison, the proposed laser system incorporating the TCTDF FSA exhibits nearly equivalent performance in terms of operating wavelength, repetition frequency, and SNR. Moreover, the TCTDF FSA utilized in this study demonstrates an exceptionally low pump power threshold, underscoring its enhanced efficiency and significant potential for advanced laser applications.

Universiti Malaya

CHAPTER 5: CONCLUSION AND FUTURE WORKS

5.1 Conclusion

In recent times, Q-switched and mode-locked fiber lasers have emerged as focal points of research due to their ability to generate pulses with higher energies over extended durations, as well as sub-picosecond pulses with intense peak power- a crucial requirement across various fields such as medical diagnostics, telecommunications, and laser material processing. While both active and passive techniques are employed for pulse generation, passive methods utilizing SAs have gained preference owing to their straightforward design, compactness, cost-effectiveness, and adaptability. These SAs function as optical switches, offering intensity-dependent transmission without the need for complex external modulators, thus simplifying the laser setup. To date, numerous saturated absorbing materials have been explored, including SESAMs, nanomaterials like CNTs, graphene, topological insulators, TMDs, and black phosphorus. However, these materials are not without limitations, prompting significant interest in the quest for novel SAs in recent years. Notably, scant attention has been directed towards exploring the potential of artificial SAs. Therefore, this research endeavors to pioneer a novel artificial SA-based technique for pulse generation.

One particularly unique type of artificial SA among the array of options is the SMS configuration, often referred to as the SMS structure, which harnesses multimode interference. This study is dedicated to exploring the efficacy of the SMS structure as an artificial SA in passive Q-switching and as a comb filter in the generation of domain-wall dark pulses through passive mode-locking operations. The central focus lies in experimentally highlighting the capability of this structure to produce either Q-switched

Universiti Malaya

pulses or mode-locked dark pulses. To achieve this main goal, three specific objectives have been delineated.

The first objective involves the design, construction, and validation of a Q-switched EYDF operating within the C-band, leveraging the Kerr effect of multimode interference. This objective has been successfully achieved, as detailed in Chapter 3. A Q-switched fiber laser operating at 1552.3 nm was effectively demonstrated utilizing a multimode double-clad EYDF as the gain medium in a linear configuration. Stable Q-switched pulses were achieved across a range of pump powers, spanning from 1.00 to 3.09 mW. At a pump power of 3.09 mW, the laser manifested a maximum repetition rate of 222.2 kHz and a minimum pulse width of 2.1 μs. Notably, a peak pulse energy of 2.7 μJ was attained at a pump power of 2.42 W. This innovative Q-switching mechanism holds promise for generating short pulses within an all-fiber laser setup across various wavelength regions.

The second objective entails leveraging a TCTDF as both the fiber FSA and interferometer within an EDFL to generate DW dark pulses. Experimental validation of harmonic domain-wall dark pulse generation has been carried out in the EDFL to fulfil this objective. This was achieved by incorporating an unpumped TCTDF to initiate multiwavelength oscillations within the laser cavity. The interaction among these oscillations precipitates the emergence of topological defects in the temporal domain, giving rise to narrow intensity dips amidst the robust CW emission background.

The final objective centers on characterizing the DW dark pulse in terms of its pulse width, spectral width, repetition rate, and harmonic order. The self-starting of the domain-wall dark pulse occurred at a pump power of 112 mW, with a fundamental repetition rate measured at 0.96 MHz, pulse duration of 250 ns, and the highest average pulse energy recorded at 3.24 nJ. With increasing power, dark pulses up to the 7th harmonic order were

Universiti Malaya

observed and quantified. As the harmonic order escalated, the temporal width of the pulses decreased, with the minimum pulse width of 60 ns documented in the 7th order. Demonstrating commendable stability, the harmonic dark pulse fiber-laser maintained SNRs above 50 dB throughout all harmonic operations. This pursuit of harmonic dark pulse dark soliton lays a robust foundation for future developments. Furthermore, owing to its low loss and exceptional noise immunity during long-haul propagation, the dark pulse fiber-laser holds promise as a potential carrier in the next generation of optical communication systems.

In conclusion, this thesis has accomplished all its objectives successfully.

5.2 Future Work

While all proposed objectives have been successfully achieved, there remains ample scope for further exploration of the SMS structure in pulsed fiber laser technology. Its potential extends to the generation of ultrashort pulses lasers within the communication window and other regions, such as the 1-micron or 2-micron domain. Future endeavors should prioritize enhancing the performance of the proposed fiber laser, focusing on reducing pulse width, increasing repetition rate, and augmenting output/pulse energy. This can be facilitated by optimizing cavity length and the characteristics of the gain medium. Moreover, there is a pressing need to extend the exploration of developed SAs to other wavelength regions, encompassing 1 µm, 2 µm, and 3.0 µm, utilizing YDF, TDF, and ZBLAN EDF, respectively, as the gain medium. Notably, investigating Q-switched and mode-locked fiber lasers operating in the 3.0 µm region presents a particularly intriguing avenue, given the absence of prior research on SMS-based SAs in this

Universiti Malaya

wavelength range. Concurrently, the pursuit of developing a new suite of artificial SAs tailored for fiber laser applications promises to be a compelling area of future research.

Universiti Malaya

REFERENCES

Ahmad, H., Tiu, Z. C., Zarei, A., Suthaskumar, M., Salim, M. A. M., & Harun, S. W. (2016). Domain-wall dark pulse generation in fiber laser incorporating MoS_2. *Applied Physics B*, *122*(4), 69. https://doi.org/10.1007/s00340-016-6343-x

Ahmed, M., Ali, N., Salleh, Z., Rahman, A. A., Harun, S. W., Manaf, M., & Arof, H. (2015). Q-switched erbium doped fiber laser based on single and multiple walled carbon nanotubes embedded in polyethylene oxide film as saturable absorber. *Optics & Laser Technology*, *65*, 25-28.

Ahmeed, M. M., Ahmad, B. A., Supian, L. S., Diblawe, A. M., & Harun, S. W. (2025). Generation of Dark Pulses in Mode-Locked Erbium-Doped Fiber Ring Laser Operating in L-Band Region Using Sc_2O_3 Absorber. *Microwave and Optical Technology Letters*, *67*(1), e70103. https://doi.org/https://doi.org/10.1002/mop.70103

Alexander, T. J., Tsolias, G. A., Demirkaya, A., Decker, R. J., Martijn de Sterke, C., & Kevrekidis, P. G. (2022). Dark solitons under higher-order dispersion. *Optics Letters*, *47*(5), 1174-1177. https://doi.org/10.1364/OL.450835

Arshad, M., Seadawy, A. R., & Lu, D. (2017). Elliptic function and solitary wave solutions of the higher-order nonlinear Schrödinger dynamical equation with fourth-order dispersion and cubic-quintic nonlinearity and its stability. *The European Physical Journal Plus*, *132*(8), 371. https://doi.org/10.1140/epjp/i2017-11655-9

Ashforth, S. A., Oosterbeek, R. N., Bodley, O. L. C., Mohr, C., Aguergaray, C., & Simpson, M. C. (2020). Femtosecond lasers for high-precision orthopedic surgery. *Lasers in Medical Science*, *35*(6), 1263-1270. https://doi.org/10.1007/s10103-019-02899-x

Bagheri, M., Frez, C., Sterczewski, L., Gruidin, I., Fradet, M., Vurgaftman, I., Canedy, C., Bewley, W., Merritt, C., Kim, C. S., Kim, M., Meyer, R., & Meyer, J. (2018). Passively mode-locked interband cascade optical frequency combs. *Scientific Reports*, *8*. https://doi.org/10.1038/s41598-018-21504-9

Baronio, F., Frisquet, B., Chen, S., Millot, G., Wabnitz, S., & Kibler, B. (2018). Observation of a group of dark rogue waves in a telecommunication optical fiber. *Physical Review A*, *97*(1), 013852.

Boiti, M., Laddomada, C., & Pempinelli, F. (1982). Nonlinear Schrödinger equation, potential nonlinear Schrödinger equation and soliton solutions. *Il Nuovo Cimento A (1965-1970)*, *68*(3), 236-248. https://doi.org/10.1007/BF02817707

Caudrey, P. J., Eilbeck, J. C., Gibbon, J. D., & Bullough, R. K. (1973). Multiple soliton and bisoliton bound state solutions of the sine-Gordon equation and related equations in nonlinear optics. *Journal of Physics A: Mathematical, Nuclear and General*, *6*(8), L112. https://doi.org/10.1088/0305-4470/6/8/002

Universiti Malaya

Cerami, L., Mazur, E., Nolte, S., & Schaffer, C. B. (2013). Femtosecond Laser Micromachining. In R. Thomson, C. Leburn, & D. Reid (Eds.), *Ultrafast Nonlinear Optics* (pp. 287-321). Springer International Publishing. https://doi.org/10.1007/978-3-319-00017-6_12

Chen, B. H., Zhang, X. Y., Wu, K., Wang, H., Wang, J., & Chen, J. P. (2015). Q-switched fiber laser based on transition metal dichalcogenides MoS_2, $MoSe_2$, WS_2, and WSe_2. *Optics Express*, *23*(20), 26723-26737. https://doi.org/10.1364/oe.23.026723

Chen, Y., Cheak, T. Z., Jin, T. S., Vinitha, G., Dimyati, K., & Harun, S. W. (2024). Domain-wall dark pulse generation with SMF-GIMF-SMF structure as artificial saturable absorber. *Scientific Reports*, *14*(1), 2141. https://doi.org/10.1038/s41598-024-52640-0

Chen, Y., Dimyati, K., Badruddin, I. A., Kamangar, S., & Harun, S. W. (2024). All-fiber Q-switched erbium-doped fiber laser generation with SMF-SIMF-SMF structure as artificial saturable absorber. *Infrared Physics & Technology*, *136*, 105088. https://doi.org/https://doi.org/10.1016/j.infrared.2023.105088

Chen, Y., Dimyati, K., & Harun, S. W. (2024). Q-switched Erbium Doped Fiber Laser Generation Using the Kerr Effect of Multimode Interference. Journal of Physics: Conference Series,

Chen, Y., Jiang, G. B., Chen, S. Q., Guo, Z. N., Yu, X. F., Zhao, C. J., Zhang, H., Bao, Q. L., Wen, S. C., Tang, D. Y., & Fan, D. Y. (2015). Mechanically exfoliated black phosphorus as a new saturable absorber for both Q-switching and mode-locking laser operation. *Optics Express*, *23*(10), 12823-12833. https://doi.org/10.1364/oe.23.012823

Chi, M., Lip, Z. H., Rosol, A. H. A., Cheng, X. S., Tiu, Z. C., Yasin, M., & Harun, S. W. (2023). Passive Q-Switching of a Cladding Pumped Erbium–Ytterbium Co-Doped Fiber Laser Induced by the Kerr Effect. *Journal of Russian Laser Research*, *44*(5), 585-589. https://doi.org/10.1007/s10946-023-10166-2

Cui, Q., Wei, M., Xiong, Z., Hu, S., Jiang, J., Wang, L., Cheng, T., Wu, X., & Jiang, H. (2019). 100–300 Hz repetition-rate acousto-optic Q-switched 2.79 µm Er: YSGG laser side-pumped by laser-diode. *Infrared Physics & Technology*, *98*, 256-259.

Cui, Q., Wei, M., Xiong, Z., Hu, S., Jiang, J., Wang, L., Cheng, T., Wu, X., & Jiang, H. (2019). 100–300 Hz repetition-rate acousto-optic Q-switched 2.79 µm Er:YSGG laser side-pumped by laser-diode. *Infrared Physics & Technology*, *98*, 256-259. https://doi.org/https://doi.org/10.1016/j.infrared.2019.03.029

Delevaque, E., Georges, T., Monerie, M., Lamouler, P., & Bayon, J. F. (1993). Modeling of pair-induced quenching in erbium-doped silicate fibers. *IEEE Photonics Technology Letters*, *5*(1), 73-75. https://doi.org/10.1109/68.185065

Deng, L., Jiang, C., Guo, X., Sun, S., Huang, H., & Cao, T. (2025). Whispering-gallery mode sensor based on coupling of tapered two-mode fiber and glass capillary. *Review of Scientific Instruments*, *96*(1). https://doi.org/10.1063/5.0227816

Dianov, E. M., Luchnikov, A. V., Pilipetskii, A. N., & Prokhorov, A. M. (1992). Long-range interaction of picosecond solitons through excitation of acoustic waves in optical fibers. *Applied Physics B*, *54*(2), 175-180. https://doi.org/10.1007/BF00331891

Ding, E., Lefrancois, S., Kutz, J. N., & Wise, F. W. (2011). Scaling Fiber Lasers to Large Mode Area: An Investigation of Passive Mode-Locking Using a Multi-Mode Fiber. *IEEE Journal of Quantum Electronics*, *47*(5), 597-606. https://doi.org/10.1109/JQE.2011.2107730

Ennejah, T., & Attia, R. (2013). Mode Locked Fiber Lasers. In S. W. Harun & H. Arof (Eds.), *Current Developments in Optical Fiber Technology*. IntechOpen. https://doi.org/10.5772/52214

Feng, M., Silverman, K. L., Mirin, R. P., & Cundiff, S. T. (2010). Dark pulse quantum dot diode laser. *Optics Express*, *18*(13), 13385-13395. https://doi.org/10.1364/OE.18.013385

Feng, X., Tam, H.-y., Liu, H., & Wai, P. K. A. (2006). Multiwavelength erbium-doped fiber laser employing a nonlinear optical loop mirror. *Optics Communications*, *268*(2), 278-281. https://doi.org/https://doi.org/10.1016/j.optcom.2006.07.010

Fu, S. J., Sheng, Q., Zhu, X. S., Shi, W., Yao, J. Q., Shi, G. N., Norwood, R. A., & Peyghambarian, N. (2015). Passive Q-switching of an all-fiber laser induced by the Kerr effect of multimode interference. *Optics Express*, *23*(13), 17255-17262. https://doi.org/10.1364/oe.23.017255

Ghafar, N. A., Zulkipli, N. F., Omar, S., Markom, A. M., Yasin, M., & Harun, S. W. (2022). Q-Switched Pulse Generation in Erbium-Doped Fiber Laser Cavity with Vanadium Aluminum Carbide Absorber. *Journal of Russian Laser Research*, *43*(6), 702-707.

Gibbon, J. D., & Eilbeck, J. C. (1972). A possible N soliton solution for a nonlinear optics equation. *Journal of Physics A: General Physics*, *5*(11), L122. https://doi.org/10.1088/0305-4470/5/11/015

Grudinin, A. B., & Gray, S. (1997). Passive harmonic mode locking in soliton fiber lasers. *Journal of the Optical Society of America B*, *14*(1), 144-154. https://doi.org/10.1364/JOSAB.14.000144

Grudinin, A. B., Richardson, D. J., & Payne, D. N. (1993). Passive harmonic modelocking of a fibre soliton ring laser. *Electronics Letters*, *29*(21), 1860-1861. https://doi.org/doi:10.1049/el:19931238

Guan, M., Chen, D., Hu, S., Zhao, H., You, P., & Meng, S. (2022). Theoretical insights into ultrafast dynamics in quantum materials. *Ultrafast science*.

Guo, J., Song, Y., Xiang, Y., Zhang, H., & Tang, D. Y. (2016). Controlled Generation of Bright or Dark Solitons in a Fiber Laser by Intracavity Nonlinear Absorber. *IEEE Photonics Journal*, *8*(3), 1-12. https://doi.org/10.1109/JPHOT.2016.2575862

Universiti Malaya

Haelterman, M., & Badolo, M. (1995). Dual-frequency wall solitary waves for nonreturn-to-zero signal transmission in W-type single-mode fibers. *Optics Letters*, *20*(22), 2285-2287. https://doi.org/10.1364/OL.20.002285

Haelterman, M., & Sheppard, A. P. (1994). Polarization domain walls in diffractive or dispersive Kerr media. *Optics Letters*, *19*(2), 96-98. https://doi.org/10.1364/OL.19.000096

Hasegawa, A., & Tappert, F. (1973). Transmission of stationary nonlinear optical pulses in dispersive dielectric fibers. I. Anomalous dispersion. *Applied Physics Letters*, *23*, 142-144. https://doi.org/10.1063/1.1654836

Hasegawa, A., & Tappert, F. (1973). Transmission of stationary nonlinear optical pulses in dispersive dielectric fibers. II. Normal dispersion. *Applied Physics Letters*, *23*(4), 171-172. https://doi.org/10.1063/1.1654847

Husaini, M. N. A. H. M., Wadi, N. I. S., Jusoh, Z., Ahmad, A. D., Apsari, R., & Dimyati, K. (2025). Dark pulse generation in mode-locked erbium-doped fiber lasers using chromium gallium carbide film-based pulse transducer. *Physica Scripta*, *100*(5), 055535. https://doi.org/10.1088/1402-4896/adcb76

Ikezi, H., Taylor, R. J., & Baker, D. R. (1970). Formation and Interaction of Ion-Acoustic Solitions. *Physical Review Letters*, *25*(1), 11-14. https://doi.org/10.1103/PhysRevLett.25.11

Keller, U. (2003). Recent developments in compact ultrafast lasers. *Nature*, *424*(6950), 831-838.

Keller, U. (2021). Linear Pulse Propagation. In U. Keller (Ed.), *Ultrafast Lasers: A Comprehensive Introduction to Fundamental Principles with Practical Applications* (pp. 25-71). Springer International Publishing. https://doi.org/10.1007/978-3-030-82532-4_2

Keller, U. (2021). Nonlinear Pulse Propagation. In U. Keller (Ed.), *Ultrafast Lasers: A Comprehensive Introduction to Fundamental Principles with Practical Applications* (pp. 131-183). Springer International Publishing. https://doi.org/10.1007/978-3-030-82532-4_4

Kharazi, S. M. S. S., Mahdiraji, G. A., Sahbudin, R. K. Z., Abas, A. F., & Anas, S. B. A. (2012). Effects of Fiber Dispersion on the Performance of Optical CDMA Systems. *Journal of Optical Communications*, *33*(4), 311-320. https://doi.org/doi:10.1515/joc-2012-0057

Korobko, D. A., Ribenek, V. A., Stoliarov, D. A., Mégret, P., & Fotiadi, A. A. (2022). Resonantly induced mitigation of supermode noise in a harmonically mode-locked fiber laser: revealing the underlying mechanisms. *Optics Express*, *30*(10), 17243-17258. https://doi.org/10.1364/OE.457023

Krökel, D., Halas, N. J., Giuliani, G., & Grischkowsky, D. (1988). Dark-Pulse Propagation in Optical Fibers. *Physical Review Letters*, *60*(1), 29-32. https://doi.org/10.1103/PhysRevLett.60.29

Lee, J. Y., & Kim, D. Y. (2006). Versatile chromatic dispersion measurement of a single mode fiber using spectral white light interferometry. *Optics Express*, *14*(24), 11608-11615. https://doi.org/10.1364/OE.14.011608

Li, G., Li, D., Cai, Y., Fu, G., Yu, W., Li, P., Xiao, Q., Gong, M., & Yan, P. (2025). Investigations of a 439 W Narrow-Linewidth Er/Yb Fiber Amplifier Pumped by 1018 nm Fiber Lasers. *Journal of Lightwave Technology*, *43*(9), 4491-4499. https://doi.org/10.1109/JLT.2024.3522203

Li, J. F., Hudson, D. D., Liu, Y., & Jackson, S. D. (2012). Efficient 2.87 µm fiber laser passively switched using a semiconductor saturable absorber mirror. *Optics Letters*, *37*(18), 3747-3749. https://doi.org/10.1364/ol.37.003747

Li, X., Huang, X., Han, Y., Chen, E., Guo, P., Zhang, W., An, M., Pan, Z., Xu, Q., Guo, X., Huang, X., Wang, Y., & Zhao, W. (2023). High-performance γ-MnO_2 Dual-Core, Pair-Hole Fiber for Ultrafast Photonics. *Ultrafast science*, *3*, 0006. https://doi.org/doi:10.34133/ultrafastscience.0006

Li, X., Huang, X., Hu, X., Guo, X., & Han, Y. (2023). Recent progress on mid-infrared pulsed fiber lasers and the applications. *Optics & Laser Technology*, *158*, 108898. https://doi.org/10.1016/j.optlastec.2022.108898

Li, Y., Harris, E., Chen, L., & Bao, X. (2010). Application of spectrum differential integration method in an in-line fiber Mach-Zehnder refractive index sensor. *Optics Express*, *18*(8), 8135-8143. https://doi.org/10.1364/OE.18.008135

Lin, R. y., Wang, Y. g., Yan, P. g., Zhang, G. l., Zhao, J. q., Li, H. q., Huang, S. s., Cao, G. z., & Duan, J. a. (2014). Bright and Dark Square Pulses Generated From a Graphene-Oxide Mode-Locked Ytterbium-Doped Fiber Laser. *IEEE Photonics Journal*, *6*(3), 1-8. https://doi.org/10.1109/JPHOT.2014.2319099

Lip, Z. H., Cheng, X. S., Chi, M., Sin Jin, T., Abdul Latiff, A., & Harun, S. W. (2024). Passively generated Q-switched pulses fiber laser in 2 µm wavelength using MXene $Ti_3C_2T_x$ and Ti_2CT_x saturable absorber. *Physica Scripta*, *99*(12), 125536. https://doi.org/10.1088/1402-4896/ad8e8b

Liu, X., & Pang, M. (2019). Revealing the Buildup Dynamics of Harmonic Mode-Locking States in Ultrafast Lasers. *Laser & Photonics Reviews*, *13*(9), 1800333. https://doi.org/https://doi.org/10.1002/lpor.201800333

Liu, X., Popa, D., & Akhmediev, N. (2019). Revealing the Transition Dynamics from Q Switching to Mode Locking in a Soliton Laser. *Physical Review Letters*, *123*(9), 093901. https://doi.org/10.1103/PhysRevLett.123.093901

Liu, X., Yao, X., & Cui, Y. (2018). Real-Time Observation of the Buildup of Soliton Molecules. *Physical Review Letters*, *121*(2), 023905. https://doi.org/10.1103/PhysRevLett.121.023905

Liu, X., Zhan, L., Luo, S., Gu, Z., Liu, J., Wang, Y., & Shen, Q. (2012). Multiwavelength erbium-doped fiber laser based on a nonlinear amplifying loop mirror assisted by

Universiti Malaya

un-pumped EDF. *Optics Express*, *20*(7), 7088-7094. https://doi.org/10.1364/OE.20.007088

Luo, Z. C., Luo, A. P., & Xu, W. C. (2011). Tunable and Switchable Multiwavelength Passively Mode-Locked Fiber Laser Based on SESAM and Inline Birefringence Comb Filter. *IEEE Photonics Journal*, *3*(1), 64-70. https://doi.org/10.1109/JPHOT.2010.2102012

Luo, Z. Q., Zhou, M., Weng, J., Huang, G. M., Xu, H. Y., Ye, C. C., & Cai, Z. P. (2010). Graphene-based passively Q-switched dual-wavelength erbium-doped fiber laser. *Optics Letters*, *35*(21), 3709-3711. https://doi.org/10.1364/ol.35.003709

Matniyaz, T. (2014). *Free-space NPR mode locked erbium doped fiber laser based frequency comb for optical frequency measurement* Kansas State University].

Mirov, S., Fedorov, V., Martyshkin, D., Moskalev, I., Mirov, M., & Vasilyev, S. (2015). Mid-IR lasers based on transition metal and rare-earth ion doped crystals. Micro- and Nanotechnology Sensors, Systems, and Applications VII,

Nakazawa, M., Tamura, K., & Yoshida, E. (1996). Supermode noise suppression in a harmonically modelocked fibre laser by selfphase modulation and spectral filtering. *Electronics Letters*, *32*(5), 461-463. https://doi.org/10.1049/el:19960318

Nazemosadat, E., & Mafi, A. (2013). Nonlinear multimodal interference and saturable absorption using a short graded-index multimode optical fiber. *Journal of the Optical Society of America B*, *30*(5), 1357-1367. https://doi.org/10.1364/JOSAB.30.001357

Nazemosadat, E., & Mafi, A. (2013). Nonlinear switching in multicore versus multimode waveguide junctions for mode-locked laser applications. *Optics Express*, *21*(25), 30739-30745. https://doi.org/10.1364/OE.21.030739

Nelson, L. E., Jones, D. J., Tamura, K., Haus, H. A., & Ippen, E. P. (1997). Ultrashort-pulse fiber ring lasers. *Applied Physics B*, *65*(2), 277-294. https://doi.org/10.1007/s003400050273

Nishida, Y. (1982). Higher Dimensional Solitons in Plasma. *BUTSURI*, *37*(5), 396-400. https://doi.org/10.11316/butsuri1946.37.396

Nishizawa, N. (2014). Ultrashort pulse fiber lasers and their applications. *Japanese Journal of Applied Physics*, *53*(9), 090101(090101)-090101(090111).

Nizamani, B., Jafry, A. A. A., Fizza, G., Memon, F. A., Salam, S., Najm, M. M., Abdul Khudus, M. I. M., Hanafi, E., Apsari, R., & Harun, S. W. (2021). Dark pulse mode-locked laser based on aluminum zinc oxide coated d-shape fiber as saturable absorber. *Fiber and Integrated Optics*, *40*(4-6), 322-334.

Panoiu, N. C., Mihalache, D., Mazilu, D., Lederer, F., & R. M. Osgood, J. (2004). Vectorial spatial solitons in bulk periodic quadratically nonlinear media. *Journal*

Universiti Malaya

of Optics B: Quantum and Semiclassical Optics, *6*(5), S351. https://doi.org/10.1088/1464-4266/6/5/025

Paschotta, R. (2006). Q Switching. In *RP Photonics Encyclopedia*: RP Photonics AG.

Paul, M. C., & Ferreira, M. F. S. (2024). 1 - Specialty optical fibers—materials, fabrication technology, and applications: introduction. In M. F. S. Ferreira & M. C. Paul (Eds.), *Specialty Optical Fibers* (pp. 3-12). Woodhead Publishing. https://doi.org/https://doi.org/10.1016/B978-0-443-18495-6.00005-6

Peng, J., Zhan, L., Luo, S., & Shen, Q. (2013). Passive Harmonic Mode-Locking of Dissipative Solitonsin a Normal-Dispersion Er-Doped Fiber Laser. *Journal of Lightwave Technology*, *31*(16), 3009-3014. https://opg.optica.org/jlt/abstract.cfm?URI=jlt-31-16-3009

Peng, W., Yan, F., Li, Q., Yin, G., Feng, S., Feng, T., & Tan, S. (2013). Tunable self-seeded multiwavelength Brillouin–erbium fiber laser using an in-line two-taper Mach–Zehnder interferometer. *Optics & Laser Technology*, *45*, 348-351. https://doi.org/https://doi.org/10.1016/j.optlastec.2012.06.025

Pérez-Millán, P., Díez, A., Andrés, M. V., Zalvidea, D., & Duchowicz, R. (2005). Q-switched all-fiber laser based on magnetostriction modulation of a Bragg grating. *Optics Express*, *13*(13), 5046-5051. https://doi.org/10.1364/OPEX.13.005046

Pierre, A., & Louis, F. D. (2004). The physics of attosecond light pulses. *Reports on Progress in Physics*, *67*(6), 813. https://doi.org/10.1088/0034-4885/67/6/R01

Pitois, S., Millot, G., & Wabnitz, S. (1998). Polarization Domain Wall Solitons with Counterpropagating Laser Beams. *Physical Review Letters*, *81*(7), 1409-1412. https://doi.org/10.1103/PhysRevLett.81.1409

Popa, D., Sun, Z., Hasan, T., Torrisi, F., Wang, F., & Ferrari, A. C. (2011). Graphene Q-switched, tunable fiber laser. *Applied Physics Letters*, *98*(7). https://doi.org/10.1063/1.3552684

Popa, D., Sun, Z., Hasan, T., Torrisi, F., Wang, F., & Ferrari, A. C. (2011). Graphene Q-switched, tunable fiber laser. *Applied Physics Letters*, *98*(7), 073106.

Pottiez, O., Deparis, O., Kiyan, R., Haelterman, M., Emplit, P., Megret, P., & Blondel, M. (2002). Supermode noise of harmonically mode-locked erbium fiber lasers with composite cavity. *IEEE Journal of Quantum Electronics*, *38*(3), 252-259. https://doi.org/10.1109/3.985565

Quimby, R. S. (2006). Optical Resonators. In *Photonics and Lasers: An Introduction* (pp. 293-306). https://doi.org/https://doi.org/10.1002/0471791598.ch16

Rahman, M. F. A., Dhar, A., Das, S., Dutta, D., Paul, M. C., Rusdi, M. F. M., Latiff, A. A., Dimyati, K., & Harun, S. W. (2018). An 8 cm long holmium-doped fiber saturable absorber for Q-switched fiber laser generation at 2-µm region. *Optical Fiber Technology*, *43*, 67-71.

Universiti Malaya

Rana, F., Lee, H. L. T., Ram, R. J., Grein, M. E., Jiang, L. A., Ippen, E. P., & Haus, H. A. (2002). Characterization of the noise and correlations in harmonically mode-locked lasers. *Journal of the Optical Society of America B*, *19*(11), 2609-2621. https://doi.org/10.1364/JOSAB.19.002609

Renninger, W. H., & Wise, F. W. (2013). Optical solitons in graded-index multimode fibres. *Nature Communications*, *4*(1), 1719. https://doi.org/10.1038/ncomms2739

Russell, J. S. (1844). Report on Waves. In *Report of the 14th Meeting of the British Association for the Advanced of Science*.

Salam, S., Azooz, S. M., Nizamani, B., Zhang, P., H. H. Al-Masoodi, A., Mukhtar Diblawe, A., Yasin, M., & Harun, S. W. (2023). A tunable-wavelength Q-switched fiber laser based on organic metal 8-hydroxyquinoline chelate as a saturable absorber. *Infrared Physics & Technology*, *131*, 104637. https://doi.org/https://doi.org/10.1016/j.infrared.2023.104637

Sanchez, F., Le Boudec, P., François, P.-L., & Stephan, G. (1993). Effects of ion pairs on the dynamics of erbium-doped fiber lasers. *Physical Review A*, *48*(3), 2220-2229. https://doi.org/10.1103/PhysRevA.48.2220

Seadawy, A. R., Rizvi, S. T. R., Akram, U., & Kamran Naqvi, S. (2022). Optical and analytical soliton solutions to higher order non-Kerr nonlinear Schrödinger dynamical model. *Journal of Geometry and Physics*, *179*, 104616. https://doi.org/https://doi.org/10.1016/j.geomphys.2022.104616

Shakaty, A. A., Hmood, J. K., Mahdi, B. R., Mahdi, R. I., & Al-Azzawi, A. A. (2022). Q-switched erbium-doped fiber laser based on nanodiamond saturable absorber. *Optics & Laser Technology*, *146*, 107569. https://doi.org/https://doi.org/10.1016/j.optlastec.2021.107569

Shiner, B. (2016). Fiber lasers continue to gain market share in material processing applications. *Manuf. Eng.*, *156*, 79-85.

Silva, L. C. B., & Castellani, C. E. S. (2021). Recent progress in optical dark pulses generation based on saturable absorber materials. *Optical Fiber Technology*, *64*, 102560. https://doi.org/https://doi.org/10.1016/j.yofte.2021.102560

Soboh, R. S., Al-Masoodi, A. H., Erman, F. N., Al-Masoodi, A. H., Nizamani, B., Arof, H., Yasin, M., & Harun, S. (2021). Lawsone dye material as potential saturable absorber for Q-switched erbium doped fiber laser. *Optical Fiber Technology*, *64*, 102537.

Sobon, G., Krzempek, K., Kaczmarek, P., Abramski, K. M., & Nikodem, M. (2011). 10 GHz passive harmonic mode-locking in Er–Yb double-clad fiber laser. *Optics Communications*, *284*(18), 4203-4206. https://doi.org/https://doi.org/10.1016/j.optcom.2011.04.050

Song, X., Diblawe, A. M., Tiu, Z. C., Salam, S., Ibrahim, F., & Harun, S. W. (2025). Domain-wall dark pulse generation with polyacrylonitrile as saturable absorber.

Universiti Malaya

Indian Journal of Physics, *99*(4), 1503-1508. https://doi.org/10.1007/s12648-024-03384-0

Supe, A., Olonkins, S., Udalcovs, A., Senkans, U., Mūrnieks, R., Gegere, L., Prigunovs, D., Grube, J., Elsts, E., Spolitis, S., Ozolins, O., & Bobrovs, V. (2021). Cladding-Pumped Erbium/Ytterbium Co-Doped Fiber Amplifier for C-Band Operation in Optical Networks. *Applied Sciences*, *11*(4), 1702. https://www.mdpi.com/2076-3417/11/4/1702

Tian, Z., Yam, S. S. H., & Loock, H.-P. (2008). Refractive index sensor based on an abrupt taper Michelson interferometer in a single-mode fiber. *Optics Letters*, *33*(10), 1105-1107. https://doi.org/10.1364/OL.33.001105

Tiu, Z. C., Harun, S., Ahmad, H., Samion, M., & Tan, S. (2022). Dark pulse generation in fiber laser system. *Optics & Laser Technology*, *151*, 108056.

Tiu, Z. C., Harun, S. W., Ahmad, H., Samion, M. Z., & Tan, S. J. (2022). Review: Dark pulse generation in fiber laser system. *Optics & Laser Technology*, *151*, 108056. https://doi.org/https://doi.org/10.1016/j.optlastec.2022.108056

Tiu, Z. C., Suthaskumar, M., Zarei, A., Tan, S., Ahmad, H., & Harun, S. W. (2015). Generation of switchable domain wall and cubic–quintic nonlinear Schrödinger equation dark pulse. *Optics & Laser Technology*, *73*, 127-129.

Tiu, Z. C., Suthaskumar, M., Zarei, A., Tan, S. J., Ahmad, H., & Harun, S. W. (2015). Generation of switchable domain wall and Cubic–Quintic nonlinear Schrödinger equation dark pulse. *Optics & Laser Technology*, *73*, 127-129. https://doi.org/https://doi.org/10.1016/j.optlastec.2015.04.010

Tiu, Z. C., Tan, S. J., Ahmad, H., & Harun, S. W. (2014). Dark pulse emission in nonlinear polarization rotation-based multiwavelength mode-locked erbium-doped fiber laser. *Chinese Optics Letters*, *12*(11), 113202. https://opg.optica.org/col/abstract.cfm?URI=col-12-11-113202

Tsai, T.-Y., Fang, Y.-C., & Hung, S.-H. (2010). Passively Q-switched erbium all-fiber lasers by use of thulium-doped saturable-absorber fibers. *Optics express*, *18*(10), 10049-10054.

Wabnitz, S., & Daino, B. (1993). Polarization domains and instabilities in nonlinear optical fibers. *Physics Letters A*, *182*(2), 289-293. https://doi.org/https://doi.org/10.1016/0375-9601(93)91073-E

Wang, J., Jia, H., Teng, H., Fang, S., Lv, Z., Liu, W., Tian, W., & Wei, Z. (2017, 2017/07/31). Generation of 408 fs Dark soliton pulse in a mode-locked ytterbium-doped fiber laser. 2017 Conference on Lasers and Electro-Optics Pacific Rim, Singapore.

Wang, L.-Y., Xu, W.-C., Luo, Z.-C., Cao, W.-J., Luo, A.-P., Dong, J.-L., & Wang, H.-Y. (2012). Dark pulses with tunable repetition rate emission from fiber ring laser. *Optics Communications*, *285*(8), 2113-2117.

Wang, M., Chen, C., Huang, C., & Chen, H. (2014). Passively Q-switched Er-doped fiber laser using a semiconductor saturable absorber mirror. *Optik*, *125*(9), 2154-2156. https://doi.org/https://doi.org/10.1016/j.ijleo.2013.10.047

Wang, M., Huang, S., Zeng, Y.-J., Yang, J., Pei, J., & Ruan, S. (2019). Passively Q-switched thulium-doped fiber laser based on oxygen vacancy MoO_3-x saturable absorber. *Optical Materials Express*, *9*(11), 4429-4437. https://doi.org/10.1364/OME.9.004429

Wang, P., Zhao, K., Xiao, X., & Yang, C. (2017). Pulse dynamics of dual-wavelength dissipative soliton resonances and domain wall solitons in a Tm fiber laser with fiber-based Lyot filter. *Optics Express*, *25*(24), 30708-30719. https://doi.org/10.1364/OE.25.030708

Wang, T., Zhang, W., Shi, X., Wang, J., Ding, X., Zhang, K., Peng, J., Wu, J., & Zhou, P. (2019). Black phosphorus-enabled harmonic mode locking of dark pulses in a Yb-doped fiber laser. *Laser Physics Letters*, *16*(8), 085102. https://doi.org/10.1088/1612-202X/ab232b

Wang, X., Wang, Z., Shen, C., Zhang, X., Huang, S., & Guo, T. (2024). Generation of spatiotemporal dark pulse or polarization domain wall solitons in a partial multimode mode-locked fiber laser. *Infrared Physics & Technology*, 105249.

Wang, Z., Zhan, L., Majeed, A., & Zou, Z. (2015). Harmonic mode locking of bound solitons. *Optics Letters*, *40*(6), 1065-1068. https://doi.org/10.1364/OL.40.001065

Wei, B.-N., Jiao, Z.-H., & Liu, W.-J. (2021). Ternary transition metal dichalcogenides for passively Q-switched Er-doped fiber laser applications. *Optik*, *248*, 168096.

Wright, L. G., Christodoulides, D. N., & Wise, F. W. (2015). Controllable spatiotemporal nonlinear effects in multimode fibres. *Nature Photonics*, *9*, 306 - 310.

Wright, L. G., Renninger, W. H., Christodoulides, D. N., & Wise, F. W. (2015). Spatiotemporal dynamics of multimode optical solitons. *Optics Express*, *23*(3), 3492-3506. https://doi.org/10.1364/OE.23.003492

Wu, M.-C., Chang, Y.-C., & Lin, G.-R. (2005). *Suppression of supermode and phase noises in mode-locked erbium-doped fiber laser with a semiconductor optical amplifier based high-pass filter* (Vol. 5709). SPIE. https://doi.org/10.1117/12.587977

Xomalis, A., Demirtzioglou, I., Jung, Y., Plum, E., Lacava, C., Petropoulos, P., Richardson, D. J., & Zheludev, N. I. (2018). Picosecond all-optical switching and dark pulse generation in a fibre-optic network using a plasmonic metamaterial absorber. *Applied Physics Letters*, *113*(5).

Xue, X., Xuan, Y., Liu, Y., Wang, P.-H., Chen, S., Wang, J., Leaird, D. E., Qi, M., & Weiner, A. M. (2015). Mode-locked dark pulse Kerr combs in normal-dispersion microresonators. *Nature Photonics*, *9*(9), 594-600.

Universiti Malaya

YANG, Q., & ZHANG, J.-F. (2005). OPTICAL QUASI-SOLITON SOLUTIONS FOR THE CUBIC-QUINTIC NONLINEAR SCHRÖDINGER EQUATION WITH VARIABLE COEFFICIENTS. *International Journal of Modern Physics B*, *19*(31), 4629-4636. https://doi.org/10.1142/s0217979205033005

Yu, H., Liu, X., Sun, W., Xu, Y., Liu, X., & Liu, Y. (2024). A brief review of Whispering Gallery Mode in sensing. *Optics & Laser Technology*, *177*, 111099. https://doi.org/https://doi.org/10.1016/j.optlastec.2024.111099

Zakharov, V., & Mikhailov, A. (1987). Polarization domains in nonlinear optics. *JETP Lett*, *45*(6), 349-352.

Zakharov, V. E., & Shabat, A. B. (1970). Exact Theory of Two-dimensional Self-focusing and One-dimensional Self-modulation of Waves in Nonlinear Media. *Journal of Experimental and Theoretical Physics*, *34*, 62-69.

Zenteno, L., Snitzer, E., Po, H., Tumminelli, R., & Hakimi, F. (1989). Gain switching of a Nd^{+3}-doped fiber laser. *Optics Letters*, *14*(13), 671-673.

Zervas, M. N., & Codemard, C. A. (2014). High power fiber lasers: a review. *IEEE Journal of selected topics in Quantum Electronics*, *20*(5), 219-241.

Zhang, A., Liu, C., Pan, H., & Guo, S. (2021). Multi-pulse operation in an actively Q-switched Er-doped fiber laser based on electro-optic modulator. *Optoelectronics Letters*, *17*(12), 729-733. https://doi.org/10.1007/s11801-021-1015-4

Zhang, C., Li, X., Chen, E., Liu, H., Shum, P. P., & Chen, X.-h. (2022). Hydrazone organics with third-order nonlinear optical effect for femtosecond pulse generation and control in the L-band. *Optics & Laser Technology*, *151*, 108016. https://doi.org/https://doi.org/10.1016/j.optlastec.2022.108016

Zhang, C., Liu, J., Gao, Y., Li, X., Lu, H., Wang, Y., Feng, J.-j., Lu, J., Ma, K., & Chen, X. (2022). Porous nickel oxide micron polyhedral particles for high-performance ultrafast photonics. *Optics & Laser Technology*, *146*, 107546. https://doi.org/https://doi.org/10.1016/j.optlastec.2021.107546

Zhang, H., Tang, D., Zhao, L., & Wu, X. (2011). Dual-wavelength domain wall solitons in a fiber ring laser. *Optics Express*, *19*(4), 3525-3530. https://doi.org/10.1364/OE.19.003525

Zhang, H., Tang, D. Y., Zhao, L. M., & Knize, R. J. (2010). Vector dark domain wall solitons in a fiber ring laser. *Optics Express*, *18*(5), 4428-4433. https://doi.org/10.1364/OE.18.004428

Zhang, H., Tang, D. Y., Zhao, L. M., & Wu, X. (2009). Dark pulse emission of a fiber laser. *Physical Review A*, *80*(4), 045803. https://doi.org/10.1103/PhysRevA.80.045803

Zhang, H., Tang, D. Y., Zhao, L. M., & Xiang, N. (2008). Coherent energy exchange between components of a vector soliton in fiber lasers. *Optics Express*, *16*(17), 12618-12623. https://doi.org/10.1364/OE.16.012618

Universiti Malaya

Zhang, P., Dimyati, K., Nizamani, B., Najm, M. M., Yasin, M., & Wadi Harun, S. (2022). Ultrashort pulse generation in All-fiber Erbium-doped fiber cavity with thulium doped fiber saturable absorber. *Optics & Laser Technology*, *149*, 107888. https://doi.org/https://doi.org/10.1016/j.optlastec.2022.107888

Zhang, W., Zhan, L., Xian, T., & Gao, L. (2019, 2019/11/11). Bidirectional dark soliton mode-locked fiber laser based on thulium-doped fiber saturable absorber.*OSA Technical Digest* International Photonics and OptoElectronics Meeting 2019 (OFDA, OEDI, ISST, PE, LST, TSA), Wuhan.

Zhang, W., Zhan, L., Xian, T., & Gao, L. (2019). Harmonic Mode-Locking in Bidirectional Domain-Wall Soliton Fiber Lasers. *Journal of Lightwave Technology*, *37*(21), 5417-5421. https://doi.org/10.1109/JLT.2019.2942185

Zhao, F., Wang, H., Zhang, T., Wang, Y., Hu, X., Sun, C., & Zhang, W. (2019). Passively Q-Switched All-Fiber Yb-Doped Lasers Based on Nonlinear Multimode Interference. *Journal of Russian Laser Research*, *40*(1), 87-93. https://doi.org/10.1007/s10946-019-09774-8

Zhao, J., Yan, P., & Ruan, S.-C. (2013). Observations of three types of pulses in an erbium-doped fiber laser by incorporating a graphene saturable absorber. *Applied Optics*, *52*(35), 8465-8470.

Zhao, L. M., Tang, D. Y., Zhang, H., & Wu, X. (2008). Polarization rotation locking of vector solitons in a fiber ring laser. *Optics Express*, *16*(14), 10053-10058. https://doi.org/10.1364/OE.16.010053

Zhao, Y., Wang, W., Li, X., Lu, H., Shi, Z., Wang, Y., Zhang, C., Hu, J., & Shan, G. (2020). Functional Porous MOF-Derived CuO Octahedra for Harmonic Soliton Molecule Pulses Generation. *ACS Photonics*, *7*(9), 2440-2447. https://doi.org/10.1021/acsphotonics.0c00520

Zhou, D.-P., Wei, L., & Liu, W.-K. (2010). *Compact passively Q-switched Er/Yb-codoped cladding pumped fiber laser* (Vol. 7750). SPIE. https://doi.org/10.1117/12.872146

Zhou, D. P., Wei, L., Dong, B., & Liu, W. K. (2010). Tunable Passively Q-switched Erbium-Doped Fiber Laser With Carbon Nanotubes as a Saturable Absorber. *IEEE Photonics Technology Letters*, *22*(1), 9-11. https://doi.org/10.1109/LPT.2009.2035325

Zhou, R., Yu, D., Liu, X., Li, Q., & Fu, H. Y. (2019). Dark rectangular noise-like pulses in a figure-nine fiber laser based on a nonlinear amplifying loop mirror. *Optics Letters*, *44*(15), 3717-3720. https://doi.org/10.1364/OL.44.003717

Zhu, X. (2008). *Multimode interference in optical fibers and its applications of fiber lasers and amplifiers* The University of Arizona].

Universiti Malaya